Imaging post-exocytic dynamics of synaptic vesicle proteins

Inaugural-Dissertation

to obtain the academic degree

Doctor rerum naturalium (Dr. rer. nat.)

submitted to the Department of Biology, Chemistry and Pharmacy

of the Freie Universität Berlin

by

Niclas Gimber

from Berlin, Germany

March, 2016

Die vorliegende Arbeit wurde in der Zeit vom Juni 2010 bis März 2016 unter Anleitung von Prof. Dr. Volker Haucke am Institut für Chemie und Biochemie der Freien Universität Berlin und am Leibniz-Institut für Molekulare Pharmakologie (FMP) durchgeführt.

1. Gutachter: Prof. Volker Haucke

2. Gutachter: Prof. Stephan Sigrist

Disputation am: 19. Mai 2016

Affidavit

I declare that my PhD thesis entitled “Imaging post-exocytic dynamics of synaptic vesicle proteins” has been written independently and with no other sources and aids than quoted.

Berlin, March 8th 2016 Niclas Gimber

Acknowledgments

I would like to express my gratitude to all the people who have supported and inspired me during my PhD studies. First of all, I would like to thank Prof. Dr. Volker Haucke for giving me the opportunity to work on this exciting project and for his excellent supervision and support throughout my PhD thesis. I would further like to thank Dr. Jan Schmoranzer for the great co-supervision, for all the fruitful discussions and for sharing his imaging expertise with me.

I am grateful for the financial support by the “Deutsche Forschungsgemeinschaft” and the Helmholtz International Research School “Molecular Neurobiology”. Furthermore, I would like to thank my PhD committee members Prof. Dr. Gary Lewin, Dr. Andrew Plested and Dr. Oliver Rocks for their scientific advices and Prof. Dr. Gudrun Ahnert-Hilger for providing the synaptophysin knockouts.

I would like to express my gratitude to all my lab colleagues, who contributed to an inspiring atmosphere. I enjoyed working with them. Special thanks to “my” Masters student Georgi Tadeus for his contribution in the initial phase of this project. His excellent programming skills made the analysis of NEP dynamics efficient enough to characterize thousands of synapses. I am grateful for the support from Dr. Tanja Maritzen, who provided the AP180 knockouts and I want to express my gratitude to the super-resolution guys Dr. Martin Lehmann and André Lampe for sharing with me all their knowledge on microscopy beyond the diffraction limit. I further thank Dr. Seong Joo Koo, who taught me how to prepare hippocampal neuron cultures and how to perform pHluorin-based imaging.

Last, but most importantly I want to thank my family and friends for being by my side and for supporting me in everything I do. I owe special thanks to Leona and my son Nils for their patience and for giving me so much energy.

Table of contents

Summary

Our central nervous system relies on synaptic transmission, which is based on the release of neurotransmitters from synaptic vesicles (SVs) by Ca^{2+}-triggered exocytosis. SV fusion with the plasma membrane at active zones is followed by endocytosis at the periactive zone. Although SV cycling is a fundamental process for neurotransmission at chemical synapses and exo- and endocytosis at the mammalian presynapse has been the subject of intense investigations over the last decades, the fate of newly exocytosed SV proteins remained largely unknown. Recent findings uncovered that upon moderate electrical stimulation, instead of newly exocytosed SV proteins, a preassembled "readily retrievable pool" of SV proteins is retrieved from the plasma membrane at the periactive zone. However, what happens to newly exocytosed SV proteins has remained unknown. To address this question, I developed an assay to spatiotemporally characterize newly exocytosed SV proteins upon moderate electrical stimulation. I furthermore identified molecular factors that mediate post-exocytic dynamics.

My data demonstrates that, in hippocampal neurons, newly exocytosed SV proteins spread out from the active zone via Brownian motion. Considering, that previous research shows that the removal of released proteins from active zones is essential for effective exocytosis, it is even more remarkable that the initial spread of newly exocytosed SV proteins is not supported by active transport. After a few seconds of diffusion, most molecules remain confined within the presynaptic plasma membrane. Only ~ 10 % of the molecules escape rapidly into the axon. After confinement, SV proteins recluster slowly. Strikingly, all investigated SV proteins show similar diffusional spread, confinement and reclustering. Super-resolution microscopy reveals that reclustered SV proteins contribute to nano-clusters that are closely associated with the clathrin-based endocytic machinery at periactive zones. It is therefore conceivable that nano-clusters of endocytic proteins mediate the trapping of newly exocytosed SV proteins at the periactive zone and transform newly exocytosed SV proteins into a preassembled readily retrievable pool.

I furthermore show that the confinement of newly exocytosed synaptobrevin 2 (Syb2) is reduced, but not abolished, by interfering with the interaction with the clathrin-based endocytic machinery, e. g. the Syb2-specific adaptors AP180 and CALM. A similar reduction

applies to the extent of reclustering. This suggests that confinement and reclustering are mediated by the clathrin-based endocytic machinery, together with a so far unidentified diffusion barrier. Furthermore, the Syb2 diffusion is accelerated by a mutation of the binding site for AP180 and CALM. This is in agreement with an early association of AP180 or CALM with Syb2. Although the acute post-exocytic confinement of AP180- and CALM-binding deficient Syb2 is only partially impaired, this study shows that Syb2 binding to its specific endocytic adaptors finally prevents a major loss into the axon over time. Taken together, these findings demonstrate that diffusional spread, confinement and reclustering are essential processes of the SV cycle and partially rely on the clathrin-based endocytic machinery.

Zusammenfassung

Signale werden an den chemischen Synapsen unseres Nervensystems durch Neurotransmitter übertragen. Diese Neurotransmitter werden durch die Ca^{2+}-abhängige Fusion von synaptischen Vesikeln (SV) mit der Plasmamembran an aktiven Zonen freigesetzt. An der periaktiven Zone werden die Bestandteile von SV wieder recycelt. Obwohl dieser Kreislauf ein elementarer Bestandteil der Signalübertragung an chemischen Synapsen ist, und die Exo- und Endozytose an der Präsynapse in der Vergangenheit eingehend untersucht wurden, ist der Verbleib von neu exozytierten SV Proteinen noch weitgehend ungeklärt. Erst kürzlich konnte gezeigt werden, dass nach einer moderaten elektrischen Stimulation nicht die neu exozytierten SV Proteine, sondern SV Proteine des sogenannten „Readily Retrievable Pool" an der periaktiven Zone endozytiert werden. Der Verbleib der neu exozytierten SV Proteine blieb jedoch weiterhin unklar. Um den Verbleib dieser Proteine aufzuklären habe ich einen Assay entwickelt mit welchem die räumliche Ausbreitung von neu exozytierten SV Proteinen nach elektrischer Stimulation untersucht werden kann. Außerdem konnte ich molekulare Faktoren identifizieren, welche die Bewegung von SV Proteinen nach der Exozytose beeinflussen.

Die vorliegende Arbeit zeigt in hippocampalen Neuronen, dass sich die neu exozytierten SV Proteine durch Diffusion ausbreiten. Frühere Arbeiten weisen darauf hin, dass das Entfernen von neu exozytierten SV Proteinen von der aktiven Zone für die effektive Exozytose essenziell ist. Daher ist es bemerkenswert, dass für die Ausbreitung von neu exozytierten SV Proteinen kein aktiver Transport benötigt wird. Nach wenigen Sekunden der Diffusion wird ein Großteil der Moleküle an der präsynaptischen Plasmamembran zurückgehalten. So gelangen nur etwa 10% der neu exozytierten Proteine in das angrenzende Axon. Nach der anfänglichen Ausbreitung kommt es zum „Reclustering", die SV Proteine ziehen sich dabei langsam wieder auf einen engeren Bereich zurück. Alle untersuchten SV Proteine zeigten auffallende Ähnlichkeiten in der Ausbreitung und im „Reclustering". Mittels hochauflösender Fluoreszenzmikroskopie zeigt diese Arbeit, dass neu exozytierte SV Proteine zusammen mit dem Clathrin-basierenden Endozytose-Apparat in dem Bereich der periaktiven Zone Nanocluster bilden. Daher ist es denkbar, dass ein in Nanoclustern organisierter Endozytose-Apparat in der periaktiven Zone neu exozytierte SV Proteine immobilisiert und daraus den „Readily Retrievable Pool" aufbaut.

Weiterhin zeige ich, dass sobald die Interaktion zu dem Clathrin-basierenden Endozytose-Apparat durch die Syb2-spezifischen Adapter AP180 und CALM fehlt, sich neu exozytiertes Syb2 zwar weiter ausbreitet, jedoch zunächst nicht frei ins Axon diffundiert. Dieser Anstieg des Ausbreitungsbereichs bleibt auch nach dem „Reclustering“ bestehen. Dies deutet darauf hin, dass neben dem Clathrin-basierende Endozytose-Apparat eine weitere Barriere für die Begrenzung der Diffusion und das „Reclustering“ von neu exozytierten SV Proteinen verantwortlich ist. Des Weiteren zeigt diese Arbeit, dass die Diffusion von Syb2 durch die Mutation von dessen AP180- und CALM-Bindungsstelle beschleunigt wird. Daher ist eine frühzeitige Interaktion von AP180 oder CALM mit Syb2 wahrscheinlich. Obwohl die akute Begrenzung von neu exozytiertem Syb2 von einer fehlenden Interaktion mit AP180 und CALM nur teilweise betroffen ist, zeige ich, dass AP180 und CALM auf lange Sicht einen maßgeblichen Verlust von Syb2 in das Axon verhindern. Zusammenfassend zeigt diese Arbeit, dass Diffusion, deren Begrenzung und das „Reclustering“ von neu exozytierten SV Proteinen wesentliche Prozesse des SV Zyklus sind und unter anderem von dem Clathrin-basierten Endozytose-Apparat vermittelt werden.

1 Introduction

1.1 The chemical synapse

Our central nervous system relies on the transmission of electrically or chemically encoded information. Signals that propagate along an axon are encoded as fast changes of the membrane potential (action potentials, APs). The depolarization of a plasma membrane from a chemical presynapse leads to Ca^{2+} influx through voltage-gated calcium channels (Katz and Miledi, 1967). The rise in the presynaptic calcium concentration increases the probability of synaptic vesicle (SV) fusion with the plasma membrane at active zones and the subsequent release of the neurotransmitter content. Neurotransmitters diffuse over the synaptic cleft and bind to ligand-gated ion channels at postsynapses, which transform the chemical signal back into an electrical signal (Südhof, 2004).

On the molecular scale, Ca^{2+} binding to synaptotagmin 1 triggers the fusion of SVs with the presynaptic plasma membrane (Fernández-Chacón et al., 2001). The actual fusion process is driven by the association of the SV protein synaptobrevin 2 with the plasma membrane proteins syntaxin and Synaptosomal-associated protein 25 (SNAP-25). All three proteins interact via their soluble NSF attachment receptor (SNARE) motifs, forming a so-called trans-SNARE complex. Thereby they pull both membranes into close proximity and induce fusion. After SV fusion with the plasma membrane, cis-SNARE complexes within the plasma membrane are disassembled by N-ethylmaleimide-sensitive factor (NSF) and its cofactor α-soluble NSF attachment protein (SNAP). Membrane and proteins are recycled and SVs are reacidified and refilled with neurotransmitter (Südhof, 2004; Jahn and Scheller, 2006).

1.2 Synaptic vesicles

Synaptic vesicles are presynaptic organelles with a spherical shape and a diameter of 42 nm. They can release their neurotransmitter content upon presynaptic Ca^{2+} entry by fusion with the plasma membrane at active zones. A tightly controlled composition of proteins and

lipids (Takamori et al., 2006; Mutch et al., 2011) ensures the reliable neurotransmission at chemical synapses. The membrane of a single SV contains on average 7000 phospholipid molecules, is enriched in cholesterol (~ 5600 molecules) and numerous transmembrane and membrane-associated proteins (Figure 1-1; Takamori et al., 2006). Most SV proteins can either be classified as transport proteins, which are involved in neurotransmitter uptake, or as trafficking proteins (Südhof, 2004). Among the transport proteins are chloride channels and the vesicular vATPase, which provide the proton gradient for neurotransmitter uptake (Stobrawa et al., 2001; Gasnier, 2000), but also neurotransmitter transporters like the vesicular glutamate transporter VGLUT. The most abundant SV trafficking proteins are synaptobrevin 2 (~ 70 molecules), synaptophysin (~ 32 molecules) and synaptotagmin 1 (~ 15 molecules) (Takamori et al., 2006; similar to the results of Wilhelm et al., 2014).

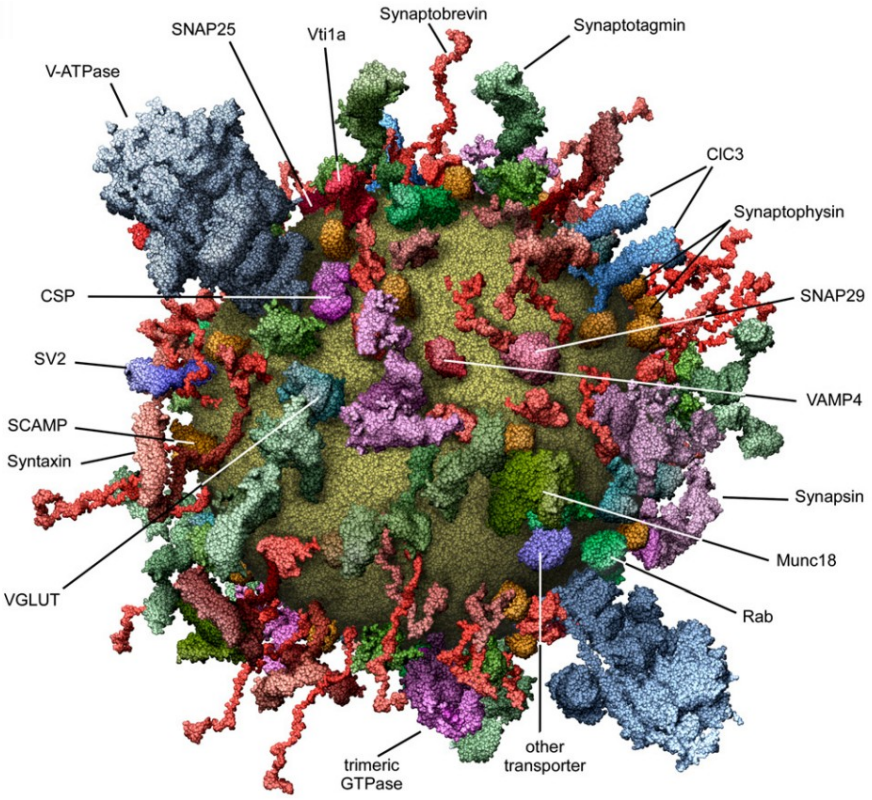

Figure 1-1: An average synaptic vesicle.

Model of an average synaptic vesicle. SV proteins are displayed at near atomic resolution. Protein numbers correspond to experimentally determined average copy numbers. Note that the SV surface is almost entirely covered with proteins. Syb2, Syt1 and Syp are the proteins with the highest abundance. Taken from Takamori et al., 2006.

1.2.1 Synaptobrevin 2

The single pass transmembrane (Bowen and Brunger, 2006) SV protein synaptobrevin 2 (Syb2) is a pivotal protein in the process of SV docking (Imig et al., 2014) and fusion with the presynaptic plasma membrane (Schoch et al., 2001). The SNARE motifs of vesicular Syb2 and syntaxin and the two SNARE motifs of SNAP-25 assemble into parallel four-helix bundles, which drives SV fusion by pulling both membranes in close proximity (Südhof, 2004). Outside SNARE complexes Syb2 exists as a monomer and as a homodimer (Fdez et al., 2010).

Uptake and release experiments with fluorescent styryl FM-dyes in hippocampal neurons of Syb2-deficient mice revealed that the complete absence of Syb2 causes major defects in SV release, in hippocampal neurons (Schoch et al., 2001). The number of Syb2 molecules that is required for the fusion of a SV with the plasma membrane is still under debate. While results from liposome fusion experiments (van den Bogaart et al., 2010; Shi et al., 2012) and experiments with chromaffin cells or hippocampal neurons (Mohrmann et al., 2010; Sinha et al., 2011) suggest that 1 - 3 SNARE complexes are sufficient for the membrane fusion, several Syb2 molecules per vesicle are most likely necessary for efficient neurotransmission (Südhof, 2013; Koo et al., 2015).

Besides the defect in exocytosis, Syb2-deficient neurons also display endocytic defects. Synaptic vesicles of neurons lacking Syb2 are elongated and enlarged. Further, styryl dye uptake experiments (Deák et al., 2004) and capacitance measurements (Xu et al., 2013a) revealed delayed SV endocytosis in Syb2 deficient neurons.

1.2.2 Synaptotagmin 1

Synaptotagmin 1 (Syt1) is a single pass transmembrane SV protein (Perin et al., 1991) and crucial for neurotransmitter release. A depolarization of the presynaptic membrane by arriving action-potentials leads to the opening of voltage-gated Ca^{2+} channels. Extracellular Ca^{2+} enters the presynapse through the open channels and binds to Syt1, which acts as a triggers for Ca^{2+}-dependent neurotransmitter release (Fernández-Chacón et al., 2001). In particular Ca^{2+} induces the binding of Syt1 to SNARE-proteins and a bending of the target membrane via the cytoplasmic C2 domains of Syt1 (Chapman et al., 1995; Gerona et al.,

2000; Hui et al., 2009; Martens and McMahon, 2008). Neurons lacking Syt1 were shown to have a profound reduction in the fast synchronous neurotransmitter release (Geppert et al., 1994).

In addition to its trigger-function in exocytosis, Syt1 is required for endocytosis. Hippocampal neurons of Syt1 knockout mice show slower rates of SV endocytosis, in comparison to WT neurons (Nicholson-Tomishima and Ryan, 2004). Interestingly, endocytic rates can be rescued by the re-expression of a membrane-targeted C2A or C2B domain or full length Syt1 in Syt1 deficient neurons, but not with mutants with abolished Ca^{2+} binding (Yao et al., 2011). Thus Syt1 acts as a Ca^{2+} sensor in both exo- and endocytosis.

1.2.3 Synaptophysin

For a long time, the function of the tetraspan (Arthur and Stowell, 2007) SV membrane protein Synaptophysin (Syp) had been unclear. Initially, it was shown that Syp does not only form homomultimers in SV membranes (Thomas et al., 1988), but also heteromers with Syb2 (Calakos and Scheller, 1994; Edelmann et al., 1995; Becher et al., 1999). It became clear that these heteromers require cholesterol (Mitter et al., 2003) and contain 25% of Syb2 associated to Syp (Khvotchev and Südhof, 2004). SV recycling experiments with the genetically encoded pH-sensitive pHluorin reporter in cortical neurons of Syp knockout mice revealed a functional relevance of the Syb2-Syp-interaction. Syp-deficient neurons show impaired Syb2 endocytosis, which results in a Syb2 accumulation at the plasma membrane (Gordon et al., 2011). This is in agreement with a faster Syb2 endocytosis and less surface accumulation in neurons overexpressing Syp (Pennuto et al., 2003; Wienisch and Klingauf, 2006). Even though the endocytosis of VGLUT1, synaptic vesicle glycoprotein 2A (SV2A) and Syt1 is also slightly affected in Syp knockout neurons (Gordon et al., 2011; Kwon and Chapman, 2011), this minor general endocytic delay may be secondary, taking the role of Syb2 in SV endocytosis into account (Deák et al., 2004; Xu et al., 2013a).

1.3 Synaptic vesicle pools

SVs can be categorized into three groups: the recycling pool, the readily releasable pool (RRP) and the reserve pool. The recycling pool is functionally defined as the fraction of SVs that are continuously released and recycled under physiological stimulation conditions (5 – 20 % of the total pool size; Richards et al., 2000; de Lange et al., 2003). The RRP represents a sub-fraction of the recycling pool. Vesicles from the RRP fuse immediately upon stimulation and are rapidly depleted during high-frequency stimulation (~ 2 % of the total pool size; Rizzoli and Betz, 2005). Morphologically the RRP corresponds to the SVs that are docked at the presynaptic active zone and primed for release (Schneggenburger et al., 1999; Schikorski and Stevens, 2001). The reserve pool acts as a buffer. It is only released upon depletion of the recycling pool during high-frequency stimulation or upon inhibition of endocytosis. It comprises 80 - 95 % of the total pool size (Richards et al., 2000; de Lange et al., 2003).

1.4 The readily retrievable pool

Under physiological conditions, most SV proteins reside at synaptic vesicles. However, even in resting neurons, a part of them can be found at the presynaptic plasma membrane. While only ~ 8 % of presynaptic Syp (Granseth et al., 2006) localizes to the plasma membrane, a substantial fraction of Syb2 and Syt1 (~ 30 %, Dittman and Kaplan, 2006; Wienisch and Klingauf, 2006; Koo et al., 2015) can be found on the presynaptic surface. Interestingly, SV proteins are not randomly distributed over the plasma membrane, but they form distinct sub-synaptic clusters with a diameter of 80 – 100 nm (Syt1: 80 – 100 nm, Syp: ~ 100 nm; Willig et al., 2006; Opazo et al., 2010) in the periphery of active zones (Syt1; Hua et al., 2011).

Recent studies found, that such clusters do not represent missorted proteins, but rather a pool of preassembled SV proteins (Readily Retrievable Pool, RRetP) that is preferentially retrieved upon electrical stimulation (Hua et al., 2011; Wienisch and Klingauf, 2006). A first indication for a stimulation-evoked retrieval of a RRetP came from single vesicle pHluorin experiments (for an introduction into pHluorin live-cell imaging see also chapter 3.4.11) with hippocampal neuron cultures, uncovering rare quantal retrieval events without

corresponding exocytic quanta (Gandhi and Stevens, 2003). Further evidence came from pHluorin experiments in hippocampal neurons, where fluorescence of a plasma membrane-localized RRetP (of Syb2-pH and Syt1-pH) was selectively eliminated by enzymatic digestion or photobleaching (similar to Figure 4-1a). In both cases, electrical stimulation, led to a fluorescence increase by exocytosis, followed by only a minor decrease. In contrast, in untreated neurons fluorescence dropped back to the baseline. This suggested that proteins of the RRetP (non-fluorescent) are preferentially retrieved, instead of newly exocytosed SV proteins (Figure 1-2; Wienisch and Klingauf, 2006). In line with that, a selective RRetP labeling with Syt1 specific antibodies, coupled to the pH-sensitive dye cypHer5E (quenched at neutral pH) revealed a stimulation induced fluorescence increase, as a result of RRetP retrieval and vesicle reacidification (Hua et al., 2011).

Thus, newly exocytosed and subsequently retrieved SV proteins are not identical. The RRetP rather represent the counterpart of the RRP, with an endocytic capacity corresponding to ~70 APs (Hua et al., 2011). While the endocytosis of the RRetP has already been described in some detail, the molecular mechanisms underlying the clustering of newly exocytosed proteins and the conversion into the new RRetP remained unknown.

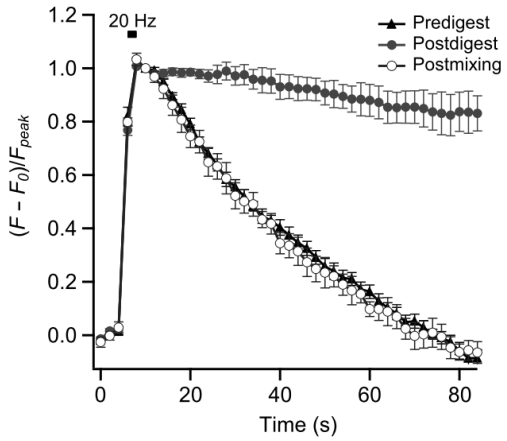

Figure 1-2: SV proteins that are exocytosed and subsequently retrieved are not identical.
Fluorescent transients from hippocampal neurons expressing pHluorin tagged Syb2. Electrical stimulation (40 AP. 20Hz) induces exocytosis, indicated by increasing fluorescence. Only a minor post-exocytic decrease in fluorescence is observed, if surface-accessible pHluorin-tags are enzymatically removed before stimulation (Postdigest). In contrast, the fluorescence drops back to the baseline, in untreated neurons (Predigest) or neurons that were surface-digested, but allowed to mix surface-stranded and vesicular proteins (Postmix). This suggests

that surface-stranded proteins (non-fluorescent) were preferentially retrieved, instead of newly exocytosed SV proteins. Taken from Wienisch and Klingauf, 2006. A detailed introduction into conventional pHluorin live-cell imaging is provided in the methods section (chapter 3.4.11).

1.5 Synaptic vesicle recycling

The huge distance between the neuronal cell body and presynaptic terminals, together with the fact that sustained exocytosis would rapidly expand the presynaptic membrane, implicate the need for a local presynaptic recycling mechanism for SVs (Figure 1-3).

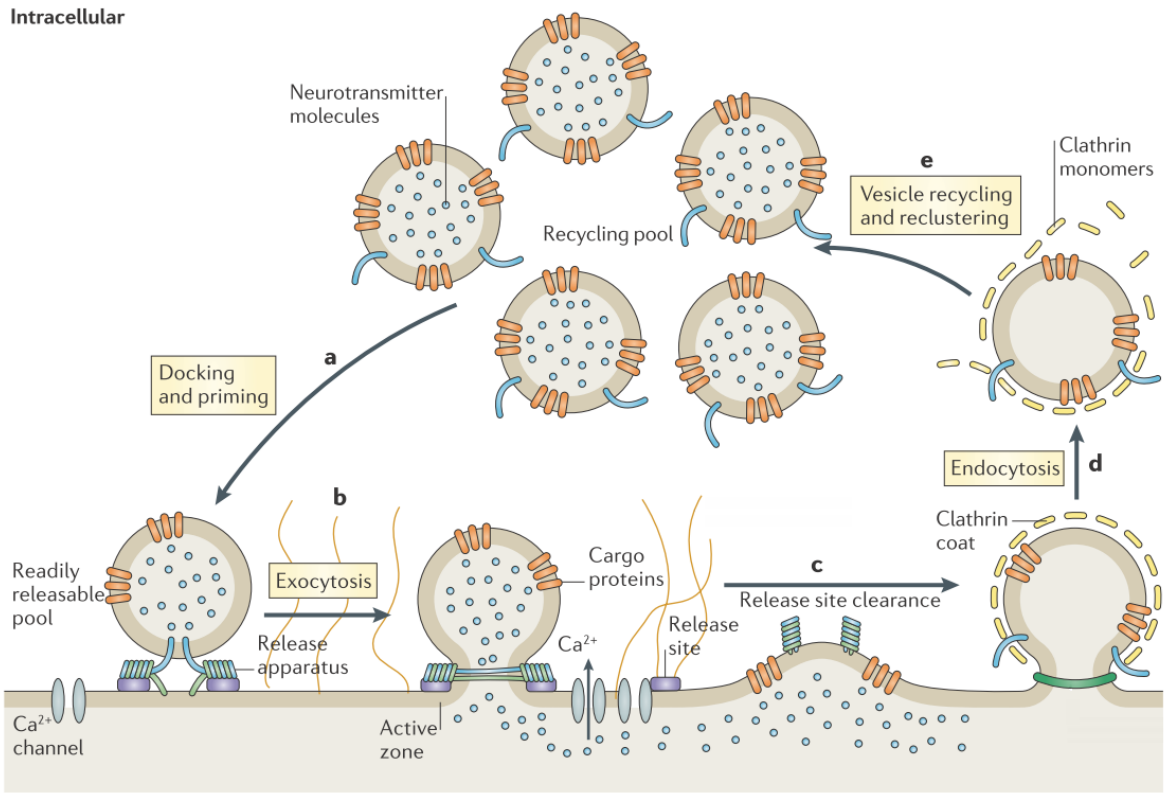

Figure 1-3: The synaptic vesicle cycle.

SVs from the recycling pool are continuously released and recycled under physiological stimulation conditions. However, just a sub-fraction of them is immediately ready for release. This so-called readily releasable pool comprises docked and primed SVs (a), which fuse with the presynaptic plasma membrane at active zones and release their neurotransmitter content. A depolarization of the plasma membrane results in the subsequent Ca^{2+} entry through voltage gated Ca^{2+}-channels and Ca^{2+} triggered exocytosis (b). Release site clearance is believed to be required to prevent active zones from getting blocked by newly exocytosed SV proteins and to allow for

further rounds of efficient exocytosis (c). Different modes of compensatory endocytosis have been proposed. However, under moderate stimulation conditions, the predominant mode seems to be clathrin-mediated endocytosis, adjacent to the active zone (d). After endocytosis, newly formed SVs are rapidly uncoated and refilled with neurotransmitter. Taken and modified from Haucke et al., 2011.

1.5.1 Models of synaptic vesicle endocytosis

Different models of synaptic vesicle endocytosis have been postulated in the past. They differ in speed and fidelity of SV retrieval (Figure 1-4). Two of them were already proposed in the 1970s, based on the ultrastructural analysis of the frog neuromuscular junction. One model, referred to as kiss-and-run, describes the transient fusion of SVs with the plasma membrane without full vesicle collapse. The narrow fusion pores is believed to close rapidly to regenerate SVs directly at active zones without the need for endocytic sorting. This model was initially proposed, based on the findings that SVs can take up horseradish peroxidase (HRP), but their recycling was too fast to experimentally capture it (Ceccarelli et al., 1973). Further evidence for the existence of a kiss-and-run mechanism comes from release experiments of lipophilic FM styryl dye in hippocampal synapses (Richards et al., 2005; Harata et al., 2006). The researchers observed uptake and partial dye release, which was taken as prove for a transient fusion pore during kiss-and-run. However, in similar experiments, kiss-and-run represented just a minor fraction of all events. Instead, most SVs lost their complete dye content, indicating full SV collapse (Chen et al., 2008).

A second model suggests that SVs are generated through clathrin-coated vesicles, which bud from the presynaptic plasma membrane outside the active zone. It is based on the observation of cisternal structures, coated pits and coated vesicles, which take up HRP upon electrical stimulation (Heuser and Reese, 1973). This model is supported by the finding that perturbing clathrin, or related cargo-specific adaptors, strongly interferes with endocytosis at presynapses, at least under moderate or low stimulation (Augustine et al., 2006; Granseth et al., 2006; Koo et al., 2011a; Kononenko et al., 2014). Single vesicle pHluorin experiments with hippocampal neurons revealed the existence of a fast and a slow mode of endocytosis, which may correspond to kiss-and-run and clathrin-mediated endocytosis (CME; Gandhi and Stevens, 2003). CME from the plasma membrane predominantly operates at low to moderate electrical stimulation (Granseth et al., 2006; Kononenko et al., 2014). In contrast to Kiss-and-

run, CME is compatible with the existence of a readily retrievable pool (Fernández-Alfonso et al., 2006; Wienisch and Klingauf, 2006; Hua et al., 2011).

Recently, two further modes of endocytosis were discovered. Rapid high pressure freezing electron microscopy revealed the existence of an ultrafast mode of endocytosis. Upon a single optogenetic stimulus, SVs were shown to collapse into the plasma membrane and being retrieved, 50 – 100 ms after stimulation, outside the active zone (Watanabe et al., 2013a, 2013b). Ultrafast endocytosis is, as kiss-and-run, in agreement with the observation of a fast component in capacitance measurements in the calyx of Held (Sun et al., 2002) and in single vesicle pHluorin experiments (Gandhi and Stevens, 2003). However, ultrafast endocytosis is not identical to kiss-and-run endocytosis, since endocytic structures appear outside active zones and with a surface area that is bigger than a single SV. Endocytosed endosomal structures rather correspond to an equivalent of four synaptic vesicles. Since endocytic invaginations of the plasma membrane lack clathrin coats and endocytosis remains unperturbed upon clathrin knockdown (KD), ultrafast endocytosis is clathrin-independent. Instead, it was shown that actin and dynamin are required for this process (Watanabe et al., 2013b, 2014). However, since ultrafast endocytosis is much faster than the endocytic kinetics, which were observed for the RRetP (Hua et al., 2011), it cannot account for SV retrieval under moderate electrical stimulation trains. Furthermore, it is unclear, whether ultrafast endocytosis retrieves exclusively lipids or the complete membrane including the SV proteins.

Bulk endocytosis operates upon strong stimulation outside active zones. Electron microscopy revealed large presynaptic plasma membrane invaginations, which give rise to endosome-like vacuoles (Miller and Heuser, 1984). Bulk endocytosis requires dynamin 1 and 3, endophilin and actin polymerization (Kononenko et al., 2014). Controversial data exists concerning the requirement of clathrin and on the incorporation of cargo (Kononenko et al., 2014; Nicholson-Fish et al., 2015). Whether bulk endocytosis is mechanistically related to ultrafast endocytosis is unknown. In conditions, where RRetP assembly and CME are too slow to compensate for the fast SV release, bulk endocytosis may step in. Thus, a spatiotemporal characterization of RRetP assembly may provide further insights on the rate limitations of CME.

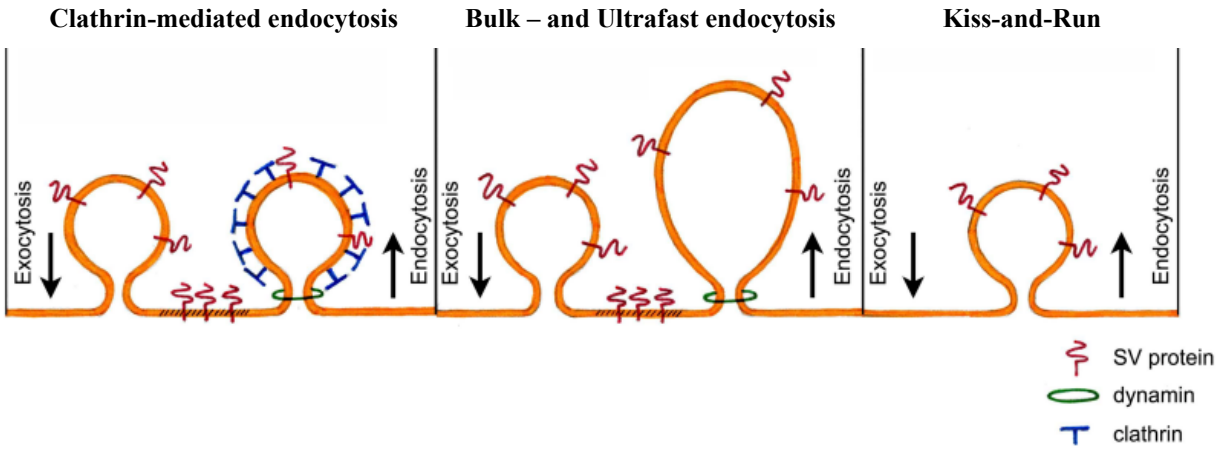

Figure 1-4: Models of SV endocytosis.

(a) Clathrin-based endocytosis occurs after a full collapse of a SV. Proteins are retrieved from the plasma membrane at sites that are distal to active zones. Retrieval is mediated by the coat protein clathrin. **(b)** Bulk – and ultrafast endocytosis involve large endocytic structures at the plasma membrane. Those endocytic structures appear distal from active zones and convert into large endosomes. These endosomes are likely further processed in a clathrin-dependent manner. CME, ultrafast- and bulk endocytosis require the GTPase dynamin to pinch off. **(c)** In kiss-and-run, SVs do not collapse into the plasmamembrane. Their neurotransmitter content is released through a transient fusion pore. Taken and modified from Kononenko et al., 2013a.

1.5.2 Clathrin-mediated endocytosis

Different modes of compensatory endocytosis at presynapses have been proposed, which probably exist in parallel or at least under different conditions. However, under moderate stimulation, CME prevails (Granseth et al., 2006; Kononenko et al., 2014) and retrieves a preassembled RRetP of SV proteins from the plasma membrane (Wienisch and Klingauf, 2006; Hua et al., 2011). The mechanism behind CME at synapses is very similar to that of constitutive or ligand-stimulated endocytosis in non-neuronal cells (Jung and Haucke, 2007). Although the exact timing is not fully understood, CME can be divided into five major processes (Figure 1-5):

Nucleation: Sites of endocytosis at the plasma membrane are defined by high local phosphatidylinositol-4,5-bisphosphate ($PI(4,5)P_2$) concentrations. $PI(4,5)P_2$, is generated by phosphatidylinositol 4-phosphate 5-kinase type I (PIPKI), precisely PIPKI γ at synapses (Wenk et al., 2001; Di Paolo et al., 2004). FCH domain only (FCHO) proteins bind to $PI(4,5)P_2$,, generate the initial membrane curvature through their F-BAR domain (McMahon

and Boucrot, 2011) and recruit the scaffold proteins epidermal growth factor receptor substrate 15 (Eps15) and intersectin which again help to recruit AP-2 (Henne et al., 2010).

Cargo selection: The accumulation of cargo in clathrin-coated pits is required for their maturation (Loerke et al., 2009). The heterotetrameric AP-2 complex can directly bind to cargo proteins including synaptotagmin and SV2A (Haucke and De Camilli, 1999). However, many SV proteins do not contain typical endocytic motifs that are recognized by AP-2. Thus, these SV proteins are sorted by clathrin-associated sorting proteins (CLASPs), which specifically bind cargo sorting signals, but also AP-2, clathrin and often $PI(4,5)P_2$ (McMahon and Boucrot, 2011). Well characterized CLASPs are AP180, CALM (both Syb2-specific; Zhang et al., 1998; Koo et al., 2011a), stonin 2 (Syt1-specific; Diril et al., 2006; Kononenko et al., 2013b), endophilin (VGlut1-specific; Voglmaier et al., 2006) and epsin (binds ubiquitinated cargo; Traub, 2005). It is not clear, whether all SV protein harbor an endocytic sorting motif or if interactions between cargo molecules themselves facilitate the clustering and subsequent internalization of the SV protein clusters (Gordon and Cousin, 2014). It is further conceivable that, after exocytosis, such proteins remain clustered over the whole SV cycle (Willig et al., 2006; Opazo et al., 2010).

Coat assembly: While SV proteins are sorted into a pit, membrane curvature is generated by accessory proteins like the ENTH (epsin N-terminal homology) domain-containing protein epsin or BAR (Bin, amphiphysin, Rvs) domain-containing proteins like amphiphysin or endophilin. Those proteins insert amphipathic helices into the cytosolic membrane leaflet and thereby bend the membrane or stabilize membrane curvature (McMahon and Gallop, 2005; Daumke et al., 2014). Each clathrin triskelion consists of three heavy and three light chains. AP-2 and accessory proteins bind to the N-terminal domain (TD) of the clathrin heavy chain, which harbors an interaction hub for clathrin ligands (Schmid and McMahon, 2007). AP-2 and accessory proteins recruit clathrin triskelia to the plasma membrane, where clathrin polymerizes into a lattice of hexagons and pentagons around the pit and thereby further stabilizes the membrane curvature (McMahon and Gallop, 2005).

Scission: The GTPase dynamin is recruited to pits through interactions with a number of proteins, including amphiphysin, endophilin and intersectin (Haucke et al., 2011). Dynamin forms helices around the neck of invaginated clathrin-coated pits. GTP hydrolysis provides the energy for conformational changes in dynamin, which lead to membrane fission (Ferguson and De Camilli, 2012). Interfering with dynamin has severe effects on endocytosis, as

demonstrated by the *Drosophila* temperature-sensitive dynamin mutant shibire^{ts}, where the acute endocytic block at non-permissive temperature completely abolishes SV endocytosis. In mammalian neurons, only the dynamin 2 isoform is implicated in CME (Kononenko et al., 2014).

Uncoating: After fission, newly formed SVs are rapidly uncoated. This allows for the reuse of endocytic proteins and for membrane fusion. Clathrin lattice disassembly from the vesicle is promoted by the ATPase heat shock cognate 70 (HSC70; Schlossman et al., 1984) and its cofactor auxillin (Ungewickell et al., 1995). Uncoating requires the endophilin dependent recruitment of synaptojanin, a phosphatase that hydrolyzes PI(4,5)P_2. This is likely to be important for auxillin recruitment or for the release of adaptor proteins from the vesicle (Cremona et al., 1999; Milosevic et al., 2011; McMahon and Boucrot, 2011). It is currently under debate, if newly endocytosed SVs, after uncoating, fuse with synaptic endosomes for further sorting or if they are directly refilled with neurotransmitter for the next round of exocytosis (Rizzoli, 2014).

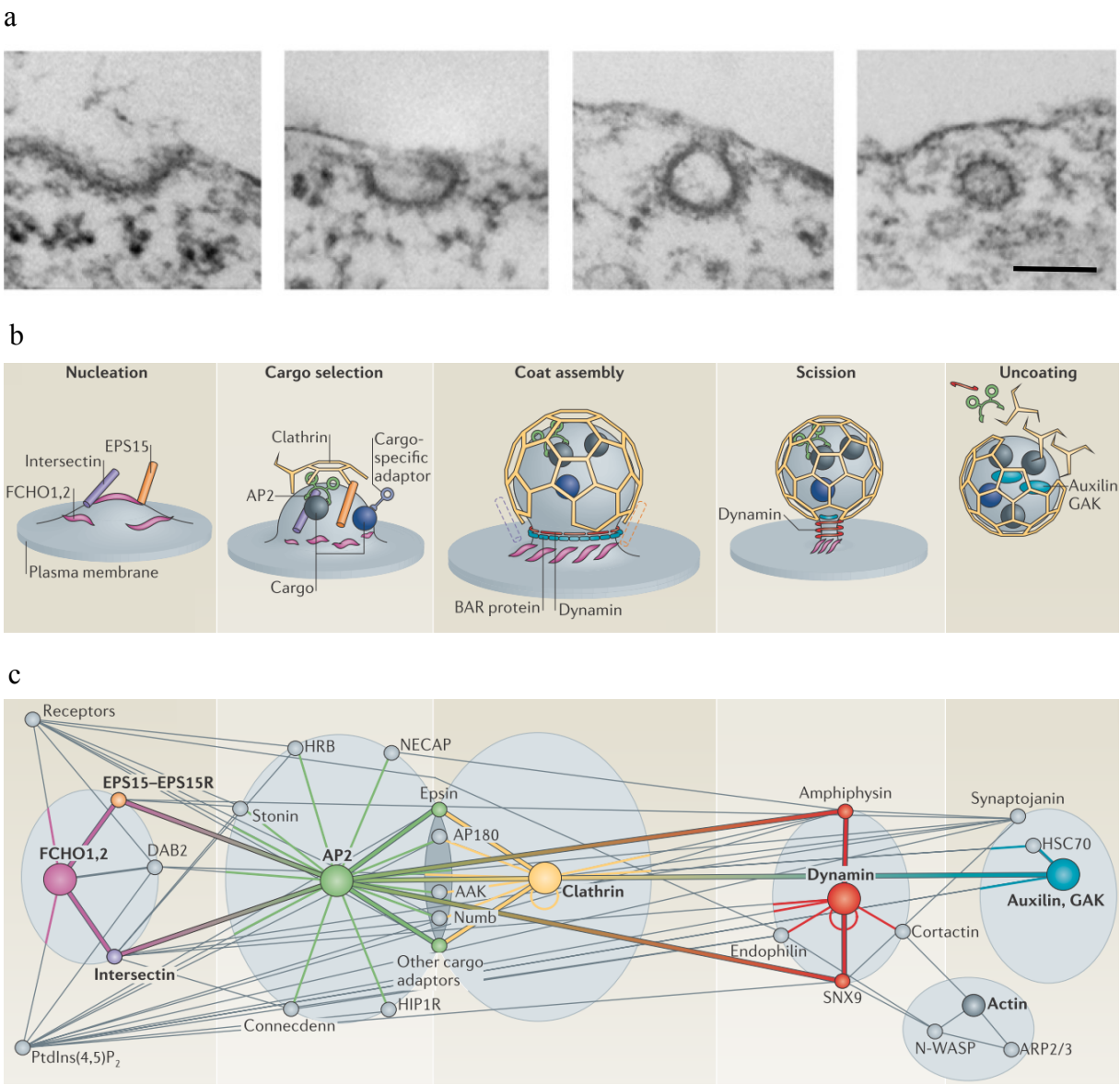

Figure 1-5: Clathrin-mediated endocytosis.

(a) Electron micrographs of different stages of clathrin-coated structures at the plasma membrane of Cos7 cells. Electron micrographs were arranged in the following order: shallow-, non-constricted, constricted clathrin-coated pits, clathrin-coated vesicles. Scale bar, 200 nm. Taken from von Kleist et al., 2011. **(b)** Temporal progression of clathrin-mediated endocytosis. CME can be devided into five major stages, although the precise timing is not known. Each stage requires a distinct set of proteins for pit maturation. **(c)** The clathrin network. Several protein-protein interactions are required for CME. Obviously different major hubs exist, which interact with several proteins that are required for CME. The hubs act at different stages of pit maturation (compare to b). Taken from McMahon and Boucrot, 2011.

1.5.3 AP180 and CALM

Neuron-specific AP180 (Puszkin et al., 1992; Zhou et al., 1992) and its ubiquitously expressed homolog CALM (clathrin assembly lymphoid myeloid leukemia; Dreyling et al., 1996) are recruited to PI(4,5)P_2-rich membrane sites via their N-terminal AP180 N-terminal homology (ANTH) domains (Ford et al., 2001). The C-terminal regions of both proteins harbors a binding-motif for clathrin and AP-2 binding (Traub, 2005), indicating the role of AP180 and CALM in clathrin recruitment to PI(4,5)P_2-rich spots in the plasma membrane. This mechanism is supported by the fact, that AP180 is able to generate flat clathrin lattices *in vitro* (Ahle and Ungewickell, 1986) and together with AP-2 induces curved clathrin-coated pits on lipid monolayers (Ford et al., 2001).

ANTH domains of AP180 and CALM were shown to directly interact with the SNARE motif of Syb2 (Koo et al., 2011a), a protein without typical endocytic sorting motifs (Traub, 2005). The mutation of methionine 46, within the SNARE motif of Syb2, to alanine (M46A) results in the major mis-localization of Syb2 to the plasma membrane in neuroendocrine cells and hippocampal neurons (Grote and Kelly, 1996; Bushlin et al., 2008; Koo et al., 2011a), indicating the function of both AP180 and CALM as Syb2 specific sorting adaptors (Koo et al., 2011b; Maritzen et al., 2012). In line with that, a knockdown of either of them in hippocampal neurons results in increased surface levels of Syb2, but not of VGLUT1. The effect is additive and thus the surface accumulations even more drastic in AP180 / CALM double-knockdown neurons (Koo et al., 2011a).

1.5.4 Presynaptic endocytic zones

Presynapses are spatially highly organized. While SVs fuse with the plasma membrane at active zones, which harbor the molecular machinery for SV docking and fusion (Südhof, 2004), compensatory endocytosis takes place in the periphery of active zones. This becomes obvious from dye uptake experiments, where loaded, and thus recently endocytosed, SVs were found in close lateral proximity to active zones (Teng and Wilkinson, 2000). In addition, clathrin-coated pits were mainly observed in the periphery of active zones (Figure 1-6; Heuser and Reese, 1973; Brodin et al., 2000). In agreement with endocytic zones adjacent to active zones, these so-called periactive zones (PAZ) exhibit a strong enrichment in actin (Bloom et

al., 2003) and endocytic proteins like dynamin, intersectin, endophilin, Eps15, amphiphysin, syndapin and calcineurin (Roos and Kelly, 1999; Koh et al., 2007; Sundborger et al., 2011; Sakaba et al., 2013; Wahl et al., 2013). Endocytic sites are not defined by cargo. This is evident from experiments with the *Drosophila* temperature-sensitive dynamin mutant shibire^{ts}, where the acute endocytic block at non-permissive temperature led to a redistribution of cargo molecules but not of the intersectin ortholog Dap160 (dynamin associated protein 160; Roos and Kelly, 1999). Instead, the large multidomain proteins intersectin and Eps15 were suggested to act as large scaffolds that organize endocytic proteins within the periactive zone (Koh et al., 2004; Marie et al., 2004; Haucke et al., 2011).

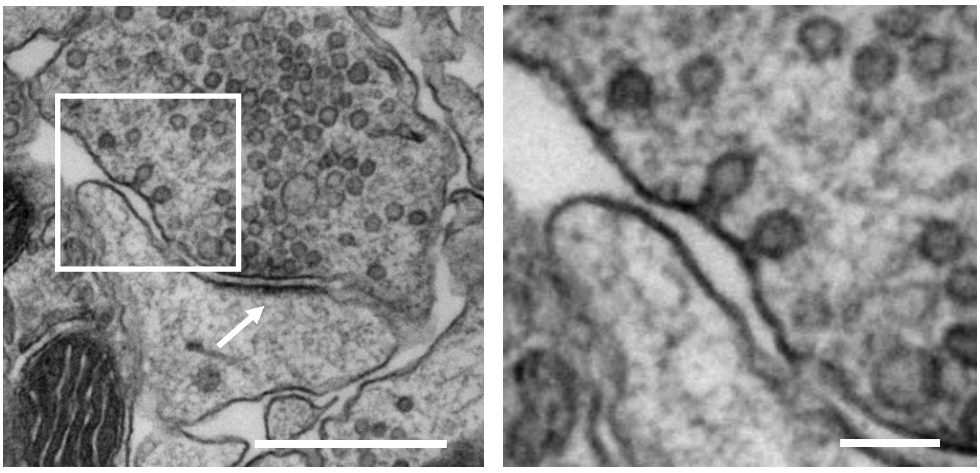

Figure 1-6: Clathrin-mediated endocytosis at the periactive zone.
Electron micrograph of a synapse of cultured murine hippocampal neurons upon electrical stimulation (200 APs, 5Hz). Note the clathrin-coated pits (white box and zoom) in the vicinity to an active zone, which is indicated by docked SVs opposing to the postsynaptic density (white arrow). Scale bar, 500 nm, zoom 100 nm. Provided by Dr. Puchkov (FMP Berlin, Germany).

1.6 Synaptic vesicle identity during cycling

Although the molecular machinery that achieves SV proteins sorting is well characterized (Jung and Haucke, 2007; Haucke et al., 2011; Rizzoli, 2014) it remains unknown, if SV proteins are sorted independently or if they remain assembled as distinct patches that preserve their identity during SV cycling (Figure 1-7). Upon moderate electrical stimulation, newly exocytosed SV proteins and the subsequently endocytosed RRetP of SV

proteins are not identical (Fernández-Alfonso et al., 2006; Hua et al., 2011; Wienisch and Klingauf, 2006). However, upon stimulation trains that exceed the capacity of the RRetP (~70 APs, 20 Hz; Hua et al., 2011), the RRetP and newly exocytosed SV proteins are endocytosed together (Fernández-Alfonso et al., 2006; Wienisch and Klingauf, 2006). Still, from these experiments it is not clear, whether SV proteins have mixed upon fusion or if the RRetP and newly exocytosed proteins were simply internalized simultaneously, but into different vesicles.

Super-resolution images from SV protein clusters in the presynaptic plasma membrane (Willig et al., 2006; Opazo et al., 2010; Hua et al., 2011) suggest that endocytic patches are preassembled well before endocytosis. However, newly exocytosed SVs could diffuse independently and reassemble into mixed clusters in the plasma membrane, which are then ready for endocytosis. More direct evidence for SVs that keep their identity during recycling comes from stimulated emission depletion (STED) images of thin sections from hippocampal neurons. Successive Syt1 labeling of different SV subsets revealed a low correlation of both labels, indicating that SVs, that were labeled in the first round did not interchange Syt1 with unlabeled SVs and thus could not be labeled in the second round (Opazo et al., 2010). However, the resolution of the STED images was insufficient to distinguish single vesicles, and the technique may thus be not accurate enough to fully prove preserved SV identity.

The stability of SV patches, no matter if newly formed or preserved upon SV fusion, may be promoted by various interactions between SV proteins with each other (Bennett et al., 1992) and with lipids (e. g. Syt1 and Syp, but not Syb2, bind to cholesterol, Thiele et al., 2000). The hypothesis of SV clustering by interactions between SV proteins is supported by the fact that the knockout of SV proteins often results in a generally slowed SV retrieval (e. g. Syb 2 knockou: Deák et al., 2004; Xu et al., 2013 / Syp knockout: Gordon et al., 2011; Kwon and Chapman, 2011 / Syt1 KO: Nicholson-Tomishima and Ryan, 2004). Evidence for a function of lipids in SV protein clustering comes from experiments with the *Drosophila* temperature-sensitive dynamin mutant shibire^{ts}. Upon acute block of endocytosis at non-permissive temperature and electrical stimulation, shibire^{ts} mutants displayed Syt1 and VGLUT clusters at the presynaptic plasma membrane of neuromuscular junctions. Syt1 clusters dissolved under cholesterol extraction. Similar results were also observed upon reduction of filamentous actin by latrunculin A (Dason et al., 2013), suggesting an

involvement of cytoskeletal elements in cluster establishment or preservation. However, likely due to fast kinetics, no convincing evidence for or against patch diffusion exists.

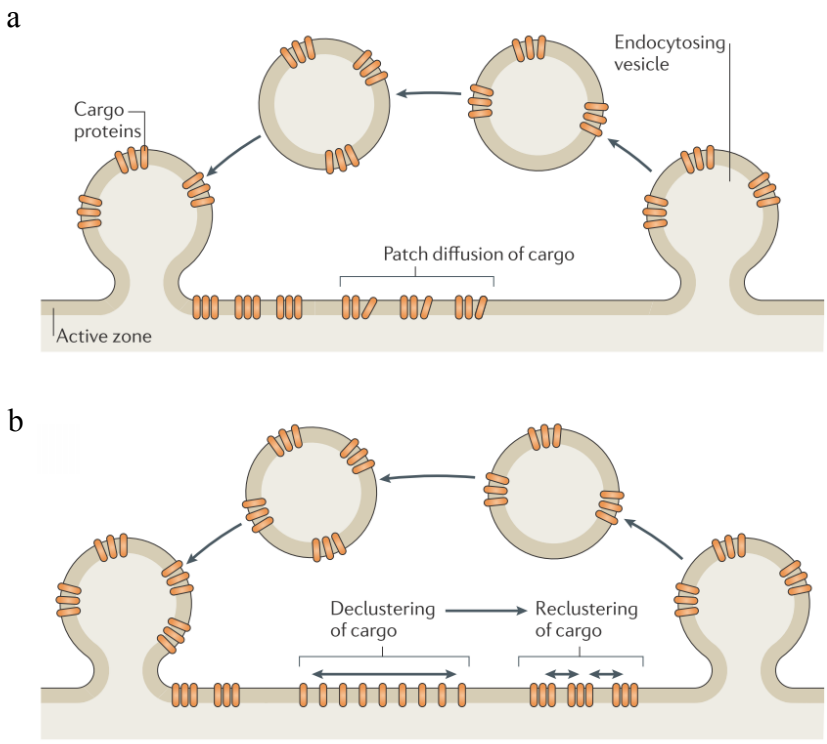

Figure 1-7: Models of SV protein movement.

(a, b) Upon exocytosis at active zones, SV proteins become part of the plasma membrane. Newly exocytosed proteins may be actively transported or diffuse passively towards the periactive zone, where they are retrieved. **(a)** The transport or diffusion of SV proteins as patches would eliminate the need for a post-exocytic sorting of single SV proteins. **(b)** A second way would be that SV proteins decluster, diffuse independently and reassemble into clusters within the plasma membrane before endocytosis. Note that declustering may lead to the intermixing of proteins from different SVs and to the intermixing of newly exocytosed SV proteins with pre-existing surface-stranded proteins that were not retrieved during the last round of endocytosis. Taken from Haucke et al., 2011.

1.7 Axonal dispersion of synaptic vesicle proteins

Stable patches may prevent newly exocytosed SV proteins from escaping into the axon. However, some studies reported that the SV proteins Syb2, Syp and Syt1 (tagged with pHluorin or non-quenchable probes), diffuse into the axon upon strong electrical stimulation (Fernández-Alfonso et al., 2006; Granseth et al., 2006; Li and Murthy, 2001; Opazo et al.,

2010; Sankaranarayanan and Ryan, 2000; Wienisch and Klingauf, 2006). However, controversial data was reported for stimulation trains within the capacity of the RRetP. Electrical stimulation either induced SV protein diffusion into the axon (Syp-mRFP: Granseth et al., 2006; Syb2-pH: Sankaranarayanan and Ryan, 2000) or no dispersion at all (Syt1: Opazo et al., 2010). Granseth et al. and Opazo et al. performed their experiments with unquenchable probes. This makes the experiments sensitive to vesicular movement. In contrast, Sankaranarayanan and Ryan addressed a combined movement of a pHluorin-tagged plasma membrane pool together with newly exocytosed proteins. A spatiotemporal characterization of newly exocytosed SV protein movements could not be investigated.

1.8 Release site clearance

Synapses often show a rapid deceleration of synaptic responses, particularly under high-frequency stimulation. This STD (short-term synaptic depression) usually reaches its maximum after 10 – 20 stimuli and was believed to be due to the availability of SVs, which is limited by the maximal rate of endocytosis. However, recent findings rather suggest that the availability of release sites may be the rate-limiting step causing STD (Neher, 2010).

Interestingly, a number of studies found an increased STD upon perturbation of the endocytic machinery. For example, STD is enhanced in the *Drosophila* temperature-sensitive dynamin mutant shibire^{ts} upon endocytic block at non-permissive temperature (Kawasaki et al., 2000). In line with that, a depression of neurotransmission was observed in the lamprey reticulospinal synapse after blocking the interaction of dynamin with SH3 domains by an injection of the amphiphysin SH3 domain or a dynamin peptide containing the SH3 binding site (Shupliakov et al., 1997). The same peptide was later found to similarly enhance STD in the calyx of held. Likewise, the dynamin inhibitor Dynasore, dynamin antibodies, a peptide that blocks the amphiphysin-AP-2 interaction, sequestration of AP-2 by the C2B domain of synaptotagmin (Hosoi et al., 2009) or depletion of intersectin (Sakaba et al., 2013) enhance STD. In agreement with a role of the clathrin-based endocytic machinery to preventing STD, Hua et al. found, through a pHluorin based assay, that dynamin inhibition by dynasore and clathrin inhibition by Pitstop 2 increase STD in hippocampal neurons. By the deconvolution of exo- and endocytic signals from pHluorin experiments, they demonstrated that STD is induced in the absence of SV reuse (Hua et al., 2013). This finding is in agreement with the

fact that STD develops so rapidly, that it cannot be caused by a depletion of the releasable pool of SVs. Rather, the removal of endocytic intermediates from release sites may be the rate-limiting step upon high-frequency stimulation and upon the disruption of the endocytic machinery (Neher, 2010; Haucke et al., 2011). In intact synapses, release site clearance may be achieved by a lateral diffusion or active transport to endocytic sites in the PAZ. Cytoskeletal elements may provide directionality (Haucke et al., 2011). Whether these proposed mechanisms, active transport or diffusion from the active- to the periactive zone, take place could be addressed with an assay that provides quantitative information about the dynamics of newly exocytosed SV proteins.

2 Aims of this study

The initial aim of this study was to develop an assay that allows to spatiotemporally describe the fate of newly exocytosed SV proteins in hippocampal neurons. This assay should then be used to investigate how released proteins distribute sub-synaptically and to which extent they escape into the axon. One aim was to examine, whether SV proteins, after exocytosis, remain at release sites, diffuse away or if they are actively transported. Another aim was to identify molecular mechanisms or structures that modulate post-exocytic SV protein dynamics.

3 Material and Methods

3.1 Material

3.1.1 Chemicals and consumables

If not indicated differently, chemicals were purchased from Carl Roth (Germany), Life Technologies (USA), Merck (Germany), Sigma-Aldrich (USA) and Thermo Fisher (USA). Disposables were obtained from B. Braun (Germany), Biozym (Germany), GE Healthcare (UK), Greiner (Germany), Millipore (USA), Sarstedt (Germany) and Schott (Germany).

3.1.2 Enzymes

Table 3-1: Enzymes

Enzyme	Source
Calf intestine alkaline phosphatase	New England BioLabs (USA)
DreamTaq DNA Polymerase	Thermo Fisher (USA)
FastDigest restriction enzymes	Thermo Fisher (USA)
Pfu DNA Polymerase	Thermo Fisher (USA)
T4 DNA Ligase	Thermo Fisher (USA)
TEV Protease	Home-made, recombinant - see chapter 3.3.2

3.1.3 Kits

Table 3-2: Kits

Kit	Supplier
Nap-5 Sephadex G-25 column	GE Healthcare (UK)
Nucleo Spin Extract II	Macherey-Nagel (Germany)
NucleoBond Xtra Midi EF	Macherey-Nagel (Germany)
NucleoSpin Plasmid	Macherey-Nagel (Germany)
ProFection	Promega (USA)

3.1.4 Buffers, media and solutions

Buffers, media and solutions were prepared with deionized water (ddH_2O; Millipore, USA). When required, solutions were autoclaved for 20 min (121 °C, 1 bar) or sterile filtered with a pore size of 0,2 µm. The pH was adjusted with HCl or NaOH.

Table 3-3: Buffers, media and solutions.

Buffer	Ingredients
Ampicillin, 500 x	50 mg / ml in ddH_2O, sterile filtered
Kanamycin, 200 x	10 mg / ml in ddH_2O, sterile filtered
DNA loading buffer, 6 x	0.25 % (v / v) bromphenol blue 0.25 % (v / v) xylen cyanol 60 % (v / v) glycerol
Ethidium bromide, 3,000 x	10 mg / ml in ddH_2O

Buffer	Ingredients
Fixative	4 % (w / v) PFA 4 % (w / v) sucrose 1 x PBS, pH 7.5
Goat serum dilution buffer (GSDB)	30 % (v / v) goat serum 385 mM NaCl 15 mM sodium phosphate buffer, pH 7.4
Goat serum dilution buffer + Triton-X 100	0.23 % Triton-X 100 GSDB
HEPES-buffered saline, 2 ×	16.4 g / l NaCl 11.9 g / l HEPES 0.21 g / l Na_2HPO_4 pH 7.1
Hippocampal neuron culture: Basic medium	1 x MEM (Minimum Essential Media; Life Technologies, USA) 5 g / l glucose 200 ml / l $NaHCO_3$ 100 mg / l Transferrin (Merck, Germany)
Hippocampal neuron culture: Plating medium	1 x Basic medium 10 % (v / v) FCS (Biochrom, Germany) 2 mM L-glutamine (Lonza, Switzerland) 25 mg / ml insulin 50 U / ml penicillin 50 µg / ml streptomycin
Hippocampal neuron culture: Growth medium	1 x Basic medium 5 % (v / v) FCS (Biochrom, Germany) 0.5 mM L-glutamine (Lonza, Switzerland) 2 % (v / v) B27-supplement (Life Technologies, USA) 50 U / ml penicillin 50 µg / ml streptomycin

Buffer	Ingredients
Hippocampal neuron culture: Digestion solution	25 mM HEPES, pH 7.4 137 mM NaCl 5 mM KCl 7 mM Na_2HPO_4
Hippocampal neuron culture: Dissociation solution	1 x HBSS (Hank's Balanced Salt Solution; Life Technologies, USA) 12 mM $MgSO_4$
pHluorin imaging: Imaging stock solution, 10 x	1.2 M NaCl 35 mM KCl 40 mM KH_2PO_4 200 mM TES 50 mM $NaHCO_3$ 50 mM glucose 12 mM Na_2SO_4 pH 7.4
pHluorin imaging: Imaging buffer, 1 x	50 mM NaCl 1.2 mM $MgCl_2$ 1.3 mM $CaCl_2$ Imaging stock solution 1 x
pHluorin imaging: Basic buffer, 1 x	50 mM NH_4Cl 1.2 mM $MgCl_2$ 1.3 mM $CaCl_2$ Imaging stock solution 1 x
pHluorin imaging: Acidic stock solution, 10 x	1.2 M NaCl 35 mM KCl 40 mM KH2PO4 200 mM MES 50 mM NaHCO3 50 mM glucose 12 mM Na2SO4 pH 5.5

Buffer	Ingredients
pHluorin imaging: Acidic buffer, 1 x	50 mM NaCl 1.2 mM $MgCl_2$ 1.3 mM $CaCl_2$ Acidic stock solution 1 x
Tail lysis buffer	100 mM Tris, pH 8.5 5 mM NaEDTA 0.2 % SDS 200 mM NaCl
2 x YT medium	1.0 % (w / v) yeast extract 1.6 % (w / v) tryptone 0.5 % (w / v) NaCl pH 7.4
LB medium	1.0 % (w / v) yeast extract 0.5 % (w / v) tryptone 0.5 % (w / v) NaCl pH 7.2
LB plates	LB medium 15 g / l agar-agar
PBS 10 x	1.37 M NaCl 27 mM KCl 43 mM Na 2 HPO 4 14 mM NaH 2 PO 4 pH 7.4
Sodium phosphate buffer, 1 M	pH — 1 M Na_2HPO_4 — 1 M NaH_2PO_4 6 — 12 ml — 88 ml 6.4 — 25.5 ml — 74.5 ml 6.8 — 46.3 ml — 53.7 ml 7 — 57.7 ml — 42.3 ml 7.2 — 68.4 ml — 31.6 ml 7.4 — 77.4 ml — 22.6 ml 7.6 — 84.5 ml — 15.5 ml 7.8 — 89.6 ml — 10.4 ml

Buffer	Ingredients
TBE, 10 x	0.89 M Tris, pH 8.0 0.89 M boric acid 0.02 M EDTA
Bacteria lysis buffer	50 mM Tris, pH 7.5 150 mM NaCl 10 mM imidazole 2 mM DTT
Protein storage buffer	20 mM Tris, pH 7.5 150 mM NaCl 20 % glycerol (w / v) 2 mM DTT
Mouse brain tissue extract: Tissue lysis buffer	20 mM HEPES, pH 7.4 100 mM KCl 2 mM MgCl2 1 mM PMSF 1 % (v / v) Triton-X100 3 % (v / v) mammalian protease inhibitor cocktail (Sigma-Aldrich, USA)

3.1.5 Primary antibodies

The following primary antibodies were used for immunocytochemistry and immunoblotting:

Table 3-4: Primary antibodies. a: alpaca; gp: guinea pig; gt: goat; m: mouse; rb: rabbit; CC: custom conjugation with fluorescent dyes (see chapter 3.3.1); IB: immunoblotting; IC: immunocytochemistry; SySy: Synaptic Systems.

Antigen	Host	Product number / clone	Dilution	Source
AP180	rb	155003	IC, 1 : 100 IB, 1 : 1000	SySy (Germany)
Bassoon	gp	141004	IC, 1 : 500	SySy (Germany)
CALM	gt	sc-6433	IC, 1 : 100	Santa Cruz (USA)
Clathrin HC	rb	ab21679	IC, 1 : 400	Abcam (UK)
c-myc	m	9E10	IC, 1 : 1000	Hybridoma cell line
GFP / pHluorin	rb	ab6556	IC, 1 : 1000	Abcam (UK)
GFP / pHluorin	a	gt-250	CC	ChromoTek (Germany)
Hsc70	m	MA3006	IB, 1 : 5000	Affinity Bioreagents (USA)
Synaptotagmin1	rb	105102	IC, 1 : 500	SySy (Germany)
Synaptophysin	m	101011	IC, 1 : 400	SySy (Germany)

3.1.6 Secondary antibodies

Fluorophore-conjugated secondary antibodies were used for immunocytochemistry at a dilution of 1 : 200 (SIM, confocal and conventional widefield imaging) or 1 : 100 (SD-*d*STORM). Only highly cross-adsorbed secondary antibodies were used in order to minimize cross-reactivity with other antibody species. Horseradish peroxidase conjugated secondary antibodies were used for immunoblotting at a dilution of 1 : 2500.

Table 3-5: Secondary antibodies. d: donkey; gp: guinea pig; gt: goat; m: mouse; rb: rabbit; HRP: Horseradish peroxidase.

Conjugate	Target Species	Host	Company
Alexa 488	gt	d	Life Technologies (USA)
Alexa 488	gp	gt	Life Technologies (USA)
Alexa 488	m	gt	Life Technologies (USA)
Alexa 488	rb	gt	Life Technologies (USA)
Alexa 568	m	gt	Life Technologies (USA)
Alexa 568	rb	gt	Life Technologies (USA)
Alexa 647	gp	gt	Life Technologies (USA)
Alexa 647	m	gt	Life Technologies (USA)
Alexa 647	rb	gt	Life Technologies (USA)
CF 680	rb	gt	Biotium (USA)
CF 680	m	gt	Biotium (USA)
HRP	rb	gt	Jackson ImmunoResearch (USA)
HRP	m	gt	Jackson ImmunoResearch (USA)

3.1.7 Plasmids

The following plasmids were used for the expression of recombinant proteins or shRNA mediated knock down in hippocampal neurons.

Table 3-6: Plasmid backbones. CMV : cytomegalovirus; kan : kanamycin; amp : ampicillin; neo : neomycin; hygro : hygromycin.

Plasmid	Description	Origin / Publication
pmCherry-N1	Mammalian expression vector for fusion proteins with mCherry, CMV promoter, resistance genes: kan / neo	Clontech (France)
pcDNA3	Mammalian expression vector, CMV promoter, resistance genes: kan / neo	Invitrogen (USA)
pcDNA5/FRT/TO	Mammalian expression vector for the generation of stable cell lines or transient expression, CMV promoter, resistance genes: amp / hygro	Invitrogen (USA)
pEGFP-N1	Mammalian expression vector for fusion proteins with EGFP	Clontech (France)
pFUGW	Mammalian expression vector, CMV promoter, resistance genes: amp	Lois et al., 2002

Table 3-7: DNA constructs for the expression of recombinant proteins. AA: amino acids; f. l.: full length protein; WT: wild type; pH: pHluorin; TEV: Tobacco Etch Virus protease cleavage site; pub: published

Construct	Species	AA	Mutation	Tag	Vector	Comment
AP180 Mutant	rat	f. l.	L219S / M244K	-	pcDNA3	pub.: (Koo et al., 2015)
AP180WT	rat	f. l.	WT	-	pcDNA3	pub.: (Koo et al., 2015)
CLC–EGFP (clathrin light chain)	rat	f. l.	WT	EGFP	pcDNA3	pub.: Posor et al., 2015
CLC–mRFP (clathrin light chain)	rat	f. l.	WT	mRFP	pcDNA5/FRT/TO	designed by Kira Brune
Lifeact-EGFP (Actin-binding protein Abp140)	yeast	1-17	WT	EGFP	pEGFP-N1	pub.: Riedl et al., 2008
Munc13-1-mCherry (Munc13-1)	rat	f. l.	WT	mCherry	pmCherry-N1	derived from Munc13-1-EFGP (Stevens et al., 2005)
Syb2_M46A-pH (Synaptobrevin2)	rat	1-116	M46A	pH, TEV	pcDNA3, modified	derived from Syb2-pH
Syb2-Myc (Synaptobrevin2)	rat	1-116	WT	Myc, TEV	pcDNA3, modified	derived from Syb2-pH
Syb2-pH (Synaptobrevin2)	rat	1-116	WT	pH, TEV	pcDNA3, modified	pub.: Wienisch et al., 2006
Syp-pH (Synaptophysin)	rat	f. l.	WT	pH	pcDNA3, modified	pub.: Granseth et al., 2006
Syt1-pH (Synaptotagmin1)	rat	f. l.	WT	pH, TEV	pcDNA3, modified	pub.: Wienisch et al., 2006

Table 3-8: DNA constructs coding for shRNAs. m: mouse; rt: rat.

Construct	Target mRNA	Sequence 5' → 3'	Vector	Comment
CALM_sh	CALM (m / rt)	GGA AAU GGA ACC ACU AAG A (Bushlin et al., 2008)	pFUGW, modified	co-expressing mKate; pub.: Koo et al., 2015
Scrambled_sh	none	ACA ACG AGC UUC CCU UCA A (Bushlin et al., 2008)	pFUGW, modified	co-expressing mKate; pub.: Koo et al., 2015

3.1.8 DNA oligonucleotides

Synthetic DNA oligonucleotides were used for polymerase chain reactions (PCR), for cloning, sequencing and genotyping. All DNA oligonucleotides were designed with the sequence editor ApE (W. Davis, University of Utah) and purchased from MWG Biotech (Germany) or BioTeZ (Germany).

Table 3-9: DNA oligonucleotides for cloning, sequencing and genotyping. Names were given the following way: amplificate _ introduced tag or restriction site _ forward or reverse _ PCR #1 or PCR #2.

Name	Sequence 5' → 3'	Application
Syb2_BamHI_Fw1	CAA TTC ACG CGT GCC ACC ATG TCG GCT ACC GCT G	Cloning: Syb2_M46A-pH & Syb2_Myc
Syb2_BamHI_Fw2	CTC GGA TCC CAA TTC ACG CGT GCC ACC ATG TCG G	Cloning: Syb2_M46A-pH & Syb2_Myc
Syb2_EcoRV_Rev1	CCC CGC CGC TTC CGC CGC TAG TGC TGA AGT AAA C	Cloning: Syb2_M46A-pH
Syb2_EcoRV_Rev2	CGG GAT ATC GTA GTC CCC GCC GCT TCC GCC GCT A	Cloning: Syb2_M46A-pH

Name	Sequence 5' → 3'	Application
Syb2_c-Myc-MfeI_Rev1	CAG AAA TAA GTT TTT GTT CCA TGT CAG CAT CAA C	Cloning: Syb2_Myc
Syb2_c-Myc-MfeI_Rev1	GAG CAA TTG TTA CAG ATC TTC TTC AGA AAT AAG T	Cloning: Syb2_Myc
CMV_Fw	CAA CGG GAC TTT CCA AAA TG	Sequencing: CMV promoter
EGFP_Rev	CGT CGC CGT CCA GCT CGA CCA G	Sequencing: EGFP
pHluorin_Fw	AAG ATG ACG GGA ACT ACA AG	Sequencing: pHluorin
pHluorin_Rev	GCC TCC ATC TTC ATG TTG TG	Sequencing: pHluorin
AP180WT_Fw	ACC TCA TGT GAA ACG	Genotyping: AP180 WT mice
AP180WT_Rev	TCT GGT GGA TAG TGT CAC TTA GGT A	Genotyping: AP180 WT mice
AP180KO_Fw	CCA GAT GAC CTG AGT TTG T	Genotyping: AP180 KO mice
AP180KO_Rev	TCT GGT GGA TAG TGT CAC TTA GGT A	Genotyping: AP180 KO mice

3.1.9 Bacterial strains

The *E. coli* strain TOP10 (Invitrogen, USA) was used for cloning, amplification of plasmid DNA and for the preservation of plasmids in bacterial glycerol stocks. The *E. coli* strain Rosetta 2 was used for the expression of TEV protease.

3.1.10 Filtersets

The following filtersets were used with epifluorescence microscopes and the SD-*d*STORM setup:

Table 3-10: Filtersets for fluorescence microscopy, all filters were purchased from AHF Analysentechnik.

Name	Excitation Filter	Emission Filter	Dichroic mirror
Cy5 ET Filterset	F49-641: 640 / 30 ET Bandpass	F47-690: 690 / 50 ET Bandpass	F48-660: Dichroic mirror T 660 LPXR
DAPI ET Filterset	F34-000: 350 / 50 AT Bandpass	F47-460: 460 / 50 ET Bandpass	F79-100: Dichroic mirror T 400 LP
EGFP ET Filterset	F49-470: 470 / 40 ET Bandpass	F47-525: 525 / 50 ET Bandpass	F48-495: Dichroic mirror T 495 LPXR
SD-*d*STORM	-	F76-635: 635 LP Edge Basic (allows only *d*STORM dyes emission)	F43-713: Dichroic mirror 700 DCXXR (in Opto Split II); Dichroic mirror Di01-R405 / 488 / 561 / 635-25x36 (for laser reflection)
TRITC HC Filterset	F39-525: 543 / 22 BrightLine HC	F37-593: 593 / 40 BrightLine HC	F38-562: Dichroic mirror HC BS 562
TxRed HC Filterset	F39-562: 562 / 40 BrightLine HC	F37-624: 624 / 40 BrightLine HC	F38-593: Dichroic mirror HC BS 593

3.1.11 Software and web applications

Table 3-11: Software and web applications

Name	Company / Author
Acrobat X Pro 10.1.1	Adobe Systems, USA
ApE , A plasmid Editor	W. Davis, University of Utah *http://biologylabs.utah.edu/jorgensen/wayned/ape/*
BioMath Calculator	Promega, *http://www.promega.com/techserv/tools/biomath/calc11.htm*
ExPASy, Expert Protein Analysis System	Swiss Institute of Bioinformatics *http://web.expasy.org*
Fiji	Schindelin et al., 2012 *http://fiji.sc/Fiji*
IGOR Pro 6.32	WaveMetrics, USA
Illustrator CS6	Adobe Systems, USA
ImageJ 1.4.8	W. Rasband, National Institute of Mental Health Schneider et al., 2012 *http://imagej.nih.gov/ij/*
MicroManager 4.11	Stuurman et al., 2010 *https://www.micro-manager.org/*
NCBI databases	National Center for Biotechnology Information *http://www.ncbi.nlm.nih.gov/*
Office, Excel	Microsoft, USA
Office, Word	Microsoft, USA
OriginPro 8.5	OriginLab Corp., USA
Photoshop CS6	Adobe Systems, USA
Prism 5.04	GraphPad Software Inc., USA

Name	Company / Author
Python 2.7	Python Software Foundation, USA
R 3.1.3	R Development Core Team, R Foundation for Statistical Computing *https://CRAN.R-project.org/*
rapidSTORM 3.1.1	Steve Wolter, Universität Würzburg Wolter et al., 2012 *http://www.super-resolution.biozentrum.uni-wuerzburg.de/research_topics/rapidstorm/*
SDmixer	A. Lampe and G. Tadeus, FMP Berlin (Lampe et al., 2015; Tadeus et al., 2015) http://sourceforge.net/projects/sdmixer/

3.2 Molecular Biology Methods

3.2.1 Cloning strategies

Cloning strategies were planned with the plasmid editor ApE (W. Davis, University of Utah). Primer sequences with mutations, restriction sites or genetically encoded polypeptide tags (Table 3-9) were purchased from MWG Biotech (Germany) or BioTeZ (Germany). The template DNA was then amplified by polymerase chain reaction. PCR product and the target vector were digested with the specific restriction enzymes, purified, ligated and transformed into chemically competent *E. coli*. Colonies were screened for positive clones by colony PCR and plasmid sequences were validated by sequencing.

3.2.2 Polymerase Chain Reaction

Polymerase chain reaction (PCR) was used to amplify DNA fragments for site-directed mutagenesis, genotyping and screening of *E. coli* colonies after ligation and transformation (colony-PCR). For cloning, PCRs were performed with Pfu DNA Polymerase (Thermo Fisher, USA). DreamTaq DNA Polymerase (Thermo Fisher, USA) was used for colony-PCRs and genotyping. The DNA samples were amplified in a thermocycler, running the following protocols:

PCR for cloning:

Table 3-12: Cloning PCR reaction.

Pfu Buffer	1x
dNTPs	200 µM of each
Forward primer	1 µM
Reverse primer	1 µM
Template DNA	10 ng / µl
Pfu DNA Polymerase	0.05 U / µl
ddH2O	50 µl

Table 3-13: Cloning PCR cycle. Tm: Calculated melting temperature of primer and template.

Step	Temperature	Time	Cycles
Initial denaturation	95 °C	2 min	1
Denaturation	95 °C	30 s	
Annealing	Tm – 5 °C	30 s	35
Extension	73 °C	2min / kb	
Final extension	73 °C	5 min	1

Colony PCR:

For colony PCR, single colonies were picked and grown in 100 µl LB-medium and the appropriate antibiotic at 37 °C for 2h on a shaker. 1 µl of the culture was used as a PCR template.

Table 3-14: Colony PCR reaction.

DreamTaq Buffer	1x
dNTPs	200 µM of each
Forward primer	0.5 µM
Reverse primer	0.5 µM
Template (*E. coli* culture)	1 µl
DreamTaq DNA Polymerase	0.5 U
ddH_2O	20 µl

Table 3-15: Colony PCR cycle. Tm: Calculated melting temperature of primer and template.

Step	Temperature	Time	Cycles
Initial denaturation	95 °C	30 s	1
Denaturation	95 °C	30 s	
Annealing	Tm – 5 °C	30 s	25
Extension	72 °C	1 min / kb	
Final extension	72 °C	5 min	1

Genotyping PCR:

AP180 KO and corresponding WT littermate mice were genotyped, as described by Koo et al. (Koo et al., 2015). Isolated genomic DNA from mouse tail (chapter 3.2.14) was used as a template for genotyping PCRs. Two separate PCR reactions were carried out in order to certainly identify WT and KO mice.

Table 3-16: Genotyping PCR reaction.

DreamTaq Buffer	1x
dNTPs	6 µM of each
Forward primer	50 µM
Reverse primer	50 µM
Template (*E. coli* culture)	1 µl
DreamTaq DNA Polymerase	1 U
ddH2O	20 µl

WT PCR:

Forward primer ACC TCA TGT GAA ACG

Reverse primer TCT GGT GGA TAG TGT CAC TTA GGT A

Table 3-17: Genotyping PCR cycle for WT.

Step	Temperature	Time	Cycles
Initial denaturation	94 °C	3 min	1
Denaturation	94 °C	30 s	
Annealing	55 °C	30 s	30
Extension	72 °C	30 s	
Final extension	72 °C	5 min	1

KO PCR:

Forward primer CCA GAT GAC CTG AGT TTG T

Reverse primer TCT GGT GGA TAG TGT CAC TTA GGT A

Table 3-18: Genotyping PCR cycle for KO.

Step	Temperature	Time	Cycles
Initial denaturation	94 °C	3 min	1
Denaturation	94 °C	30 s	
Annealing	64 °C (-0,5 °C per cycle)	30 s	12
Extension	72 °C	45 s	
Denaturation	94 °C	20 s	
Annealing	58 °C	30 s	25
Extension	72 °C	45 s	
Final extension	72 °C	2 min	1

3.2.3 Agarose Gel Electrophoresis

Agarose gel electrophoresis was used to separate DNA fragment for size analysis or gel extraction. Depending on the size of the DNA fragments, agarose gels were prepared with 0.7 % - 2 % (w / v) agarose in 1 x TBE buffer. DNA samples were loaded with 1x DNA loading buffer and separated by electrophoresis at 100 V in 1 x TBE. Gels were stained in 3 µg / ml ethidium bromide in ddH_2O for 15 min. DNA fragments were visualized with UV-light.

3.2.4 Isolation of DNA from Agarose Gels and PCR

DNA fragments that were further used for cloning were cut out of the agarose gel under minimized UV-exposure and purified with the gel extraction kit Nucleo Spin Extract II from Macherey-Nagel (Germany) according to the manufacturer's instructions. Restriction digested PCR products were isolated with the same protocol.

3.2.5 DNA Restriction Digest

For cloning and for the identification of positive clones after cloning and transformation, plasmid DNA or purified PCR products were digested with FastDigest enzymes (Fermentas, USA) in 1 x FastDigest buffer in a volume of 20 – 30 µl at 37 °C for 3 h. 1 µl FastDigest enzyme was used for the digestion of 1 µg DNA or 0.2 µg PCR product.

3.2.6 Dephosphorylation of vector DNA

To prevent religation, linearized plasmid DNA was 5'-dephosphorylated by adding 10 units of calf intestine alkaline phosphatase (New England BioLabs, USA) to the DNA mix, directly after restriction digest. Dephosphorylation reactions were performed at 37 °C for 5 min.

3.2.7 Ligation of DNA fragments into linearized vectors

Ligation reactions were performed with 1 U T4 DNA Ligase (Thermo Fisher, USA) in 20 µl of 1 x T4 DNA Ligase buffer. 20 - 100 ng of the linearized vector and a 2- to 5-fold molar excess of insert DNA was added to the mix. The ligation reaction was carried out at 16 °C overnight. The ligation-product was directly used to transform competent *E. coli* TOP10.

3.2.8 Preparation of chemically competent E. coli

Chemically competent *E. coli* Top10 were prepared by inoculating 50 ml of LB medium with *E. coli* TOP10 cells from a fresh agar plate. Cells were grown at 37 °C until an optical density of 0.4 was reached at 600 nm. This equals ~ 2 x 10^8 cells / ml. Cells were harvested for 10 min at 2500 x g and 4 °C. After removing the supernatant, cells were resuspended in 10 ml of 0.1 M $CaCl_2$ and incubated on ice for 30 min or up to 3 h. Cells were harvested as described before and resuspended in 2 ml of 0.1 M $CaCl_2$. 50 % glycerol was added to the bacterial suspension to a final concentration of 10 %. 50 µl aliquots were snap-frozen in liquid nitrogen and stored at -80°C.

3.2.9 Transformation of chemically competent E. coli

50µl aliquots of chemically competent *E. coli* Top10 were thawed on ice. Up to 0.2 µg of purified plasmid DNA or 5 µl of a ligation reaction mix was added to the bacteria and incubated on ice for 30 min. Bacteria were heat-shocked at 42 °C for 45 s, kept on ice for 2 min and plated on a LB agar plate, supplemented with the appropriate antibiotic for selection. In the case of a kanamycin resistance, bacteria were incubated with 600 µl pre-warmed LB medium without antibiotics for 20 min at 37°C prior plating. Plates were incubated overnight at 37 °C.

3.2.10 Plasmid DNA purification

Plasmid DNA was prepared with the small-scale kit (mini) NucleoSpin Plasmid (Macherey-Nagel, Germany). Higher amounts of DNA (midi) or high purity DNA, free from

endotoxin was prepared with the kit NucleoBond Xtra Midi EF (Macherey-Nagel, Germany). *E. coli* cultures were inoculated with bacterial colonies from agar plates or with bacteria from glycerol stocks and grown overnight in LB media with the appropriate antibiotic for selection (mini: 5 ml, midi: 100 ml). Plasmid DNA was isolated according to the manufacturer's instructions.

3.2.11 Spectrophotometric determination of DNA concentrations

The concentration of DNA was determined by its absorption at a wavelength of 260 nm. A drop of 1 µl DNA was placed on the Sensor of a NanoDrop 1000 (Thermo Fisher, USA) Spectrophotometer. Concentrations were calculated with use of the Beer-Lambert equation:

DNA concentration:

$$c = \frac{A_{260\,nm}}{\varepsilon_{260\,nm} \cdot b} \qquad (1)$$

c: DNA concentration ; $A_{260\,nm}$: absorbance at 260 nm; $\varepsilon_{260\,nm}$: extinction coefficient of double-stranded DNA at 260 nm (E = 20 $mg^{-1}cm^{-1}ml$; b: path length, 0.01cm for NanoDrop 1000)

3.2.12 DNA Sequencing

Plasmid DNA was purified (mini or midi) and sent in a separate tube with specific sequencing primers to MWG Biotech (Germany) or Source BioScience (Germany), who carried out the sequencing reaction using the chain-termination method (Sanger and Coulson, 1975). Sequencing results were analyzed with the sequence editor ApE (W. Davis, University of Utah).

3.2.13 Glycerol Stocks

For long-term storage, *E. coli* overnight cultures were mixed 1:1 with 50 % (v / v) sterile glycerol and stored at -80 °C.

3.2.14 Isolation of genomic DNA from mouse tail

Genomic DNA for mouse genotyping was isolated from tail biopsies. The tip of a tail was cut with sterilized scissors. Tails were incubated for 1 h in 200 µl tail lysis buffer and 2 µl Proteinase K (800 units / ml, New England BioLabs, USA) on a shaker at 58 °C. Debris was removed by centrifugation (11,000 g, 3 min) and DNA was precipitated from the supernatant by the addition of 200 µl cold isopropanol (- 20 °C). Tubes were inverted before centrifugation (11,000 g, 3 min). The supernatant was removed and the pellet was washed with 200 µl 70 % ethanol. Samples were centrifuged again (11,000 g, 3 min), supernatant was removed and the pellet was dried for 8 min at 55°C. The pellet was then dissolved in 50 µl ddH_2O. DNA was then used for genotyping (chapter 3.2.2).

3.3 Biochemical Methods

3.3.1 Antibody labeling with amine-reactive fluorescent dyes

If not commercially available, secondary antibodies were labeled with the specific fluorophore. Succinimidyl esters of fluorescent Alexa- (Life Technologies, USA) or CF-dyes (Biotium, USA) were coupled to primary amines of antibodies. In order to obtain optimal labeling, reactions were carried out at a five-fold molar excess of amine-reactive fluorescent dyes over the number of antibodies. This typically resulted in a degree of labeling (DOL) of ~2 (two fluorophores bind one antibody). Therefore, 100 µg of the antibody was mixed with 400 µl of $NaHCO_3$ (50 mM, pH 8.1) in a reaction tube. The amine-reactive fluorescent dye was dissolved in DMSO (10 µM) and the required volume was added to the tube. Remaining dye was stored at - 20°C. The mix was incubated in the dark on a rotating wheel for 1 h at room temperature. Unbound dye was removed by running the mix on a Nap-5 Sephadex G-25 column (GE Healthcare, UK). Columns were equilibrated with PBS and the labeling mix was loaded to the column. Labeled antibody was eluted with PBS and fractions of 200 µl were collected.

The absorbance of the antibody at 280 nm and the maximal absorbance of the coupled fluorophore were measured for each fraction with the NanoDrop 1000 (Thermo Fisher, USA). The antibody-concentration and the DOL were determined for each fraction with equation 2. Fractions with a high protein concentration were used for immunolabeling, if the DOL was ~ 2.

Degree of labeling:

$$DOL = \frac{A_{fl} \cdot \varepsilon_{prot}}{(A_{280\,nm} - A_{fl} \cdot C_{280\,nm}) \cdot \varepsilon_{fl} \cdot b} \qquad (2)$$

DOL: degree of labeling; $A_{280\,nm}$: absorbance at 280 nm; A_{fl}: absorbance maximum of the fluorophore; $\varepsilon_{280\,nm}$: extinction coefficient of the pure antibody at 280; ε_{fl}: extinction coefficient of the fluorophore at its absorbance maximum; $C_{280\,nm}$: correction factor which depends on the absorbance of the fluorophore at 280 nm (provided by the manufacturer); b: path length (0.01cm for NanoDrop 1000)

3.3.2 Expression of recombinant TEV protease in E. coli

TEV protease was expressed and purified in cooperation with Wen-Ting Lo (Leibniz Institute for Molecular Pharmacology, Berlin). Hexa-histidine tagged TEV protease was expressed in the *E. coli* strain Rosetta 2. 1 l of 2 x YT medium was inoculated with an overnight culture of the TEV protease-expressing bacteria and grown at 37°C (180 rpm) until an optical density of 0.8 - 1.0 was reached at 600 nm. Protein expression was induced by adding 0.5 mM Isopropyl-β-D-thiogalactopyranoside (IPTG). Hexa-histidine tagged TEV protease was expressed overnight at 20 °C. Cells were harvested at 4,000 x g (4 °C, 15 min). Harvested cells were resuspended in lysis buffer for bacteria and Hexa-histidine tagged TEV protease was purified with Nickel-NTA beads (Quiagen, Germany) according to the manufacturer's instructions. The buffer of the purified hexa-histidine tagged TEV protease was exchanged to protein storage buffer, adjusted to 1 mg / ml, snap-frozen in liquid nitrogen and stored at -80°C.

3.3.3 Preparation of protein extract from mouse brain and western blot analysis

Mouse brain extracts and western blot analysis was performed in cooperation with Dr. Tanja Maritzen (Leibniz Institute for Molecular Pharmacology, Berlin). In order to verify the AP180 expression in AP180 KO and WT mouse brains, brains were homogenized in tissue lysis buffer with 15 strokes of a potter at 1,000 rpm. Lysates were incubated for 30 min on ice and centrifuged at 20,800 g for 10 min at 4°C. The protein concentration was determined by Bradford assay (Bradford, 1976). Samples were analyzed by SDS-PAGE (Shapiro et al., 1967) and immunoblotting (Towbin et al., 1992; antibody dilutions: anti AP180 1 : 1000 / anti Hsc70 1 : 5000). Bound primary antibodies were detected by the incubation with secondary HRP conjugated antibodies (antibody dilution 1 : 2500) and chemiluminescent substrate.

3.4 Cell Biological Methods

3.4.1 Preparation of primary hippocampal neuron cultures

Coverslips were cleaned for neuronal cell culture once with HCl (1M, overnight) and washed multiple times with acetone and ethanol. For poly-L-lysine (PLL) coating, 25 mm coverslips were incubated with a drop of 100 µl PLL in ddH_2O (15 µg / ml; Biochrom, Germany) in the middle of each coverslip for at least 2 h (room temperature), before PLL was removed with a Pasteur pipette. Cultures of primary hippocampal neurons were prepared from mice (postnatal, P1 – P3) in sparse culture. Hippocampi from up to four mice were dissected under sterile conditions and transferred into a dish with sterile ice-cold Hank's Balanced Salt Solution (HBSS; Life Technologies, USA), supplemented with 20 % fetal calf serum (FCS), 50 U / ml penicillin and 50 µg / ml streptomycin (P / S). Hippocampi were sliced into small pieces before they were washed twice in a Falcon tube with 5 ml HBSS, supplemented with FCS and P / S and washed twice with HBSS, containing P / S but no serum. The tissue was then digested (37 °C, 15 min) with 10 mg Trypsin (Sigma-Aldrich, USA) and 20 µg DNase (Sigma-Aldrich, USA) in 2 ml sterile digestion solution. The tissue was washed, as described before, and taken up into 2 ml dissociation solution with 20 µg DNase. Fragments were dissociated with siliconized and fire-polished Pasteur pipettes, with decreasing opening sizes (2 - 0.5 mm), until no tissue pieces were visible. 2 ml of HBSS with FCS and P / S was added to the cell suspension and cells were sedimented for 8 min at 200 x g (4 °C). Cell pellets were resuspended in 1 ml plating medium and cells were counted with a hemocytometer. The cell suspension was adjusted with plating solution to 100,000 cells / 50 µl and plated as a 50 µl drop in the middle of a 25 mm PLL coated coverslip in a 6-well plate. Cells were allowed to attach to the coverslip for 1 h in an incubator at 37 °C, 5 % CO_2 and 95 % humidity, before 2 ml of pre-equilibrated plating medium was added. Cells were fed on the next day (1 DIV) by removing 1 ml of the plating medium and adding 1 ml of pre-equilibrated growth medium. One day later (2 DIV), 1 ml of pre-equilibrated growth medium, supplemented with 2 µM Cytosine β-D-arabinofuranoside (AraC; Sigma-Aldrich, USA) was added to each well. Cells were fed again one week after preparation (7 DIV) by removing 1 ml of the old medium and adding 1 ml of pre-equilibrated growth medium with 2 µM AraC. Neuron cultures were used for experiments after 14 – 15 DIV.

3.4.2 Transfection of primary hippocampal neurons

Primary hippocampal neurons were prepared, as described in chapter 3.4.1, and transfected after 7 - 8 DIV with plasmid DNA by calcium phosphate transfection using the mammalian transfection kit ProFection (Promega, USA). The osmolarity of Neurobasal A medium (NBA; Life Technologies, USA) and HBSS (Life Technologies, USA) was adjusted with D-Mannitol (Sigma-Aldrich, USA) to the osmolarity of the medium from the neuron culture and pre-equilibrated in an incubator with 37 °C and 5 % CO_2 for 1 h. Coverslips from neuron cultures were transferred to 6-well plates, prepared with 1 ml NBA per well. Cells were kept in the incubator during the preparation of the transfection reagent. 3 – 6 µg of DNA were used for the transfection of one 25 mm coverslip. The DNA was mixed with 12.5 µl of CalCl2 (2 M) and ddH_2O in a volume of 100 µl (values represent the volume per coverslip). DNA and calcium phosphate precipitates were formed by adding the DNA mix drop-wise under continuous vortexing into a 15 ml falcon tube containing 100 µl of 2 x HEPES-buffered saline per coverslip. Calcium phosphate precipitates were kept in the dark for 30 min and added drop-wise to the prepared neurons in NBA. Cells were kept in the incubator for ~20 min to allow for the sedimentation of the precipitates. Once sediments were visible, cells were briefly washed three times with pre-equilibrated HBSS, before coverslips were transferred back to the original plate.

3.4.3 Generation of AP180 / CALM deficient neurons

Heterozygous mice of a recently published AP180 KO mouse line (Koo et al., 2015) were interbred, in order to obtain WT and AP180 KO litter mates. Mice were genotyped by detecting the AP180 WT and KO alleles via PCR-analysis of isolated genomic DNA from mouse tails (chapter 3.2.14). The 323 bp product of the WT-PCR and the 401 bp product of the KO-PCR (chapter3.2.2) were analyzed on an agarose gel. Primary hippocampal neuron cultures were prepared (chapter 3.4.1) from AP180 KO mice and transfected (chapter 3.4.2) with a plasmid co-expressing mKate and specific shRNA directed against CALM to obtain AP180 / CALM-depleted neurons. As a control, hippocampal neurons from WT littermates were transfected with a plasmid co-expressing mKate and a scrambled control shRNA (Table 3-8).

3.4.4 Immunocytochemistry of hippocampal neurons

Primary hippocampal neurons were prepared as described in chapter 3.4.1 and transfected via calcium phosphate transfection (chapter 3.4.2). After 14 - 15 DIV, cells were fixed with 4 % (w / v) paraformaldehyde (PFA), 4 % (w / v) sucrose in PBS (pH 7.5) for 15 min. Coverslips were washed three times with PBS. Neurons were blocked and permeabilized upside down with 50 µl GSDB + 0.23 % (v / v) Triton X-100 in a humidity chamber (30 min, room temperature). Primary antibodies were diluted (according to Table 3-4) in GSDB + 0.23 % (v / v) Triton X-100 and aggregates were removed by centrifugation (10,000 x g, 5 min, 4 °C). Coverslips were incubated with 50 µl of the supernatant upside down (1 h, room temperature) in a humidity chamber and washed three times with PBS. Fluorescently labeled secondary antibodies were diluted 1 : 200 (or 1 : 100 for SD-*d*STORM) in GSDB + 0.23 % (v / v) Triton X-100 and aggregates were removed by centrifugation, as described before. After incubating cells with 50 µl of the supernatant in a humidity chamber upside down (30 min, room temperature), coverslips were washed at least three times with PBS and mounted for widefield microscopy with Immu-Mount (Thermo Fisher, USA) on glass slides. Coverslips for super resolution microscopy (SD-*d*STORM) were mounted with *d*STORM imaging buffer on microscopy slides with 100 µl spherical voids (Carl Roth, Germany) and sealed with nail polish.

Variations from the standard protocol:

- For the detection of surface-stranded proteins, all labeling steps were carried out without Triton X-100.
- For immunocytochemistry with the anti CALM antibody (raised in goat), goat serum was replaced in all buffers by 5 % BSA.
- A detailed protocol for the detection of newly exocytosed SV proteins is provided in chapter 3.4.5.

3.4.5 Selective labeling of newly exocytosed SV proteins

Primary hippocampal neurons were prepared as described in chapter 3.4.1 and transfected with c-myc epitope-tagged Syb2. At 14 - 15 DIV, cultures were used for immunocytochemistry. In order to prevent uncontrolled antibody uptake, all labeling steps before fixation were carried out in the presence of the AMPA and NMDA receptor antagonists APV (DL-2-Amino-5-phosphonopentanoic acid, 50 µM) and CNQX (6-Cyano-7-nitroquinoxaline-2,3-dione, 10 µM). First, neurons were incubated with primary anti c-myc antibodis in imaging buffer (20 min, room temperature), to saturate all surface-epitopes. Then, neurons were washed three times with imaging buffer, placed in an electric field stimulation chamber with two platinum electrodes on each sides of a bath (RC-47FSLP; Warner Instruments, USA) with imaging buffer, stimulated with 40 AP (20 Hz, 100mA) and fixed with 4 % (w / v) PFA, 4 % (w / v) sucrose in PBS for 15 min at room temperature. Further labeling steps were carried out in GSDB. Unbound antibodies were removed by washing three times with PBS. Primary antibodies on the neuronal surface were saturated with Alexa 488-labeled Fab fragments of secondary antibody (overnight, 4 °C), followed by a labeling of newly exocytosed proteins with primary anti c-myc (1 h, room temperature) and Alexa 647 labeled FAB fragments of secondary antibody (30 min, room temperature). Further labeling of intracellular proteins was performed with primary and secondary antibodies as described in the chapter “Immunocytochemistry of hippocampal neurons”, (chapter 3.4.4) in GSDB + 0.23 % (v / v) Triton X-100.

3.4.6 Determination of Syb2 surface levels by immunocytochemistry

AP180 / CALM deficient neurons and control neurons were generated as described in chapter 3.4.3. Neurons were transferred into medium containing 1 µM tetrodotoxin (TTX; in 10 mM sodium acetate, pH 5.3) or an equal volume of 10 mM sodium acetate (pH 5.3). TTX was renewed after DIV 10. At DIV 14, cells were fixed for 10 min at room temperature with 4% (w/v) PFA, 4% (w/v) sucrose in PBS. After 3x washing with PBS, the cells were blocked with GSDB (10 min, room temperature). Cells were then incubated with custom labeled (chapter 3.3.1) CF647 labeled anti GFP / pHluorin nanobodies (ChromoTek, Germany) in blocking solution (1.6 µg / ml, 1 h room temperature). After 4x washing with PBS, cells were

mounted with ImmuMount (Thermo Fisher, USA), which has a basic pH and thus unquenches all pHluorin fluorescence. Images were acquired by widefield microscopy. For the calculation of surface levels, see also chapter 3.5.12.

3.4.7 Widefield microscopy - diffraction limited

Fluorescence microscopy is a technique that is broadly used for the visualization of proteins in fixed or living cells. Proteins are usually marked with a genetically encoded fluorescent protein-tag or an antibody that was raised against a specific epitope of a target protein in combination with fluorescent dyes. Fluorescence microscopy takes advantage of the fact that fluorophores can be efficiently excited with light of a certain wavelength and emit light at a longer wavelength. The emitted light is separated from excitation light coming from the light source by a dichroic mirror and spectral emission filters. Since each fluorophore has a characteristical excitation- and the emission-wavelength, multi-color images can be generated from samples that were labeled with different fluorescent markers. Therefore, filters and mirrors have to be chosen accordingly to the fluorescent properties of the fluorophore (Table 3-10).

If not stated differently, widefield microscopy was used for fluorescence imaging. This technique was chosen for the fast acquisition in live-cell experiments and for experiments that do not require super-resolution or confocal microscopy. Images were acquired with an inverted epifluorescence microscope (Eclipse Ti; Nikon, Japan), controlled by MicroManager 4.11 (Stuurman et al., 2010), equipped with either a 40x (NA, numerical aperture = 1.30; Nikon, Japan) or a 60x oil-immersion objective (NA = 1.49; Nikon, Japan), a sCMOS camera (Neo; Andor Technology, UK) and a 200 Watt mercury lamp (Lumen 200; Prior Scientific, Germany). An incubator (Okolab, Italy) around the microscope and the PerfectFocus (Nikon, Japan) autofocus system made the system compatible for live-cell imaging. Filter sets (Table 3-10) were chosen according to the excitation and emission properties of the fluorescent labels.

3.4.8 Confocal microscopy

Confocal microscopy provides a better z-resolution than widefield microscopy. This is achieved by the addition of a pinhole in the light-path that reduces out-of-focus light. Confocal microscopy was only used in Figure 4-10c for the verification of CALM knockdowns, since it was required to distinguish between the CALM expression in transfected hippocampal neurons and CALM expression in the underlying astrocyte layer. Images were therefore acquired with the laser-scanning microscope LSM780 (Carl Zeiss Microscopy GmbH) under control of the Imaging-Software ZEN (Carl Zeiss, Germany). The confocal microscope was equipped with a 488nm Argon-Laser and a 561nm DPSS-Laser. Emission was detected at 500–550 or 565–700 nm.

3.4.9 Super-resolution microscopy: SD-dSTORM

Conventional microscopy generates images with a limited resolution by the diffraction barrier (Abbe, 1873; chapter 3.5.6, equation 11). Single spots become blurred and thus overlap in densely labeled structures. However, as longs as the distance between the two spots is large enough (Rayleigh, 1879), both spots can be localized. Single molecule localization-based super-resolution microscopy comprises diverse microscopy techniques, which follow a common underlying principle. They circumvent the diffraction barrier by taking image series from samples, where only a subset of molecules emits light at a time (Huang et al., 2009). Fluorescent blinking is achieved in *d*STORM (direct stochastic optical reconstruction microscopy) by inducing prolonged OFF states of organic dyes by strong excitation and the incubation with reducing buffers in absence of oxygen (Heilemann et al., 2008). The fluorophores that are stochastically in an ON state can be localized by fitting algorithms. However, multi-color approaches in localization-based super-resolution microscopy often suffer from registration errors. This is highly problematic for co-localization experiments (Annibale et al., 2012). In contrast to other localization-based super-resolution microscopy approaches, SD-*d*STORM is free of errors in multicolor registration because different fluorophores with overlapping emission spectra are localized in the same image. Colors are assigned after spectrally demixing the emission (Figure 3-1). This technique has the further advantage, that it provides minimal color-crosstalk and reduced noise (Lampe et al., 2012,

2015). The lateral resolution of SD-*d*STORM is 20 – 35 nm, which is a ~10-fold gain, compared to conventional diffraction limited microscopy (Lampe et al., 2012; Lehmann et al., 2015).

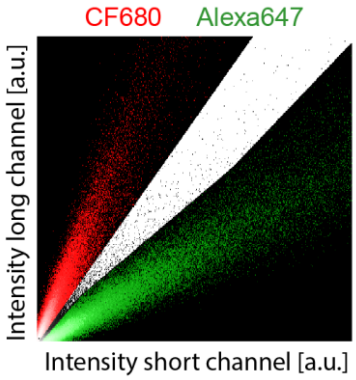

Figure 3-1: Representative intensity space from spectral-demixing *direct* stochastic optical reconstruction microscopy.
Representative intensity space to assign colors for single-molecule localizations in SD-*d*STORM imaging. Localizations were either assigned to the CF680 channel (black area, left), Alexa647 channel (black area, right) or not assigned (white area).

Immunocytochemistry for SD-*d*STORM was done as described in the chapter 3.4.4. Labeled secondary antibodies carried the SD-*d*STORM-compatible fluorescent dyes Alexa Fluor 647 (Invitrogen, USA) or CF 680 (Biotium, USA). Directly before imaging, labeled and fixed samples were incubated for five minutes with 100 µl of 1 : 200 diluted 100 nm sized fluorescent TetraSpeck beads (Life Technologies, USA; stock concentration ~ 2.3 x 10^{10} beads / ml) and 0.01 % (w / v) PLL in PBS. Non-sedimented beads were washed off two times with PBS and samples were mounted in *d*STORM imaging buffer: 0.5 mg / ml glucose oxidase (Sigma-Aldrich, USA), 40 mg / ml catalase (Roche, Switzerland), 10 % (w / v) glucose, 100 mM MEA (β-mercaptoethylamine; Sigma-Aldrich, USA) in PBS. Samples were mounted with nail polish.

SD-*d*STORM images were acquired with an inverted epifluorescence microscope (Eclipse Ti; Nikon, Japan), controlled by MicroManager 4.11 (Stuurman et al., 2010). The microscope was equipped with a 100x oil-immersion objective (NA = 1.49; Nikon, Japan), an additional 1.5 x lens, a EMCCD camera (DU-897E; Andor Technology, UK) and an emission splitter (OptoSplit II; Cairn Research, UK) between the camera and the 1.5 x lens. Samples were illuminated with a 300 mW 640 nm laser diode. An autofocus system (PerfectFocus II; Nikon, Japan) was used to reduce focus drift. The Drift was further minimized by stabilizing the room temperature with a customized incubator (Okolab, Italy) around the microscope. Alexa Fluor 647 (Invitrogen, USA) and CF 680 (Biotium, USA) were used as dye pair for

dual color imaging. The emission splitter was equipped accordingly with a dichroic mirror (700-DCXXR; AHF Analysentechnik, Germany) and an emission bandpass filter (F76-635; AHF Analysentechnik, Germany). The acquisition and analysis procedure was done, as previously described (Lampe et al., 2012) with the localization software rapidSTORM (Wolter et al., 2012) and the demixing software SDmixer (Tadeus et al., 2015). In order to reduce errors from remaining drift, SD-*d*STORM movies were registered on the basis of the fluorescent TetraSpec beads (Life Technologies, USA) with a custom written Python skript (written by Gregor Lichtner, Leibniz Institute for Molecular Pharmacology, Berlin). The same beads were used to register SD-*d*STORM channels with widefield channels in ImageJ (Schneider et al., 2012).

3.4.10 Super-resolution microscopy: Structured illumination microscopy

Structured illumination microscopy (SIM) is another technique to circumvent the diffraction barrier. SIM increases the image resolution by measuring the pattern resulting from the interference of an illumination pattern with the sample and computationally restoring the sample information (Gustafsson, 2000). SIM was used in this thesis to resolve the nanoscale synaptic organization of the active- and periactive zone. SIM offers only a 2-fold gain in resolution, compared to conventional diffraction limited microscopy (Gustafsson, 2000). However, in contrast to SD-*d*STORM used system allows for the acquisition of up to four different colors in one sample.

For SIM imaging of the active- and periactive zone, hippocampal neurons were silenced for 5 min with 50 µM APV and 10 µM CNQX in imaging buffer, stimulated (40 APs, 20 Hz) or directly fixed and stained with primary and secondary antibodies, as described before (chapter 3.4.4). Samples were mounted in Vectashield (Vector Laboratories, USA). 3D 3-color SIM images were acquired using the 488 nm, 568 nm and 643 nm laser lines, standard filter sets of the OMX V4 Blaze (GE Healthcare, UK) system and 125 nm z-sectioning. 100 nm fluorescent beads (TetraSpeck; Invitrogen, USA) were used for registration of detection channels. This method achieves less than 40 nm registration error for all three channels. Images were exported with Imaris 7.6 (Bitplane, Switzerland).

3.4.11 pHluorin live-cell imaging

The pH-sensitive pHluorin-tag was used to study the spatiotemporal dynamics on the plasma membrane or cycling of synaptic vesicle proteins. pHluorin was fused to the luminal domain a target proteins. pHluorin is a modified GFP (green fluorescent protein) that was optimized towards high pH-sensitivity. In the unprotonated form, pHluorin is efficiently excitable at 488 nm wavelength. However, in the protonated state, fluorescence is reduced by 20-fold (the pKa of pHluorin is 7.1; Miesenböck et al., 1998). These properties make it possible to study the exo- / endocytic cycling of pHluorin-tagged synaptic vesicle proteins. pHluorin-tags are hardly detectable in the acidic lumen (pH ~5.5) of synaptic vesicles. However, upon electrical stimulation and subsequent synaptic vesicle fusion with the plasma membrane, pHluorin becomes exposed to the neutral pH of the extracellular space (pH ~7.4), resulting in an fluorescence increase (Miesenböck et al., 1998; Sankaranarayanan et al., 2000). In the meantime the much slower endocytosis of the readily retrievable pool of synaptic vesicle proteins, a pre-clustered pool of SV proteins at the synaptic surface (Fernández-Alfonso et al., 2006; Wienisch and Klingauf, 2006; Hua et al., 2011), starts to occur. The endocytosis of tagged synaptic vesicle proteins and re-acidification of the vesicle leads to a drop in fluorescence by subsequent pHluorin protonation (Sankaranarayanan and Ryan, 2000).

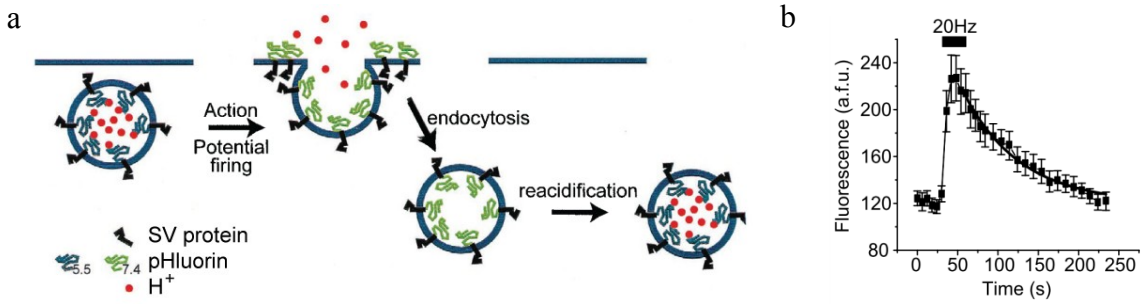

Figure 3-2: pHluorin live-cell imaging of the SV-cycle.

SV proteins that are lumenally fused to pHluorin are widely used as reporters for exo- and endocytosis. Inside the acidic lumen of a SV (pH ~5.5), pHluorin fluorescence is quenched due to protonation. During stimulation, SVs fuse with the plasma membrane. The pHluorin-tag becomes unquenched by de-protonation in the neutral extracellular environment (pH ~7.4). The fast fluorescence rise drops during endocytosis and reacidification of SVs. Taken and modified from (Sankaranarayanan et al., 2000). **(a)** Schematic illustration of pHluorin

unquenching and quenching during the SV cycle. **(b)** Fluorescence intensity traces of hippocampal neurons expressing pHluorin-tagged synaptobrevin 2, upon electrical stimulation (600 AP, 20 Hz). Taken and modified from (Sankaranarayanan and Ryan, 2000).

- General pHluorin live-cell imaging procedure

  Primary hippocampal neuron cultures were prepared as described in chapter 3.4.1 and transfected after 7 - 8 DIV with the expression construct for the pHluorin-tagged SV protein. Neurons were placed with imaging buffer in an electric field stimulation chamber with two lateral electrodes (RC-47FSLP; Warner Instruments, USA). Recurrent action potentials of the culture were inhibited with the AMPA and NMDA receptor antagonists APV (50 µM) and CNQX (10 µM) in the imaging buffer. Image-series were acquired with an EGFP filter set (F46-002; AHF Analysentechnik) at 30 °C. Neutral density filters and imaging rate were chosen according to the requirements of the experiment.

- Imaging exo- / endocytic cycling

  Neurons were stimulated by electric field stimulation with 40 APs (20 Hz, 100 mA). Movies were recorded at 0.5 Hz frame rate and 100 ms exposure.

- Detection of newly exocytosed SV proteins

  In experiments where only newly exocytosed SV proteins were under examination, unquenched surface pHluorin was either selectively bleached (Wienisch and Klingauf, 2006) by illuminating the neurons for 400 s or the pHluorin-tag was removed by enzymatic digestion with Tobacco Etch Virus (TEV) protease (Hua et al., 2011) in imaging buffer (4 µg / ml, 5 min, 30 °C; only Figure 4-5e-g, Figure 4-14 and Figure 4-17) prior to electric field stimulation (40 APs, 20 Hz, 100 mA). Movies were recorded at 2.5 Hz frame rate and 400 ms exposure.

3.4.12 Determination of Syb2 surface fractions by pHluorin imaging

The fraction of Syb2-pH on the synaptic plasma membrane was determined by pHluorin-imaging in combination with an acid-base protocol. Acidic buffer (pH 5.5) was used to quench all surface pHluorin, whereas basic buffer was used to unquench all vesicular pHluorin. Hippocampal neurons were prepared and tranfected with Syb2-pH, as described above. Movies were recorded, at 0.2 Hz frame rate and 100 ms exposure. At the beginning of a movie, neurons were kept in imaging buffer. The medium was replaced, after intensity values reached a steady state, in the following order: acidic-, physiological-, basic-, physiological imaging buffer. Buffers were released from syringes by a perfusion setup under the control of a VC-6 valve controller (Harvard Apparatus, USA). Excessive medium was removed with a Mini-Peristaltic Pump II (Harvard Apparatus, USA). After applying acid-base washes, neurons were stimulated with 200 AP (20 Hz, 100 mA), in order to identify functional synapses. The calculation of surface fractions is described in chapter 3.5.11.

3.5 Image Analysis and Mathematic Models

3.5.1 Identification of responding synapses

Synaptic areas, displaying stimulation-induced pHluorin responses were identified based on stimulus-evoked changes in the local fluorescence signal (F) using a custom-written ImageJ macro. The synaptic area was then calculated from the differential image (F_{after} - F_{before}) with the implemented histogram-based threshold procedure of ImageJ.

3.5.2 Correction for photobleaching and background

Identified synaptic areas (chapter 3.5.1) were expanded by 3 x 3 to a rectangular region of interest and images series were extracted. Intensity traces were fit with an exponential decay (equation 3) for each single pixel until the start of stimulation.

Exponential Decay:

$$I(t) = bg + a \cdot e^{-t/\tau} \quad (3)$$

I(t): Intensity at time t; bg: background signal; a: intensity at time 0; τ: lifetime

The bleach rate was calculated from the lifetime of the pHluorin decay for each pixel (equation 4).

Bleach rate:

$$\lambda = e^{-1/\tau} \quad (4)$$

λ: bleach rate; τ: lifetime

The bleach rate was used to correct the pixel-specific bleaching over the entire image sequence (equation 5)

Bleach Correction:

$$I_{bc}(t) = I(t) + \sum_{i=0}^{t}(1-\lambda) \cdot (I(i) - bg) \quad (5)$$

I_{bc}(t): bleach corrected intensity at time t; I(t): Intensity at time t; λ: bleach rate; bg: background

To reduce background and to correct for the residual fluorescence signal, coming from partially quenched luminal pHluorin molecules, after photobleaching or TEV treatment, the median of 5 images before stimulation was subtracted from the entire image sequence, resulting in ΔF image series.

3.5.3 Quantification of pHluorin intensity signal and escape

The pHluorin intensity signal over time was measured from selected (responding) synapses (chapter 3.5.1) with ImageJ (Schneider et al., 2012). The escape of newly

exocytosed SV proteins into the axon was measured from manually selected axonal regions of 0.9 µm² with a distance of 1.2 µm to a responding synapse.

3.5.4 Determination of endocytic time constants and endocytosis-resistant fractions

Endocytic time constants and endocytosis-resistant fractions were calculated with Origin Pro (OriginLab, USA) by applying a single exponential fit (equation 3) to pHluorin intensity traces. τ represents the endocytic time constant and bg is the endocytosis-resistant fractions.

3.5.5 Quantification of local protein spread by Gaussian fit

The bleach- and background corrected image sequences (chapter 3.5.2) of responding synapses were fit frame-by-frame to a 2D Gaussian distribution using equation 6-8 with a Igor Pro (WaveMetrics, USA) macro, which was written by Georgi Tadeus (Leibniz Institute for Molecular Pharmacology, Berlin). To compensate for synapses that are not parallel aligned to the imaging plane, only the longer FWHM of the 2d Gaussian fit was analyzed over time (equation 9).

Gaussian Fit 2D:

$$I(x,y) = I_0 + A \cdot e^{-\frac{1}{2}\left(\frac{x'}{\sigma_x}\right)^2 - \frac{1}{2}\left(\frac{y'}{\sigma_y}\right)^2} \quad (6)$$

$$x' = x \cdot \cos(\theta) + y \cdot \sin(\theta) - x_0 \cdot \cos(\theta) - y_0 \cdot \sin(\theta) \quad (7)$$

$$y' = -x \cdot \sin(\theta) + y \cdot \cos(\theta) + x_0 \cdot \sin(\theta) - y_0 \cdot \cos(\theta) \quad (8)$$

$$FWHM = 2 \cdot \sqrt{2 \cdot \ln(2)} \cdot \sigma \quad (9)$$

I(x,y): pixel intensity at the image coordinates x, y; I_0: intensity offset; A: amplitude; σ: standard deviation; θ: rotation angle; FWHM: full width at half maximum intensity; x_0, y_0: Gaussian center

3.5.6 Diffraction-limited rendering of SD-dSTORM images

To compare the SD-dSTORM images with images of conventional widefield resolution the SD-*d*STORM images were blurred with a Gaussian in ImageJ (Schneider et al., 2012) using σ_{Render} from equation 10.

Rendering:

$$\sigma_{Widefield} = \sqrt{\sigma_{dSTORM^2} + \sigma_{Render^2}} \quad (10)$$

$\sigma_{Widefield}$: standard deviation of widefield image (equation 9, 11); σdSTORM: standard deviation of SD-dSTORM (Lehmann et al., 2015); σR_{ender}: standard deviation for rendering.

Widefield resolution (Abbe, 1873):

$$FWHM = \frac{\lambda}{2NA} \quad (11)$$

FWHM: full width at half maximum intensity; λ: emission wavelength of the dye; NA: numerical aperture of the objective

Finally, the blurred images were displayed with the original camera pixel size of 105 nm.

3.5.7 Ripley's L(r)-r function

The Ripley's L(r)-r function was used to describe the clustering properties of protein localizations from SD-*d*STORM experiments. Estimations of normalized and edge-corrected Ripley's K(r) and L(r)-r functions (equations 12, 13) were calculated using the splancs package for the R software environment for statistical computing (Rowlingson and Diggle, 1993) with the following equations (El-Shaarawi and Piegorsch, 2002):

Ripley's :

$$K(r) = \frac{A}{N}\sum_i \sum_{j \neq i} \frac{I(d_{ij}<r)}{N \cdot w(I_i,I_j)} \quad (12)$$

$$L(r) - r = \sqrt{\frac{K(r)}{\pi}} - r \quad (13)$$

K(r): Edge-corrected Ripley's K to estimate the number of individual localizations (i) within a distance r of another (j) localization normalized by the number of total localizations N per area A; d_{ij} is the distance between localization i and j; $I(d_{ij}<r)$ is the indicator function that equals 1 if dij < r or 0 otherwise; $w(l_i,l_j)$ is the weight function for edge correction.

L(r)-r: Normalized K(r), equals 0 for a random distribution (Kiskowski et al., 2009). Upper envelopes of complete spatial randomness (CSR) were taken from 10 simulations for each region of interest.

3.5.8 k-nearest neighbors

k-nearest neighbors distributions were calculated, in order to describe the spatial relation of localizations from two different color-channels. *k*-nearest neighbors distributions were only obtained from localizations within synaptic regions (identified by bassoon labeling) in SD-*d*STORM images. $k = 10$ was chosen in order to reduce the likelihood of false positive hits due to noise. A custom-written ImageJ macro was measuring distances from all localizations in a reference channel to all localizations in a second channel. Only the distance to each 10^{th} ($k = 10$) nearest neighbor was counted for each reference localization and further used for statistics. The negative control for co-localization was generated by performing a toroidal shift of one channel for half the size of the region of interest against the other channel, along the x-Axis.

3.5.9 Radial intensity profiles

Radial intensity profiles were generated with the ImageJ (Schneider et al., 2012) macro "Radial Profile". First, local sub-synaptic maxima were found automatically in the NEP channel with the ImageJ function "find maxima". Next, radial profiles for NEP and AP180 were measured around centers of sub-synaptic NEP-clusters. Averaged intensity

values were plotted against their radial distance to the local maximum in the NEP reference channel.

3.5.10 Determination of diffusion coefficients

Diffusion from a point-source generates a Gaussian distribution. The FWHM of that distribution solely depends on the elapsed time and on the diffusion coefficient of the diffusing items (Crank, 1975). The intensity distribution resulting from overlaid successive SV fusion events in pHluorin experiments was modelled by using intensity changes between two successive images as a measure for the relative number of fused SVs. Gaussian distributions were calculated for all fused SV (binned by the imaging-rate). Each Gaussian distribution was weighted by its corresponding intensity increase (experimental data) and integrated with the previous Gaussian intensity distributions (equations 14, 15). In analogy to the pHluorin movies, the sum of all distributions was fit with one Gaussian distribution (equation 16) and plotted over time. The diffusion coefficients were determined by matching the mean slope from the experimental $FWHM^2$ to the $FWHM^2$ from the model. The validity of the model was validated by comparing traces obtained from the model and experimentally obtained traces, using a two-way repeated measures ANOVA.

Integrated Gaussian:

$$I(r,t) = \sum_{j=0}^{N} \frac{I_j - I_{j-1}}{4 \cdot \pi \cdot D \cdot (n-j)} \cdot e^{\left(-\frac{r^2}{4 \cdot D \cdot (n-j)}\right)} \quad (14)$$

$$N = \frac{t}{f} \quad (15)$$

I(r, t): Intensity at the radial distance r (from Gaussian center) and time t; D: diffusion coefficient, N: frame number; f: frame duration;

Gaussian Fit 1D:

$$I(r) = I_0 + A \cdot e^{-\frac{1}{2}\left(\frac{r}{\sigma}\right)^2} \quad (16)$$

I(r): intensity at the radial distance r (from Gaussian center); I_0: intensity offset; σ: standard deviation

3.5.11 Calculation of Syb2 surface fractions from pHluorin images

Data were acquired, as described in the chapter "Determination of Syb2 surface fractions by pHluorin imaging" (chapter 3.4.12). Synapses were manually selected in ImageJ (Schneider et al., 2012). Average intensity values from synapses responding to electrical stimulation were then measured (after intensity values reached a steady state) at all buffer conditions. Syb2 surface fractions were determined from acid-base washes with equation 17.

Calculation of surface fractions:

$$Surface\ fration = \frac{I_P - I_A}{I_B - I_A} \quad (17)$$

I_A: Synaptic intensity at acidic buffer; IB: Synaptic intensity at basic buffer; I_P: Synaptic intensity at physiological buffer;

3.5.12 Calculation of Syb2 surface levels by immunocytochemistry

Data were acquired, as described in the chapter "Determination of Syb2 surface levels by immunocytochemistry" (chapter 3.4.6). Synapses were identified in the Syb2-phluorin channel, with the implemented histogram-based threshold procedure of ImageJ (Schneider et al., 2012). Synaptic intensity values were measured in all channels. The synaptic intensity of surface-Syb2 (signal from the antibody labeling) was divided by the total synaptic Syb2-intensity (unquenched pHluorin channel). Values were normalized to the mean value of all experimental groups of each experiment and were transformed into Z scores before statistical evaluation to compensate for differences in absolute fluorescence intensities between independent experiments.

3.6 Statistical analysis

If not indicated differently, traces were recorded from 4 - 12 neurons per individual experiment. From each neuron several tens to hundreds of synapses were analyzed. Data were pooled in two steps: i) by calculating the median from all synapses from one neuron and ii) by using this value to generate the median for all neurons within each individual experiment. N

individual experiments were averaged and used for statistical analysis. Maximal spread, FWHM² of the last time point and the half-time of reclustering were obtained from median filtered original traces in order to reduce noise. All values are depicted as mean ± s.e.m. Statistical significance was calculated with Prism (Graphpad, USA) using a two-way ANOVA with repeated measures (for curves) or a two-tailed t-test (all bar graphs). Statistical significance is indicated as followed: *** $p < 0.001$, ** $p < 0.01$, * $p < 0.05$, not significant (n. s.) $p > 0.05$.

4 Results

4.1 The fate of newly exocytosed synaptic vesicles

While exo- and endocytosis at the mammalian presynapse has been the subject of intense investigations over the last decades (Heuser and Reese, 1973; Haucke et al., 2011; Saheki and Camilli, 2012; Südhof, 2013; Kononenko and Haucke, 2015), comparably little is known about the mobility of SV proteins within plasma membranes immediately after exocytosis. This knowledge gap was mainly due to the methodical challenges that investigating the fate of newly exocytosed SV proteins poses, including the small size of the synapse and the small time-window between exocytosis and compensatory endocytosis. Until recently, it was assumed that the newly exocytosed pool of SV proteins (NEP) is immediately retrieved. However, it became evident that instead of an immediate retrieval of the NEP, neurons rather internalize a preexisting "readily retrievable pool" of SV proteins (RRetP; Fernández-Alfonso et al., 2006; Wienisch and Klingauf, 2006; Hua et al., 2011). The time-window for precisely investigating the spatiotemporal behavior of the NEP is thus much longer than initially expected. Research on the NEP may be important to understand the processes that lead to the formation of the RRetP and might provide answers to central questions, including "What drives release site clearance?" and "Do newly exocytosed SV proteins escape into the axon?"

4.1.1 Monitoring newly exocytosed SV proteins

The selective microscopic detection of fluorescently labeled proteins of the NEP is still hindered by the comparatively large signal from SVs and from preexisting SV proteins on the axonal surface (Dittman and Kaplan, 2006; Wienisch and Klingauf, 2006; Koo et al., 2015). In order to specifically study the dynamics of SV proteins upon SV fusion with the plasma membrane, I developed a novel assay based on employing the pH-sensitive fluorescent protein pHluorin GFP (green fluorescent protein; Miesenböck et al., 1998). pHluorin-tagged SV proteins are an effective tool to trace SV proteins during the SV cycle

(Sankaranarayanan et al., 2000). The pHluorin-tag remains quenched in the acidic lumen of SVs, whereas electrical stimulation and subsequent SV fusion with the plasma membrane, unquenches pHluorin due to the neutral extracellular environment. In a classical pHluorin assay, subsequent endocytosis and reacidification causes pHluorin requenching (Figure 1-2, Figure 3-2). Hence, local changes in fluorescence can be caused by several, at least partially simultaneous processes: exocytosis, endocytosis and the lateral movement of surface-stranded proteins. Thus, the classical pHluorin assay is unsuitable for a specific detection of NEP dynamics.

However, exocytosis is followed by the endocytosis of a preexisting surface-stranded RRetP, which is not identical to the NEP (Fernández-Alfonso et al., 2006; Wienisch and Klingauf, 2006; Hua et al., 2011). In order to separate exocytosis from endocytosis, the fluorescence of extracellular pHluorin was selectively removed (surface-eclipsed). This was achieved either by enzymatic tag removal with Tobacco Etch Virus (TEV) protease (similar to Hua et al., 2011) or by selective photobleaching (similar to Wienisch and Klingauf, 2006) of unquenched surface-stranded pHluorin molecules prior imaging. Consequentially, stimulation should induce pHluorin-signal changes that originate only from NEP dynamics and not from RRetP endocytosis (Figure 4-1a). I tested both methods in hippocampal neurons expressing the pHluorin tagged SNARE-protein Syb2 (Syb2-pH). Synaptic Syb2-pH fluorescence was massively reduced upon either treatment (Figure 4-1b, c). This indicates that selective photobleaching or enzymatic tag removal are sufficient to eclipse the fluorescence signal originating from the RRetP. Lumenal pHluorin remained efficiently quenched in resting surface-eclipsed neurons. However, electrical stimulation (40 AP, 20Hz) induced a fluorescence increase at synaptic boutons, indicating that exocytosis remains unperturbed (Figure 4-1d).

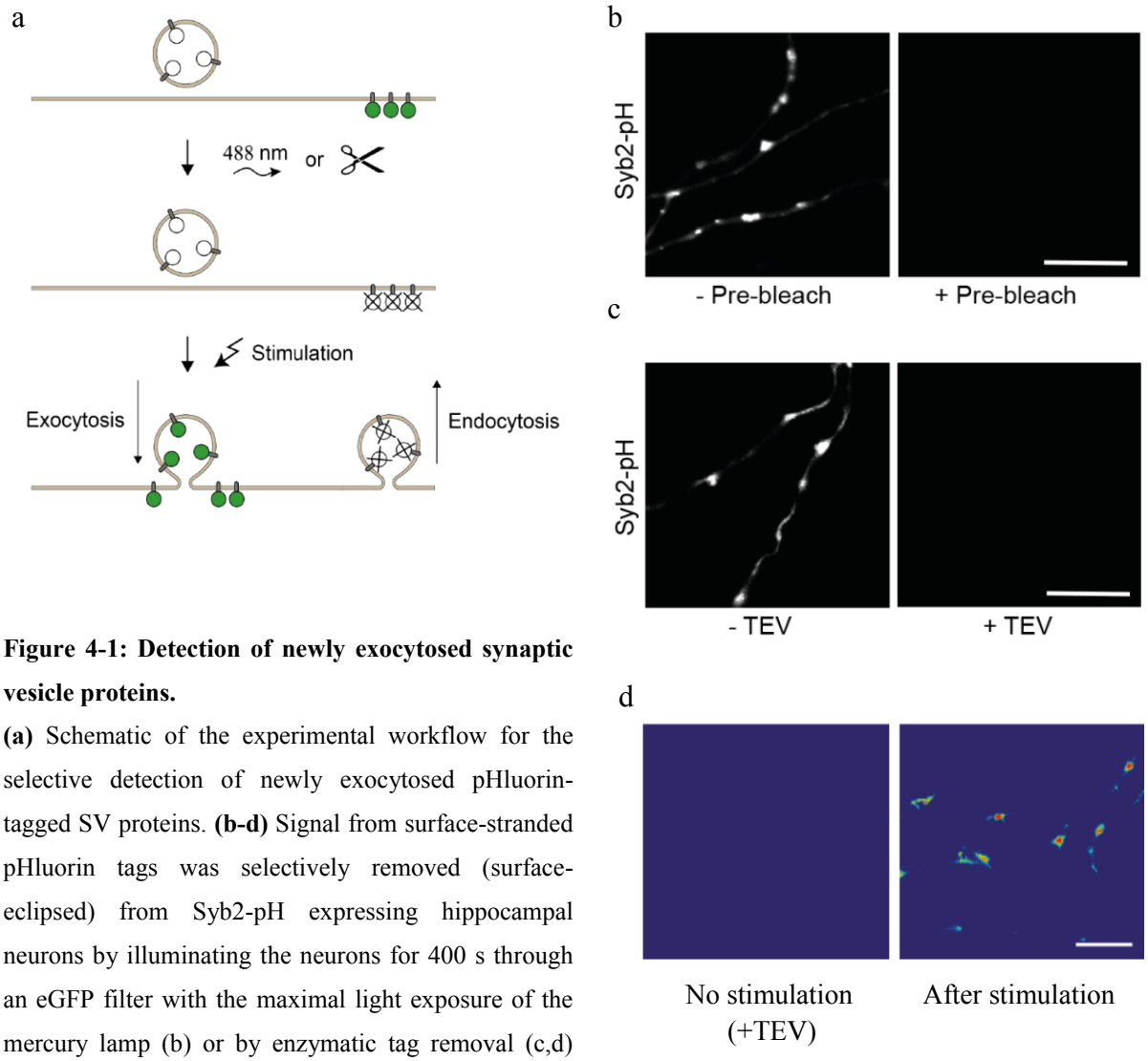

Figure 4-1: Detection of newly exocytosed synaptic vesicle proteins.

(a) Schematic of the experimental workflow for the selective detection of newly exocytosed pHluorin-tagged SV proteins. **(b-d)** Signal from surface-stranded pHluorin tags was selectively removed (surface-eclipsed) from Syb2-pH expressing hippocampal neurons by illuminating the neurons for 400 s through an eGFP filter with the maximal light exposure of the mercury lamp (b) or by enzymatic tag removal (c,d) with TEV protease. Scale bar, 5µm. (d) Surface-eclipsed neurons before and after electric field stimulation (40 AP, 20 Hz). Stimulation leads to an unquenching of the pHluorin-tag upon exocytosis and a selective detection of the NEP. Scale bar, 10µm.

4.1.2 Restricted movement of newly exocytosed proteins

Next, pHluorin imaging of surface-eclipsed neurons was used as a tool to study the fate of newly exocytosed SV proteins. First, I investigated whether the movement of newly exocytosed SV proteins is restricted to presynaptic boutons or if proteins undergo unlimited

escape into the axon. Therefore, Syb2-pH expressing hippocampal neurons were surface-eclipsed, stimulated (40AP, 20Hz) and the fluorescence intensity from automatically detected (chapter 3.5.1) synapses was measured over time. The pHluorin intensity within synaptic boutons increased during the stimulation, indicating that the lumenal pHluorin tag was exposed to the neutral extracellular pH after SV fusion with the plasma membrane. In contrast to pHluorin experiments without surface-eclipsing (Figure 4-9a; Sankaranarayanan et al., 2000) the fast initial rise in fluorescence was followed by a small decrease (~ 10 %) of fluorescence to a plateau level (Figure 4-2a) and not back to the baseline. This small decrease could be explained by endocytosis and reacidification of a minor fraction of newly exocytosed Syb2-pH or by escape of Syb2-pH from the synaptic area into the axon.

To investigate the cause of this decay in more detail, I measured the fluorescence intensities from axonal regions, in 1.2 µm distance to synaptic boutons, over time. Interestingly, the axonal regions displayed a rise in fluorescence that temporally correlated with the observed synaptic decrease in fluorescence after stimulation. This strongly suggests that a small fraction of newly exocytosed Syb2-pH escaped into the axon (Figure 4-2b).

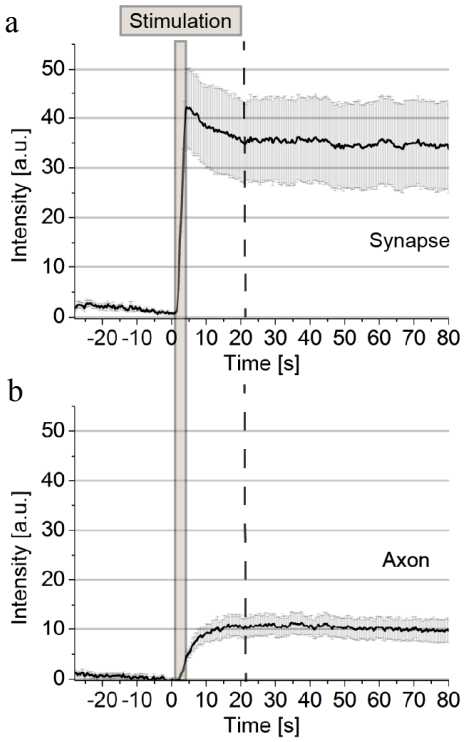

Figure 4-2: Newly exocytosed Syb2 is largely restricted to the surface of presynaptic boutons. Hippocampal neurons expressing Syb2-pHluorin were surface-eclipsed and stimulated in an electric field with 40 AP, 20 Hz. Fluorescence intensity changes upon stimulation were recorded from automatically detected (according to chapter 3.5.1) presynaptic boutons (a) or from axonal areas with 1.2 µm distance to the synapse (b). Mean ± s.e.m.; n = 10 neurons. Note the similar kinetics of the small fluorescent decay after exocytosis within synaptic boutons and the increase in fluorescence in the axon.

I further tested, whether the post-exocytic decay was solely caused by a minor NEP escape into the axon without any contribution of endocytosis and reacidification by using the vATPase inhibitor folimycin (Droese et al., 1993) that prevents fluorescence decays by endocytosis and subsequent reacidification. Hippocampal neurons expressing Syb2-pH were either surface-eclipsed, treated with folimycin, or both conditions were combined prior to electric stimulation (40AP, 20Hz). All three conditions resulted in a fast initial rise in synaptic fluorescence upon exocytosis, followed by a small fluorescence decrease to a plateau level (Figure 4-3). This confirms that the small synaptic intensity decay does not represent endocytosis but represents a small Syb2-pH escape into axons displayed in Figure 4-2. pHluorin imaging in combination with surface-eclipsing is therefore suitable to precisely image and quantify dynamics of newly exocytosed SV proteins.

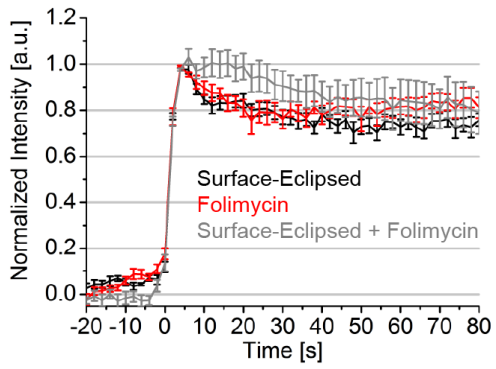

Figure 4-3: pHluorins traces from surface-eclipsed neurons show no contribution of endocytosis and subsequent reacidification.
Hippocampal neurons expressing Syb2-pHluorin were stimulated in an electric field (40 AP, 20 Hz) and imaged over time. Neurons were either surface-eclipsed by photobleaching, reacidification was blocked (folimycin), or both treatments were combined prior to electrical stimulation (mean ± s.e.m.; n = 7 neurons).

4.1.3 Newly exocytosed Syb2 undergoes fast spread, confinement and reclustering within presynaptic boutons

The majority of newly exocytosed proteins remains confined within presynaptic boutons (see chapter 4.1.2). However, it is unclear, how SV proteins distribute sub-synaptically after exocytosis. Revealing the precise distribution of NEP proteins is particularly interesting as the spatiotemporal relationship between exocytosis and the assembly of the RRetP prior to endocytosis and mechanisms underlying release site clearance are poorly understood (Neher, 2010; Haucke et al., 2011).

In order to characterize sub-synaptic dynamics of newly exocytosed SV proteins, it is of prime importance to know, if proteins originate from one or multiple active zones. In order to find out if newly exocytosed SV proteins in our assay originate from single active zones, surface-eclipsed hippocampal neurons were co-transfected with Syb2-pH and a fusion protein of the active zone marker Munc13-1 (Stevens et al., 2005) with the fluorescent protein mCherry. From 160 spots of newly exocytosed Syb2-pH, only 9 contained more than one Munc13-1-mCherry spot (Figure 4-4a), suggesting that the majority of newly exocytosed proteins arises from single active zones. This is in agreement with previous ultrastructural studies (Schikorski and Stevens, 1997). Centers of automatically determined spots of newly exocytosed proteins were reliably detected and served as a basis for the further characterization of NEP dynamics. Centers were marked with yellow crosses in Figure 4-4a.

In order to describe the spatiotemporal behavior of newly exocytosed Syb2, I combined high-resolution time-lapse imaging with synchronized electric field stimulation of surface-eclipsed hippocampal neurons and semi-automated image analysis. The signal from newly exocytosed Syb2-pH was background- and bleach-corrected (ΔF) and fitted to a 2-dimensional (2d) Gaussian distribution (Figure 4-4b), using a customized software tool. The full with at half maximum (FWHM) of the Gaussian fit was used as a measure of signal width that is independent from the overall signal intensity. Noise-like residuals (Figure 4-4b) demonstrate the good quality of the fit and confirm the 2d Gaussian distribution as an appropriate model.

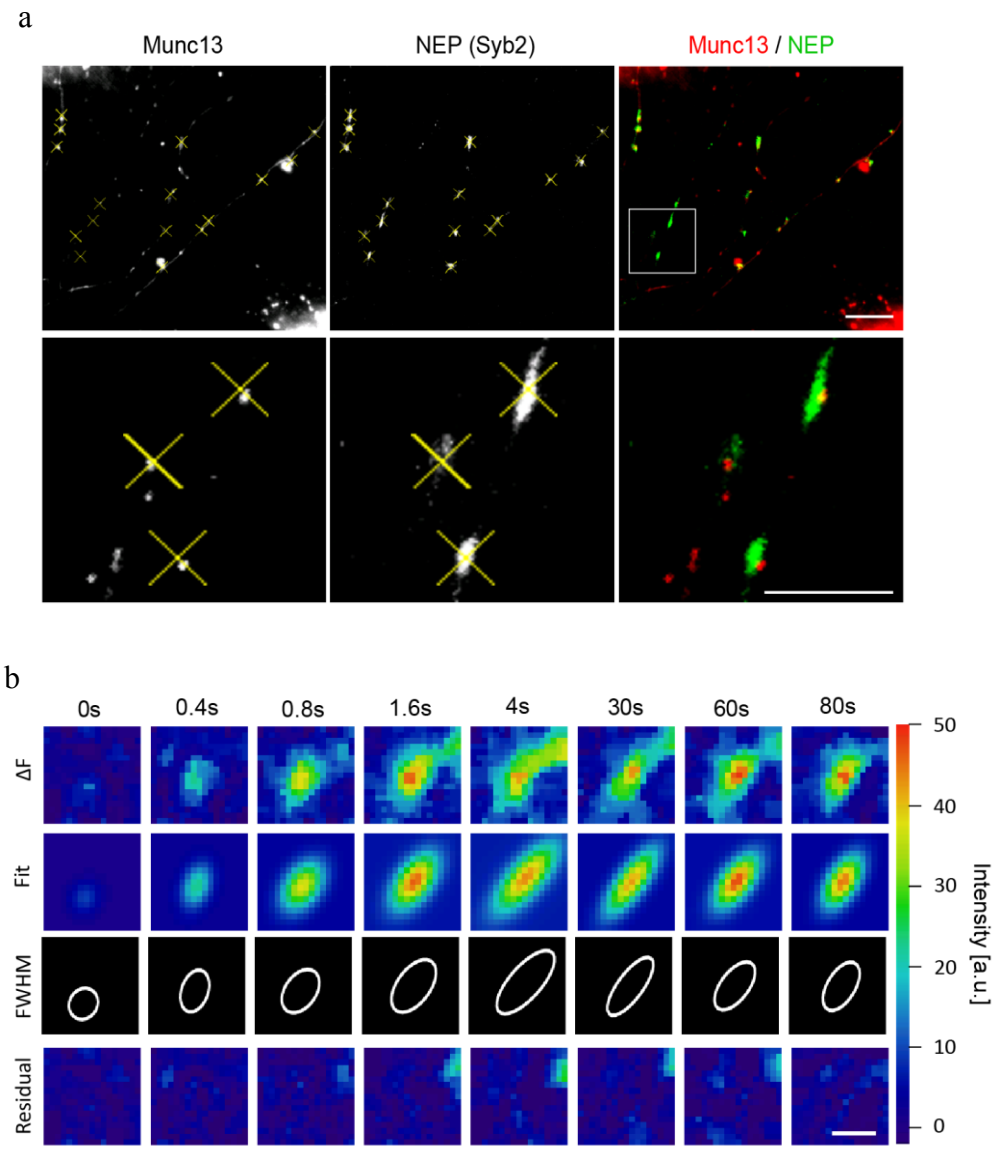

Figure 4-4: Sub-synaptic redistribution of newly exocytosed Syb2-pH.

(a) Hippocampal neurons coexpressing Syb2-pHluorin and Munc13-1-mCherry were surface-eclipsed, stimulated in an electric field (40 AP, 20 Hz) and imaged over time. Yellow crosses represent automatically detected centers (chapter 3.5.1) of newly exocytosed Syb2-pH, which are passed to the Gaussian fit routine. Note the overlap of newly exocytosed proteins with single Munc13-1 puncta. Scale bar, 10 µm, zoom 5 µm. **(b)** Representative images of a Syb2-pHluorin expressing synapse of a stimulated (40 APs, 20 Hz) surface-eclipsed neuron, either background subtracted (ΔF), 2d Gaussian fit (Fit), FWHM (white line) or Gaussian fit residual. Scale bar, 1 µm.

The square of the FWHM ($FWHM^2$) from 2d Gaussian fits of newly exocytosed Syb2-pH was then plotted over time, as a measure for the covered area. From the sample images (Figure 4-4b) and from the quantifications (Figure 4-5a) it is obvious that newly exocytosed Syb2-pH underwent a fast phase of spreading, indicated by the increasing $FWHM^2$ during the first seconds. The spread reached a plateau ~ 2 s after the end of stimulation at about the size of an average synaptic bouton (Wilhelm et al., 2014). Thus, newly exocytosed proteins remained confined within the synaptic bouton. Confinement was followed by a phase of reclustering into a smaller area, indicated by a slow $FWHM^2$ decrease.

The maximum area reached during the plateau phase was independent from Syb2-pH expression levels, demonstrated by the lack of correlation of maximal spread ($FWHM^2$ max) and initial Syb2-pH intensity before surface-eclipse (Figure 4-5c). In addition, no effect of photobleaching on reclustering was observed when light exposure was decreased 20-fold during acquisition (Figure 4-5d), showing that this effect was not due to any photodamage. Furthermore, surface-eclipse by selective photobleaching or by enzymatic tag removal showed no statistically significant difference with respect to maximal spread, covered area after reclustering and half-time ($t_{1/2}$) of reclustering (Figure 4-5e-g), indicating that both procedures did not interfere with spread, confinement and reclustering.

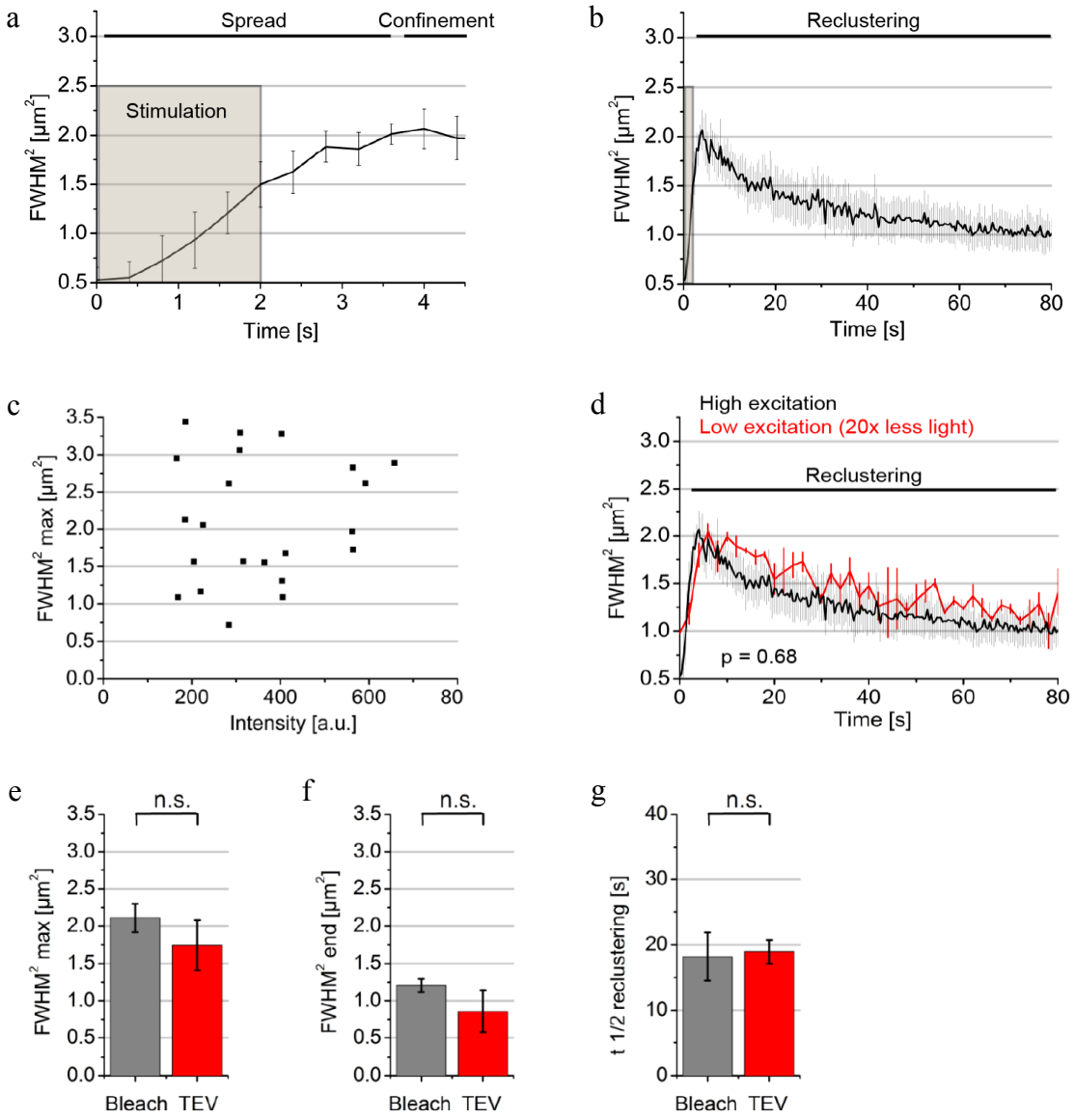

Figure 4-5: Newly exocytosed Syb2-pH reveals spread, confinement and reclustering within presynaptic boutons. Hippocampal neurons expressing Syb2-pHluorin were surface-eclipsed and stimulated in an electric field (40 AP, 20 Hz). Newly exocytosed Syb2-pH was fitted with a 2d Gaussian distribution. **(a,b)** The $FWHM^2$ of the Gaussian fit is plotted over time. Fast spread during and after the stimulation is followed by confinement (a) and reclustering (b). Mean ± s.e.m.; N = 5 independent experiments. **(c)** The maximal spread ($FWHM^2$ max) is plotted as a function of Syb2-pHluorin expression levels (synaptic pHluorin intensity before eclipsing surface proteins). Each data point corresponds to one neuron. **(d)** $FWHM^2$ traces for time-lapse imaging of Syb2-pHluorin using high excitation (black, 2.5 Hz, no neutral density filter) or low excitation (red, 0.5 Hz, 4 x neutral density filter). Mean ± s.e.m.; high excitation N = 5 (replotted from b), low excitation N = 2 individual experiments; Statistical significance was tested using two-way ANOVA test with repeated measures. **(e-g)** Neurons were surface-eclipsed by photobleaching or enzymatic cleavage of Syb2-pHluorin (harboring a TEV

cleavage site) by TEV protease. The $FWHM^2$ of Gaussian fit shows no statistically significant difference, between the two conditions, with respect to maximal spread (e), last time point (f), and half-time ($t_{1/2}$) of reclustering (g). Mean ± s.e.m.; independent experiments: photobleach (N = 5), TEV cleavage (N = 3). Statistical analysis was done using a two-tailed unpaired t-test.

4.2 Major SV proteins have similar post-exocytic dynamics

I next investigated whether the post-exocytic spread, confinement and reclustering are specific properties of Syb2, the SV transmembrane protein with the highest copy number (Takamori, 2006), or if they also hold true for other SV proteins. Since it is unknown, whether newly exocytosed SVs remain as patches at the plasma membrane or if proteins diffuse alone (Haucke et al., 2011) different proteins may have different spatiotemporal properties.

I therefore decided to compare the post-exocytic dynamics of the three major (Takamori, 2006) SV transmembrane proteins Syb2, Syp and Syt1. Transfected neurons were surface-eclipsed, stimulated (40 AP, 20 Hz) and the spatiotemporal NEP dynamics were analyzed as described above. Not only Syb2-pH, but also pHluorin-tagged Syp (Syp-pH) and Syt1 (Syt1-pH) underwent spreading, confinement (Figure 4-6a) and reclustering (Figure 4-6b). No statistically significant differences were observed with respect to the maximal area covered upon spreading (Figure 4-6c), the area covered after reclustering (Figure 4-6d), or the half-time of reclustering (Figure 4-6e).

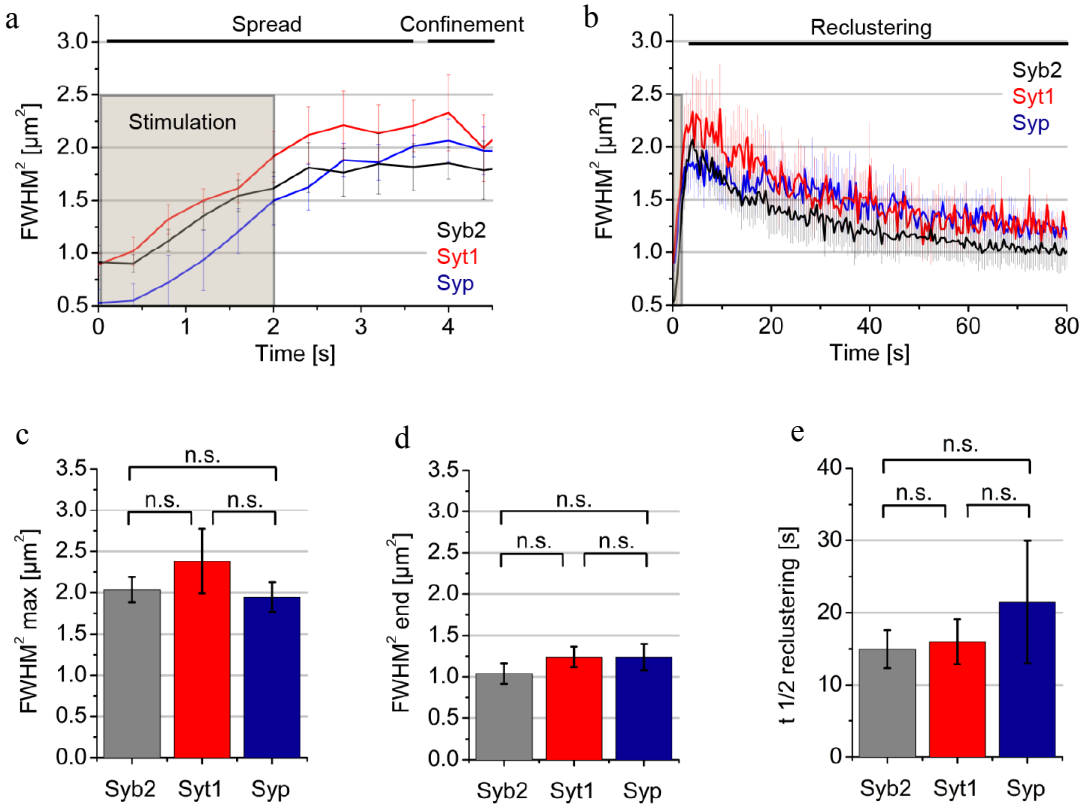

Figure 4-6: The three most abundant SV proteins show similar spread, confinement and reclustering upon exocytosis.

Hippocampal neurons expressing pHluorin tagged SV proteins were surface-eclipsed and stimulated in an electric field (40 AP, 20 Hz). The fluorescent signal of newly exocytosed proteins was fit with a 2d Gaussian distribution. **(a,b)** The $FWHM^2$ of the Gaussian fit over time shows spreading, confinement (a), and reclustering (b) of Syb2-, Syt1-, and Syp-pHluorin. **(c-e)** Maximal spread (c), last time point (d), and half-time $t_{1/2}$ of reclustering (e) were measured from data in (b). Mean ± s.e.m.; independent experiments: Syb2 (N = 5, replotted from Figure 4-5); Syt1 (N = 3); Syp (N = 3). Statistical analysis was done with a two-tailed unpaired t-test.

4.3 Filamentous actin does not affect post-exocytic Syb2 dynamics

Recent experiments with the *Drosophila* temperature-sensitive dynamin mutant shibire^{ts} demonstrated that filamentous actin is important to preserve SV protein clusters in the plasma membrane (Dason et al., 2013).

In order to investigate, if actin filaments are also involved in the confinement and reclustering of newly exocytosed SV proteins, the actin polymerization in hippocampal neurons was inhibited by the incubation with Latrunculin A (LatA; Coué et al., 1987). First, the effect of LatA on removing filamentous actin in hippocampal neurons was tested with the actin filament reporter LifeAct-eGFP, which is the fusion protein of eGFP (enhanced green fluorescent protein) and the first 17 amino acids of the actin-binding protein Abp140 (Riedl et al., 2008). LifeAct-eGFP was expressed in hippocampal neurons. Images from neurons expressing LifeAct-eGFP were taken first in the presence of DMSO and then after 5 min of treatment with 10 µM Latrunculin A. While in the control (DMSO) condition, LifeAct-eGFP accumulated in boutonic structures, the signal dispersed after the treatment with LatA (Figure 4-7a, b), consistent with a disruption of synaptic actin filaments.

To examine, if filamentous actin is required for the confinement of newly exocytosed SV proteins or their reclustering, hippocampal neurons expressing Syb2-pH were treated with 10 µM LatA 5 min prior surface-eclipse and stimulation (40 AP, 20 Hz). LatA remained in the imaging buffer throughout the experiment. Time-lapse imaging revealed no obvious difference between spread, confinement and reclustering of Syb2-pH between control- and LatA treated neurons (Figure 4-7c). This suggests that filamentous actin is not involved in NEP dynamics.

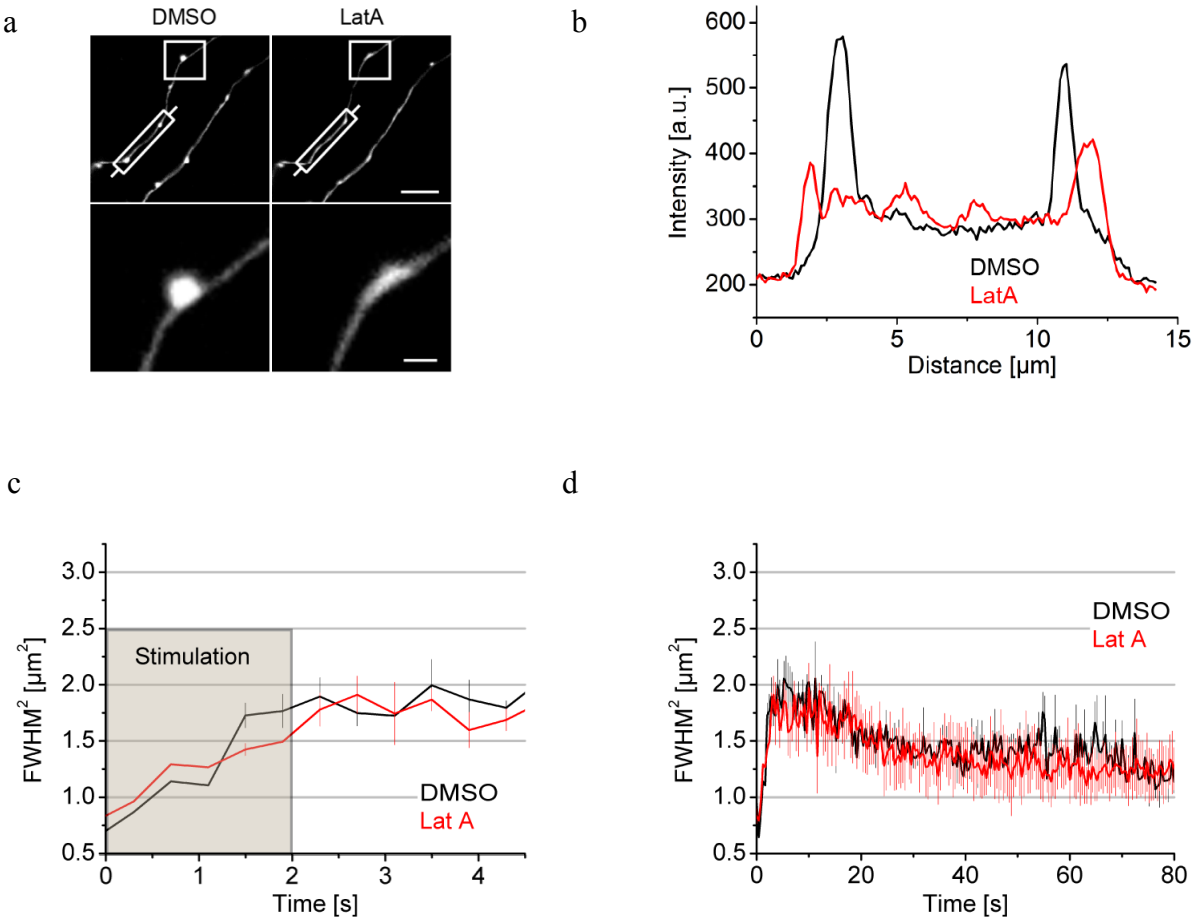

Figure 4-7: Actin filaments are not required for spreading, confinement, and reclustering of newly exocytosed SV proteins.

(a,b) Hippocampal neurons expressing LifeAct-eGFP were first imaged in the presence of DMSO and then after incubation with Latrunculin A (10 µM, 5 min). (a) Representative images. Scale bar, 5 µm, zoom 1 µm. (b) Line plot of the data shown in (a). **(c,d)** Hippocampal neurons expressing Syb2-pH were treated with DMSO or 10µM Latrunculin A (Lat A) for 5 min, surface-eclipsed and stimulated in an electric field (40 AP, 20 Hz). The fluorescent signal of newly exocytosed proteins was fitted with a 2d Gaussian distribution. Note that for both, DMSO and Lat A treated neurons, the $FWHM^2$ of the Gaussian fit over time shows spreading, confinement (c), and reclustering (d) with no obvious differences between the conditions. Mean ± s.e.m.; N = 3 individual experiments.

4.4 Syp does not mediate Syb2 confinement

The retrieval of Syb2 is impaired at synapses lacking Syp. However, contradictory results regarding a frequency-dependent requirement of Syp were reported (Gordon et al., 2011; Rajappa et al., 2016). The interaction between both proteins (Calakos and Scheller, 1994; Edelmann et al., 1995; Becher et al., 1999) was shown to depend on cholesterol (Mitter et al., 2003), whereby only Syp, and not Syb2 binds to cholesterol (Thiele et al., 2000). Furthermore, cholesterol is particularly enriched in SVs (Takamori, 2006) and required for the stability of SV proteins clusters at the presynaptic plasma membrane of the *Drosophila* neuromuscular junctions (Dason et al., 2010, 2013). It is therefore tempting to hypothesize that Syp is involved in post-exocytic Syb2 confinement via cholesterol-microdomains.

A previously published Syp knockout mouse strain (McMahon et al., 1996) was used to analyze the dynamics of newly exocytosed Syb2-pH. Syp knockout (KO) and wildtype (WT) littermate mice were genotyped and provided by the group of Prof. Ahnert-Hilger (Charité Universitätsmedizin Berlin). The Syp deficiency of KO neurons was verified by a co-immunolabeling of Syp and Syt1 in Syp KO and WT hippocampal neurons (Figure 4-8a). As expected, Syp co-localized with Syt1 in synaptic structures of WT neurons, whereas no specific Syp signal was observed in Syp KO neurons, confirming the absence of Syp in the KO.

In order to find out, if Syp is involved in the confinement and reclustering of Syb2, Syb2-pH transfected hippocampal neurons were surface-eclipsed, stimulated (40AP, 20Hz) and post-exocytic Syb2-pH dynamics were analyzed. Both WT and Syp KO neurons displayed spreading, confinement (Figure 4-8b) and reclustering (Figure 4-8c) with no obvious kinetic differences between WT and KO neurons. This suggests that Syp is not crucial for Syb2 confinement and reclustering.

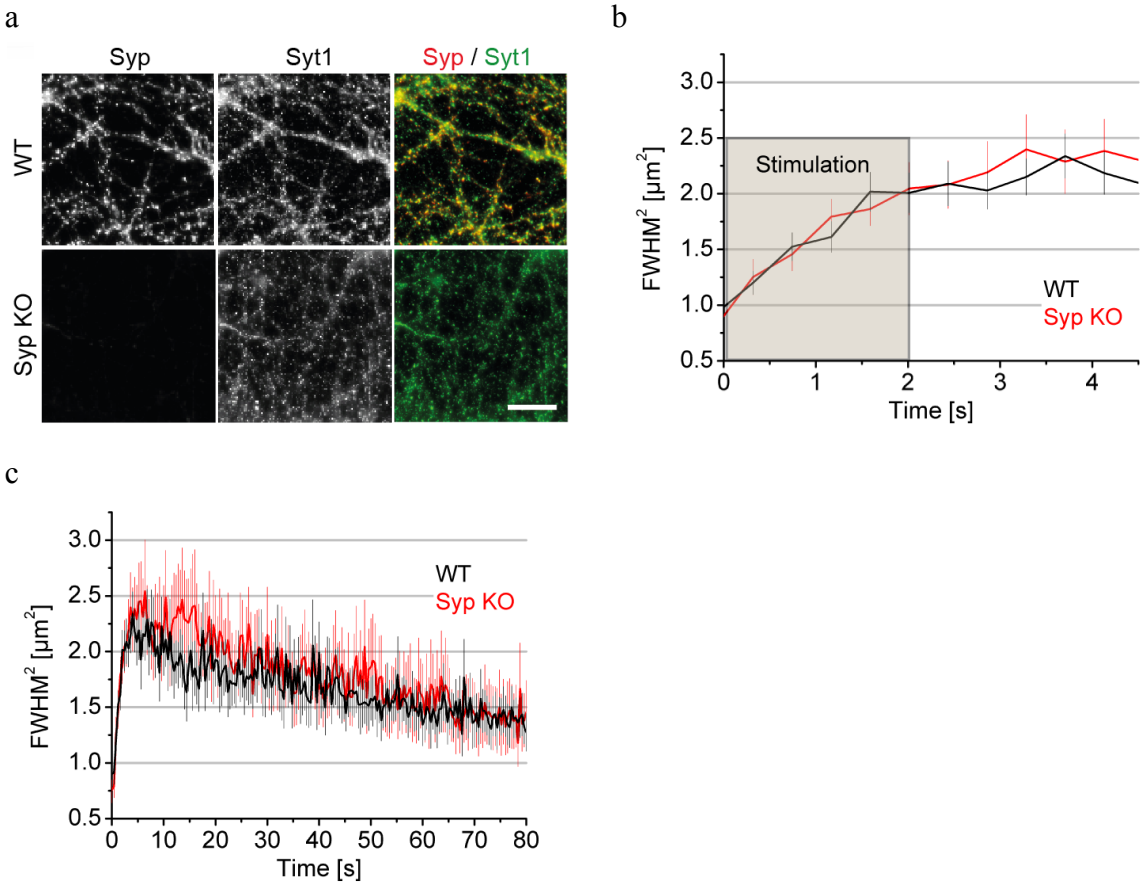

Figure 4-8: Synaptophysin is not crucial for Syb2 confinement and reclustering.

(a) Syp and Syt1 immunolabeling of synaptophysin KO and WT hippocampal neurons. Scale bar, 20 µm. **(b,c)** Syp KO and WT hippocampal neurons expressing Syb2-pH were surface-eclipsed and stimulated in an electric field (40 AP, 20 Hz). The fluorescent signal of newly exocytosed Syb2-pH was fitted with a 2d Gaussian distribution. For both genotypes, the $FWHM^2$ of the Gaussian fit over time shows spreading, confinement (b) and reclustering (c) with no obvious differences between the both genotypes. Mean ± s.e.m.; n = 12 neurons.

4.5 The clathrin-based endocytic machinery modulates post-exocytic protein dynamics

SV proteins undergo an activity-dependent cycle of exo- and endocytosis (Südhof, 2004). Under conditions of low-to-moderate electrical stimulation SV proteins cycle via the RRetP at the plasma membrane (Fernández-Alfonso et al., 2006; Wienisch and Klingauf, 2006; Hua et al., 2011) and are retrieved in part by the clathrin-based endocytic machinery (Granseth et al., 2006; Kononenko et al., 2014). I therefore speculated that the clathrin-based endocytic machinery is not only involved in cargo retrieval, but also in the confinement and reclustering of newly exocytosed SV proteins. This hypothesis was tested with three different manipulations of the clathrin-based endocytic machinery. Post-exocytic dynamics of Syb2 were analyzed upon treatment with the clathrin-specific inhibitor Pitstop 2 (von Kleist et al., 2011; Stahlschmidt et al., 2014), upon depletion of the Syb2-specific endocytic adaptors AP180 and CALM and upon point mutation of the Syb2 SNARE motif, which is crucial for binding to AP180 and CALM (Harel et al., 2008; Koo et al., 2011a, 2015).

4.5.1 Confinement is modulated by the clathrin-based endocytic machinery

Acute clathrin inhibition was achieved by applying the small molecule inhibitor Pitstop 2 to neurons. Pitstop 2 interferes with ligand binding to the N-terminal domain of clathrin HC, which serves as a recruitment hub for AP-2 and accessory proteins including CALM and AP180. Pitstop 2 blocks CME by dramatically increasing the lifetime of clathrin-coated pits (von Kleist et al., 2011). It therefore sequesters endocytic proteins that otherwise may be involved in NEP confinement, in non-productive pits.

The Pitstop 2 efficiency in blocking endocytosis was validated by pHluorin-based imaging of exo- / endocytic cycling (without surface-eclipse). Hippocampal neurons expressing Syb2-pH were stimulated (40AP, 20 Hz) and imaged over time (Figure 4-9a). DMSO treated neurons performed efficient exocytosis, endocytosis, and reacidification, revealed by the rise in Syb2-pH fluorescence, followed by a decline to baseline levels. However, in Pitstop 2 treated neurons, the fluorescence rise was followed by a smaller drop, indicating that endocytosis was impaired. The endocytosis-resistant fraction was increased to ~ 60 % upon Pitstop 2 treatment (Figure 4-9b), whereas the endocytic time constant of the

remaining endocytosed fraction was slightly but not significantly increased (Figure 4-9c). These findings are in agreement with the observation that Pitstop 2 arrests clathrin-coated pits at the plasma membrane (von Kleist et al., 2011). A similar reduction in endocytosis was reported previously upon the depletion of clathrin heavy chain with the same stimulation protocol and Syp-pH as a reporter (Granseth et al., 2006; but see Kononenko et al., 2014).

Next, I examined the effect of acute clathrin inhibition on newly exocytosed SV protein dynamics. In order to sequester a large amount of endocytic proteins into non-productive clathrin-coated pits, multiple stimulations were applied. First, hippocampal neurons expressing Syb2-pH were surface-eclipsed, stimulated (40 AP, 20 Hz) and imaged in the presence of DMSO. After pre-incubation with Pitstop 2 and a second stimulus (Figure 4-9d) to efficiently saturate the clathrin-based endocytic machinery, the procedure was repeated in the presence of Pitstop 2. Both, DMSO-treated and Pitstop 2-treated neurons displayed spreading, confinement (Figure 4-9e) and reclustering (Figure 4-9f). However, newly exocytosed Syb2-pH covered a significantly larger area on Pitstop 2 treated neurons compared to the DMSO control (Figure 4-9g). This suggests that spread and confinement of newly exocytosed Syb2 are limited by the association with the clathrin-based endocytic machinery. Interestingly, the difference in the covered area remained also after reclustering (Figure 4-9h).

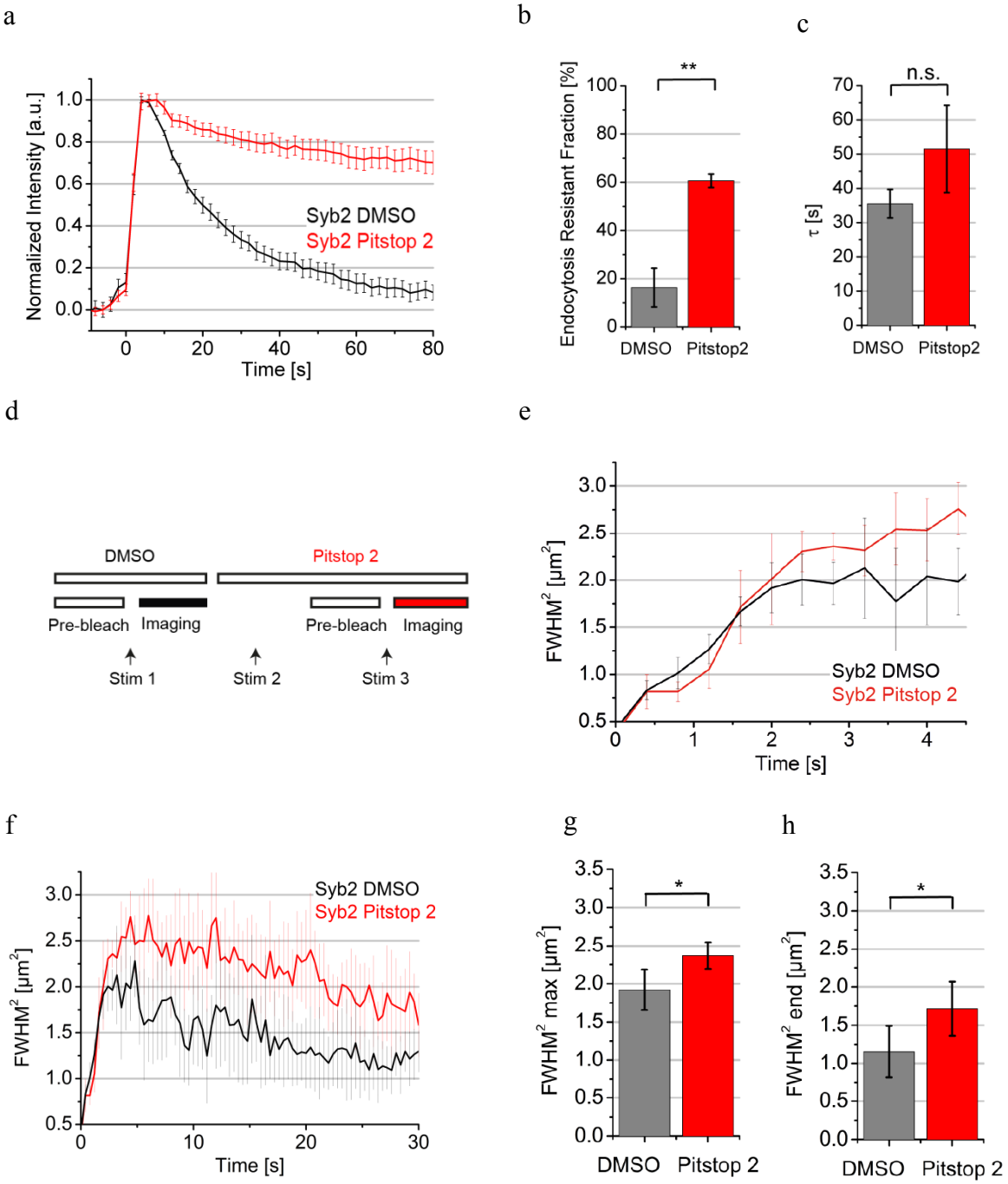

Figure 4-9: Effect of clathrin inhibition on spread and confinement of newly exocytosed proteins.
Hippocampal neurons expressing Syb2-pHluorin were treated with DMSO or Pitstop 2 (20 µM, 2 min). **(a-c)** In order to determine the effect of Pitstop 2 on endocytic kinetics, neurons were stimulated (40 AP, 20 Hz) and imaged over time without surface-eclipse (a). The endocytosis resistant fraction (b) and the endocytic time constant τ (c) were obtained from a single exponential fit on the data displayed in (a). **(d-h)** To study spread and confinement, neurons were treated with DMSO or Pitstop 2 (20 µM, 2 min) and stimulated (each stimulation: 40 AP, 20 Hz) as displayed in the scheme (d). $FWHM^2$ of the Gaussian fit of pHluorin signals from

newly exocytosed proteins over time show phases of spreading, confinement (e) and reclustering (f) at both conditions. Maximal spread (g) and the last time point (h) were measured from data in (f). Mean ± s.e.m.; N = 3 individual experiments (a-c, e-h); Statistical significance was tested with a two-tailed paired t-test. ** $p < 0.01$, * $p < 0.05$.

4.5.2 Depletion of AP180 and CALM reduces Syb2 confinement

Pitstop 2 increases lifetimes of several endocytic proteins in clathrin-coated pits (von Kleist et al., 2011). It is therefore conceivable that arresting CME by Pitstop 2 results in the sequestration of endocytic proteins, possibly including factors such as endophilin and dynamin with roles in both CME as well as clathrin-independent endocytosis (Kononenko et al., 2014; Boucrot et al., 2015). Thus, it remains unclear, which specific endocytic proteins are required for the observed Syb2 confinement. As the endocytic adaptors AP180 and CALM have been implicated in the specific retrieval of Syb2 (Grote and Kelly, 1996; Bushlin et al., 2008; Koo et al., 2011a) I hypothesized that either one or both of these proteins are required for Syb2 confinement.

AP180 deficient mice were generated, genotyped and validated by western blot, as recently described by Koo et al. (Koo et al., 2015) in collaboration with Dr. Tanja Maritzen (Leibniz Institute for Molecular Pharmacology, Berlin). To obtain homozygote AP180 KO and WT mice, AP180 heterozygous mice were bred with each other. Mice were then genotyped by PCR analysis of genomic DNA (Figure 4-10a). Western blots against AP180 confirm the lack of AP180 in KO animals by the lack of the specific 180 kDa band in KO brain lysates (Figure 4-10b). Hippocampal neurons were then prepared from mice homozygous for either the WT or the KO allele.

In order to obtain AP180 and CALM double-deficient neuronal cultures (AP180 KO / CALM KD), AP180 KO neurons were transfected with a CALM-specific shRNA. WT neurons were transfected with a scrambled (Scr) control shRNA and used as control cells (WT / Scr). The fluorescent protein mKate served as a marker for transfected cells and was co-expressed from the same vector as the shRNA. CALM knockdowns were verified by a CALM-specific immunolabeling on transfected neuron cultures. Confocal images of WT / Scr neurons show an intense CALM-specific staining that is almost absent in AP180 KO / CALM

KD neurons, but not in untransfected neurons within the same images (Figure 4-10c). This demonstrates the efficient knockdown.

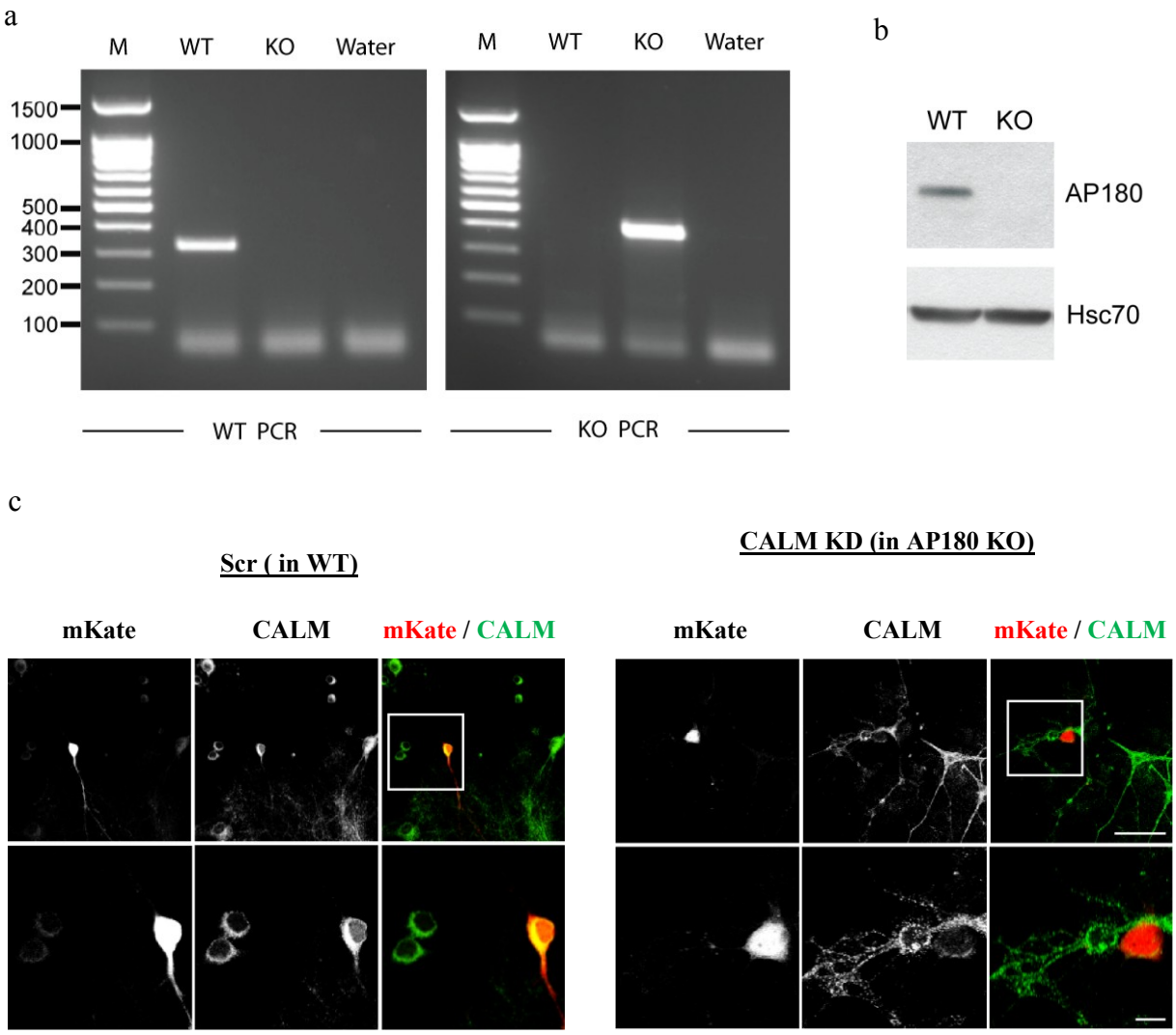

Figure 4-10: Validation of AP180 and CALM deficiency.

(a) AP180 KO verification by PCR on genomic DNA using a primer set generating a 323 bp product in the presence of the WT allele (WT PCR) and a primer set generating a 401 bp product in presence of the KO allele (KO PCR). A reaction without genomic DNA (water) was run as control. **(b)** Western blot of brain lysates from WT and AP180 KO mice (p1), detected with an anti AP180 and anti Hsc70 (Heat Shock Cognate Protein 70, loading control) antibody. **(c)** CALM and AP180 deficient hippocampal neurons were generated from AP180 KO neurons by shRNA mediated CALM knockdown (KD). Confocal images of CALM in wild-type (WT) neurons expressing scrambled (scr) shRNA and in AP180 KO neurons expressing CALM-specific shRNA demonstrate the efficient knockdown of CALM. mKate expressed from the same vector as the shRNA serves as a marker for transfected cells. Scale bar, 50 µm, zoom 10 µm.

Next, post-exocytic Syb2-pH dynamics in surface-eclipsed AP180 / CALM deficient neurons and corresponding WT / Scr control neurons were analyzed upon electrical stimulation (40AP, 20 Hz). Both genotypes displayed spreading, confinement (Figure 4-11a), and reclustering of Syb2-pH (Figure 4-11b). However, in AP180 KO / CALM KD neurons, newly exocytosed Syb2-pH covered a significantly larger area after spreading, compared to control neurons (Figure 4-11c). This difference remained also after reclustering (Figure 4-11d). However, the half-time of reclustering was unaltered (Figure 4-11e), demonstrating that endocytic adaptors like AP180 or CALM are required for confinement, but do not affect the reclustering rate of newly exocytosed Syb2. Interestingly Syb2-pH appeared to spread a little faster in AP180 KO / CALM KD neurons (Figure 4-11a). This could be explained by a faster diffusion of Syb2 alone, in comparison to a complex of Syb2 with AP180 or CALM and potential further indirect binding partners (see also chapter 4.6.3).

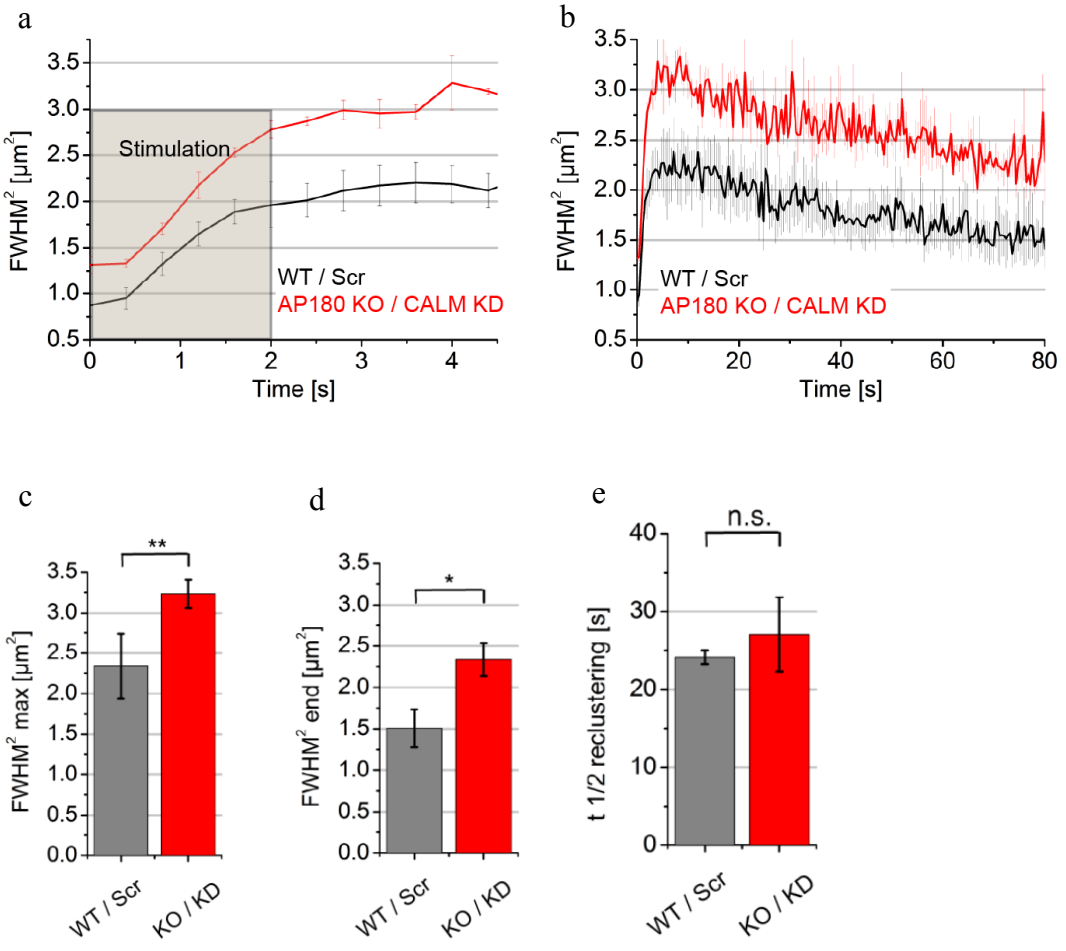

Figure 4-11: AP180 and CALM modulate the spread and confinement of newly exocytosed Syb2.

Syb2-pH expressing hippocampal neurons lacking AP180 (KO) and depleted of CALM (KD) or wild-type (WT) neurons treated with scrambled (Scr) shRNA were surface-eclipsed and stimulated in an electric field (40 AP, 20 Hz). The fluorescence signal of newly exocytosed Syb2-pH was fitted with a 2d Gaussian distribution. **(a,b)** The $FWHM^2$ of the Gaussian fit over time shows spreading, confinement (a), and reclustering (b) for both conditions. **(c-e)** Maximal spread (c), last time point (d), and half-time $t_{1/2}$ of reclustering (e) were measured from data in (b). Mean ± s.e.m.; N = 3 independent experiments. Statistical analysis was done by two-tailed paired t-test. ** $p < 0.01$, * $p < 0.05$.

4.5.3 AP180- and CALM-deficient neurons fail to sort Syb2 into SVs

A previous study from our group showed, that the KD of AP180 or CALM results in increased surface levels of Syb2 in hippocampal neurons. This effect was additive and accumulated to a ~ 2-fold increase in Syb2 surface levels in double-knockdown neurons, compared to WT control neurons (Koo et al., 2011a).

I hypothesized that this is a consequence of post-exocytic Syb2 mis-sorting and that AP180 KO / CALM KD neurons would similarly accumulate Syb2 on their surface. In order to substantiate this hypothesis, Syb2-pH surface levels of transfected AP180 KO / CALM KD and WT / Scr hippocampal neurons were measured in cultures that were silenced with the voltage-gated sodium channel blocker tetrodotoxin (TTX) and untreated neurons. Surface-stranded Syb2-pH was detected on fixed neurons with fluorescently labeled anti-GFP nanobodies. The signal of nanobody-labeled surface-stranded Syb2-pH was compared with the fluorescence of total Syb2-pH after unquenching (Figure 4-12a). As expected from the recent findings in AP180 / CALM double-knockdown cells (Koo et al., 2011a), Syb2-pH surface levels were ~ 2-fold increased in AP180 KO / CALM KD neurons. Strikingly, silencing of neuronal activity by the application of TTX rescued elevated Syb2 surface accumulations of AP180 / CALM deficient neurons to WT / Scr levels, suggesting that increased surface levels are indeed the long-term consequence of impaired post-exocytic Syb2 mis-sorting.

Previous work from our group demonstrates that KD of AP180 slightly (~ 20 %) increases Syb2 surface levels in hippocampal synapses (Koo et al., 2011a). Since AP180 KD neurons may still express small amounts of AP180, I wanted to determine, how strong the complete loss of AP180 would affect Syb2 sorting. To address this question, Syb2-pH surface levels were measured in transfected hippocampal neurons by applying acid-base washes.

Acidic buffer quenches surface pHluorin, whereas basic buffer unquenches all vesicular pHluorin. Acid-base washes can thus be used to calculate surface levels of pHluorin-tagged SV proteins (see also chapter 3.4.12 and Diril et al., 2006). The Syb2-pH surface fraction was increased by ~ 40 % in AP180 KO neurons (Figure 4-12b). Surface levels could be rescued completely by the re-expression of AP180 WT in AP180 KO neurons, but not by mutant AP180 (L219S/M244K) that cannot bind Syb2 (Koo et al., 2015).

Syb2 surface-levels of neurons lacking only AP180 were affected much milder than that of AP180 and CALM double-deficient neurons, suggesting that CALM in addition to neuron-specific AP180 is required to maintain Syb2 sorting.

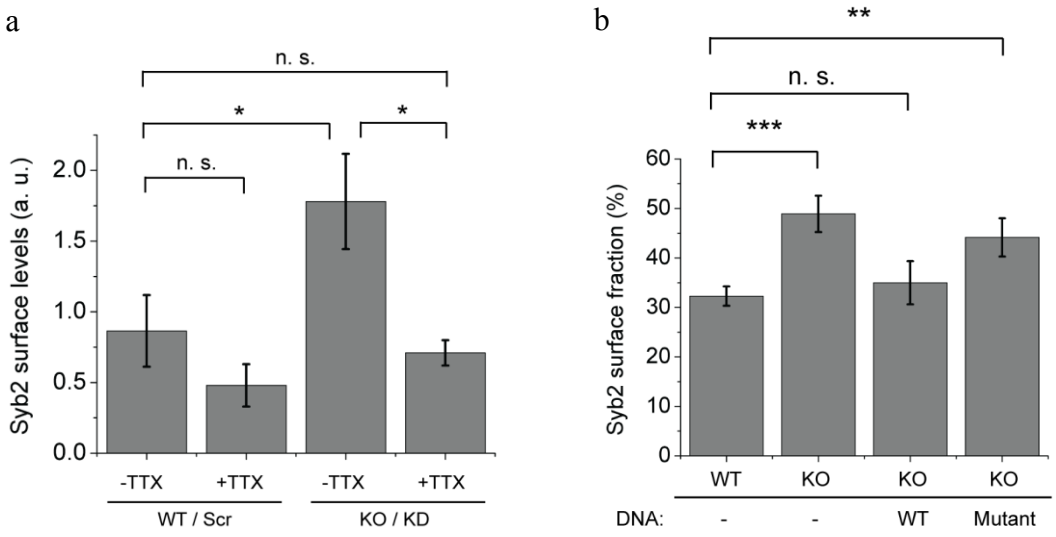

Figure 4-12: Activity dependent Syb2 surface accumulation of neurons lacking AP180 or AP180 / CALM. **(a)** Relative Syb2-pH surface levels of transfected hippocampal WT / Scr and AP180 KO / CALM KD neurons. Neuron cultures were silenced for eight days with 1 µM tetrodotoxin (TTX). Surface-stranded Syb2-pH was stained on fixed cells with anti-GFP nanobody (CF647 labeled). Surface levels correspond to the surface labeling normalized to the total pHluorin fluorescence after unquenching. Mean ± s.e.m.; N = 3 independent experiments. Statistical analysis was done with a one-way-ANOVA after transformation into Z scores to compensate for differences in absolute fluorescence intensities between independent experiments. **(b)** Syb2-pH surface fraction of WT and AP180 KO hippocampal neurons re-expressing AP180 WT or mutant (L219S / M244K), determined by applying acid-base washes (chapter 3.4.12). Mean ± s.e.m.; Neurons from 2 independent experiments: WT (n = 12), AP180 KO (n = 30), AP180 KO re-expressing AP180 WT (n = 25), AP180 KO expressing mutant AP180 (n = 24). Statistical analysis was done with a one-way-ANOVA. *** $p < 0.001$, ** $p < 0.01$, * $p < 0.05$.

4.5.4 Efficient Syb2 confinement requires the association with AP180 or CALM

AP180 and CALM deficiency may lead to secondary effects, since both adaptors are involved in clathrin recruitment to $PI(4,5)P_2$ in the plasma membrane (Ahle and Ungewickell, 1986; Ford et al., 2001). To avoid potential biases from AP180 and CALM deficiency, the influence of both endocytic adaptors on post-exocytic Syb2 dynamics was further studies with a Syb2 recycling mutant. The point-mutation of methionine 46 within the Syb2 SNARE motif to alanine (M46A) abolishes the association with AP180 and CALM. This leads to a major redistribution of Syb2 (M46A) to the plasma membrane (Grote and Kelly, 1996; Harel et al., 2008; Koo et al., 2011a), similar to Syb2 (WT) in AP180- and CALM-deficient neurons (Figure 4-12a).

To investigate whether the localization of surface-stranded Syb2 M46A is altered in comparison to Syb2 WT, Syb2-c-myc (WT) and Syb2-pH (M46A) surface pools of co-transfected hippocampal neurons were immunolabeled and analyzed with the super-resolution microscopy technique “spectral-demixing direct stochastic optical reconstruction microscopy” (SD-*d*STORM; Lampe et al., 2012; Lehmann et al., 2015). Intriguingly, Syb2 (M46A) predominantly localized at axonal structures, in contrast to Syb2 (WT) which revealed a distinct boutonic localization (Figure 4-13). This indicates that, beside their relevance for acute NEP confinement (Figure 4-11), the endocytic adaptors AP180 and CALM are also implicated in the long-term maintenance of synaptic confinement on neuronal surfaces.

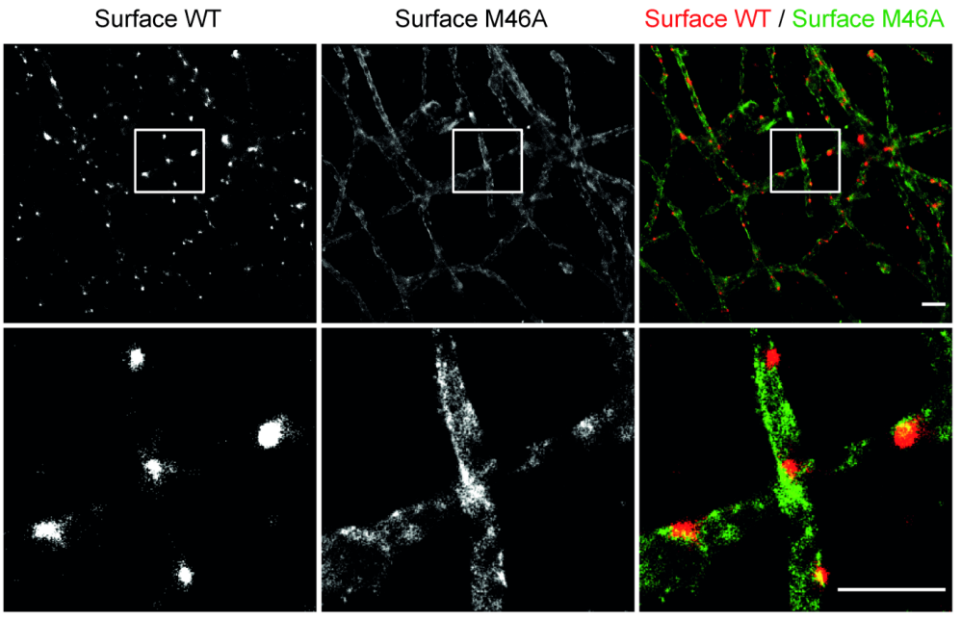

Figure 4-13: Syb2 (WT) but not (M46A) displays boutonic localization.
SD-*d*STORM imaging of hippocampal neurons expressing both, Syb2-c-myc (WT) and Syb2-pH (M46A). Syb-2 proteins on the neuronal surface were immunolabeled with primary and fluorescent secondary antibodies (WT: CF 647-labeled, M46A: Alexa 647-labeled) without plasma membrane permeabilization. Note the axonal localization of Syb2 (M46A) in contrast to a bouton-like localization of Syb2 (WT). Scale bar, 1.5 µm, zoom 1.5 µm.

Considering, that the absence of the endocytic adaptors AP180 and CALM causes defects in acute Syb2 confinement (chapter 4.5.2), it is very likely that the Syb2 (M46A) redistribution on the plasma membrane originates at least in part from a reduced confinement of the newly exocytosed mutant. In order to address this issue, pHluorin tagged Syb2 WT or M46A was expressed in hippocampal neurons. In line with the super-resolution images in Figure 4-13, unquenched plasma membrane localized Syb2-pH (WT) was found on bouton-like structures, while Syb2-pH (M46A) localization was less distinct, with a major fraction being localized on the axon (Figure 4-14a). Neurons were surface-eclipsed and stimulated (40AP, 20Hz). Fluorescence intensity changes were recorded in the synaptic regions that were also used for the spatiotemporal analysis of the NEP spreading. Note that these regions are larger than the narrow regions that were selected to determine synaptic escape in Figure 4-2 and Figure 4-3, as they must provide enough spatial information for the analysis of NEP dynamics. Both WT and M46A displayed a fluorescence increase, corresponding to

exocytosis and no signs of endocytosis (Figure 4-14b). Since no fluorescence decay was observed, newly exocytosed SV proteins did not escape from these enlarged regions. The spatiotemporal analysis of Syb2 WT and M46A revealed spreading, confinement (Figure 4-14c) and reclustering (Figure 4-14d) of both proteins. However, the mutant Syb2-pH showed a slightly faster spread (Figure 4-14c). Directly after spreading (Figure 4-14e) and until the end of reclustering (Figure 4-14f), the mutant covered a significantly larger area compared to WT Syb2-pH, while the half-time was unaltered (Figure 4-14g). Hence, Syb2-pH (M46A) phenocopied the post-exocytic dynamics of Syb2-pH (WT) in AP180 KO / CALM KD neurons.

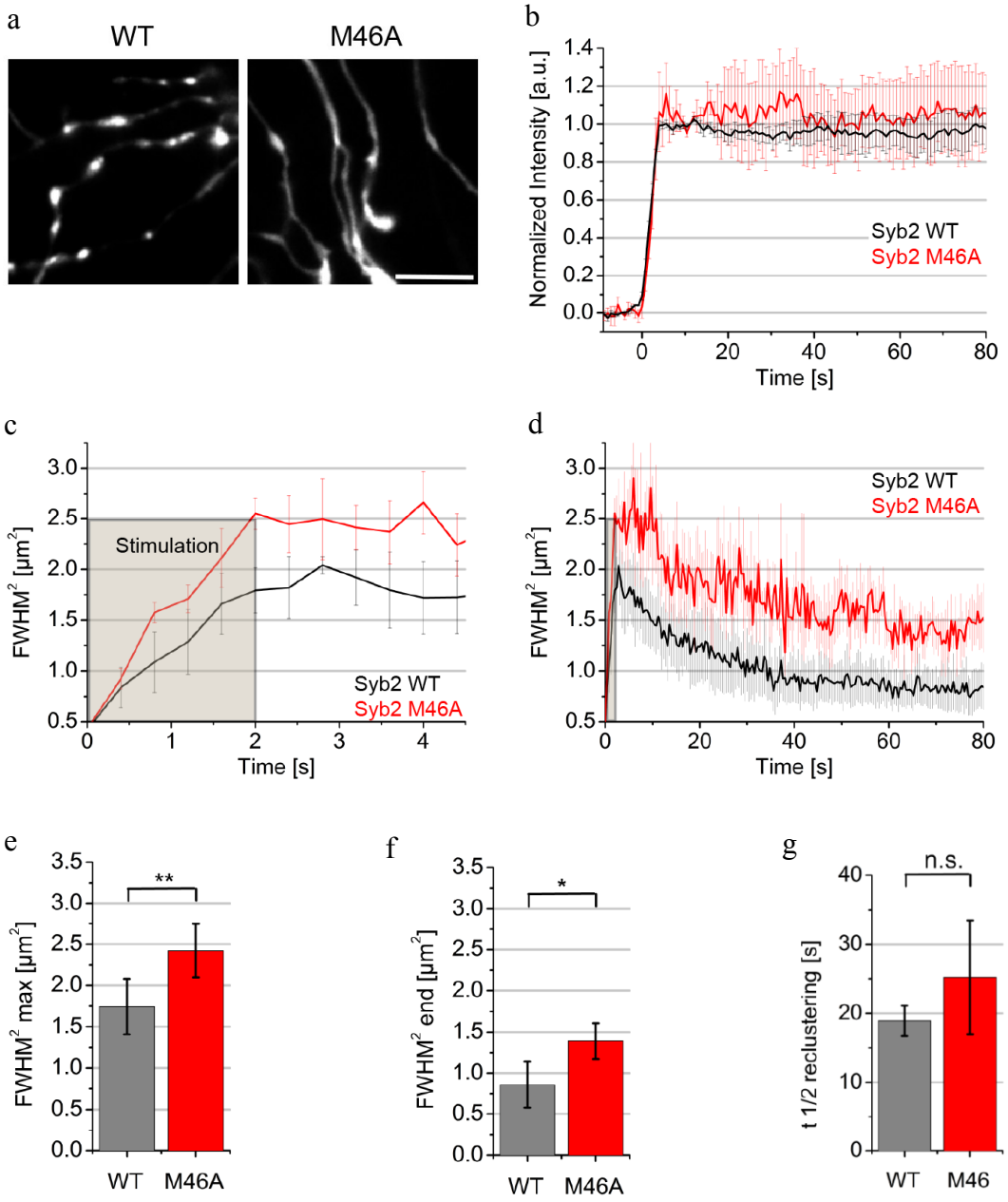

Figure 4-14: Spread and confinement of Syb2 are modulated by the association with AP180 or CALM.

(a) Widefield images of hippocampal neurons expressing wild-type (WT) or mutant (M46A) Syb2-pH. Scale bar, 5 µm. Note the large axonal surface pool of Syb2 (M46A). **(b-g)** Hippocampal neurons expressing wild-type or mutant Syb2-pH were surface-eclipsed and stimulated in an electric field (40 AP, 20 Hz). Fluorescence intensity changes upon stimulation were recorded from expanded synaptic regions, corresponding to the regions for the fitting procedure (b). The fluorescence signal of newly exocytosed proteins was fitted with a 2d Gaussian distribution in each single image. The $FWHM^2$ of the Gaussian fit over time shows spreading, confinement (c), and reclustering (d) at both conditions. Maximal spread (e), last time point (f), and half-time $t_{1/2}$ of reclustering (g) were measured from data in (d). Mean ± s.e.m.; N = 3 independent experiments. Statistical analysis was done with a two-tailed paired t-test. ** $p < 0.01$, * $p < 0.05$.

4.6 Diffusion drives release site clearance

The disruption of the clathrin-based endocytic machinery leads to short-term synaptic depression in various model organisms. Several lines of evidence suggest that this phenomenon is not due to a depletion of SVs (Hosoi et al., 2009; Kawasaki et al., 2000; Sakaba et al., 2013; Hua et al., 2013). A model was suggested in which SV proteins block release sites and efficient release site clearance is required for sustained neurotransmission (Neher, 2010). Lateral diffusion and the directed actin-dependent transport were suggested as driving force for release site clearance (Haucke et al., 2011). However, up to date, no data exists that validates either model.

4.6.1 Mathematical modeling of diffusional spread

To test whether the initial spread of newly exocytosed SV proteins is mediated by their diffusion or by active transport we used mathematical modelling in comparison to the experimental data. The fluorescence signal originating from the fusion of a single SV can mathematically be treated as a single point source of diffusive material. In the case of pure diffusion the $FWHM^2$ increase linearly over time (Crank, 1975). However, single SV fusion signals are very low. Thus, multiple action potentials were applied in the experiment, leading to the fusion of most of the vesicles of the readily releasable pool (Schikorski and Stevens, 2001). The measured fluorescence was thus an overlay from several fusion events at different time-points. To nevertheless be able to interpret the $FWHM^2$ time-trace we assumed the signal as a superposition of multiple successive fusion events in the mathematical model. This assumption is corroborated by the stimulation-induced increase in pHluorin-derived fluorescence over the time-course of stimulation (Figure 4-15a). Intensity changes between two successive images served as a measure for the relative number of fused SVs during that timeframe. Each exocytic event generates a signal that follows a Gaussian distribution and is defined by the elapsed time, the amount of released material and the diffusion coefficient (Crank, 1975). Gaussian distributions from single fusion events were summed up (Figure 4-15b) and compared to the experimentally determined $FWHM^2$ of the initial SV protein spread during stimulation (see also chapter 3.5.10). Diffusion coefficients were adjusted to yield the best match between the modelled and the experimental data. This procedure allowed

us to identify the mode of movement and, in the case of Brownian motion, to measure the corresponding diffusion coefficient.

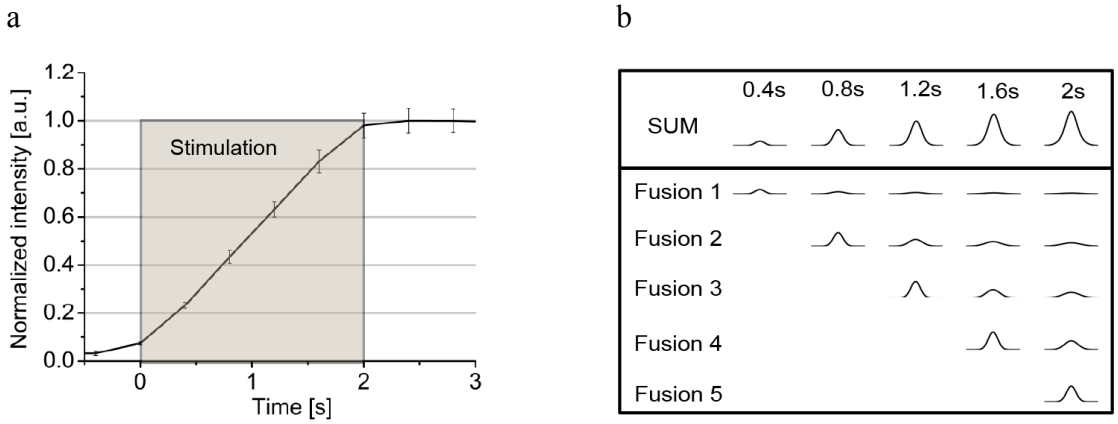

Figure 4-15: A model to describe the distribution of newly exocytosed proteins from overlaid, successive fusion events.

In order to determine diffusion coefficients for newly exocytosed proteins, a model of free diffusion after successive fusion of synaptic vesicles was applied. The relative amount of fused vesicles at a given time was experimentally determined from the pHluorin increase after stimulation (40 AP, 20Hz) of surface-eclipsed hippocampal neurons. **(a)** The Syb2-pHluorin fluorescence increase was used to model free diffusion of successively fusing Syb2-pH. Mean ± s.e.m.; N = 5 independent experiments. **(b)** Assuming that released proteins travel by Brownian motion, the pHluorin signal in (a) can be spatially approximated by the overlay of several Gaussian distributions (SUM) from multiple exocytic events (e. g. Fusion 1 - 5). The FWHM of each Gaussian distribution depends on the elapsed time from exocytosis and on the diffusion coefficient of the pHluorin-tagged protein. The amplitude is defined by the intensity changes during the corresponding frame in (a).

4.6.2 Newly exocytosed SV proteins spread by Brownian motion

The above described mathematical diffusion model was applied to the experimentally determined initial spread of Syb2-pH, Syt1-pH and Syp-pH from Figure 4-6 to investigate whether their post-exocytic spread is caused by diffusion. During the first time-point the model underestimated the $FWHM^2$ of the microscopic data, probably due to limitations in resolution and sensitivity of the microscopy setup. However, for all following values, $FWHM^2$ time-courses displayed no significant difference between model and experimental

data (Figure 4-16a-c) after adjusting the diffusion coefficients for all three SV proteins. The fact that no further assumption had to be made to match modelled and experimental data indicates that Brownian motion, rather than active transport is the "driving force" behind the initial spread of newly exocytosed SV proteins. Diffusion coefficients from the best-fit model of Syb2-pH, Syt1-pH and Syp-pH did not differ significantly from each other. They were all in the range of ~ 0.2 - 0.3 $\mu m^2/s$ (Figure 4-16d).

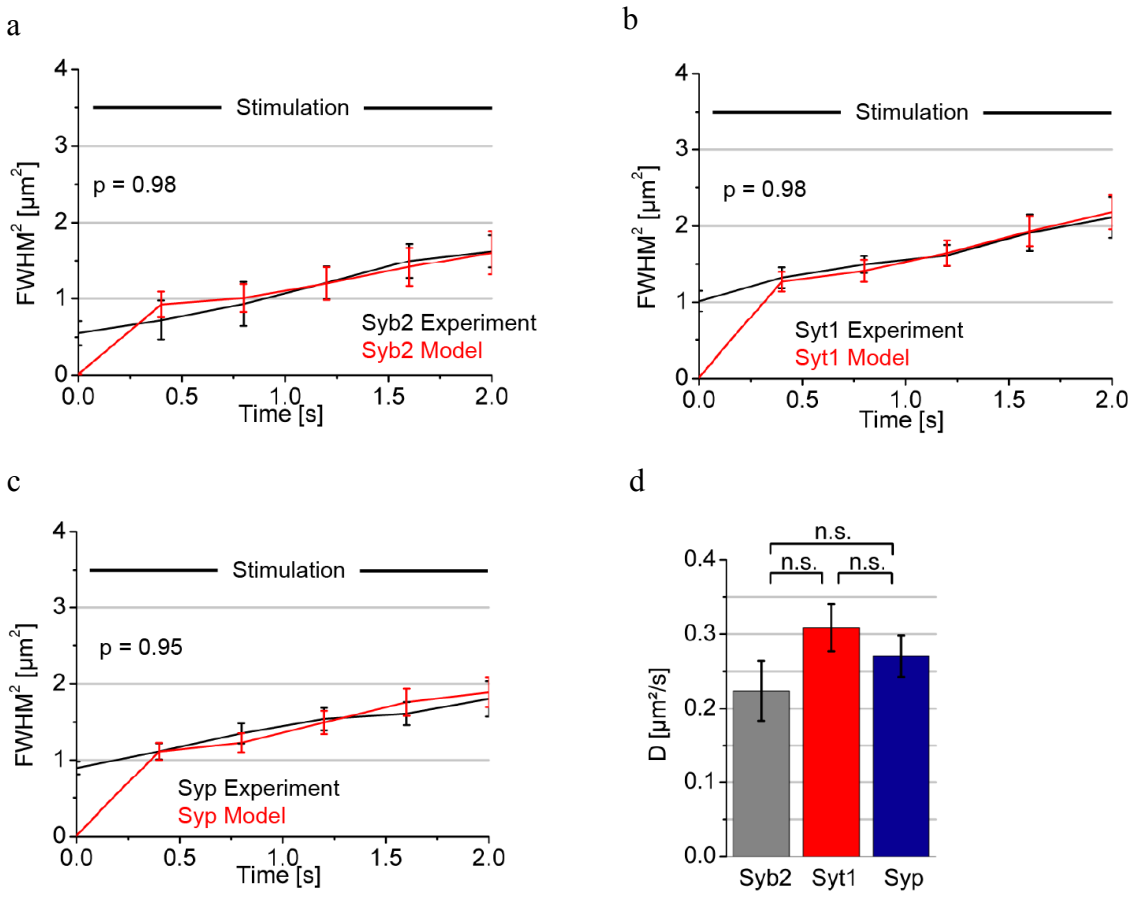

Figure 4-16: The initial spread of newly exocytosed SV proteins is mediated by diffusion.
Diffusion coefficients were adapted to yield the best match between modelled FWHM² and experimentally determined FWHM² during the initial SV protein spread. **(a-c)** Best fit of the model FWHM² and experimentally determined FWHM² of newly exocytosed Syb2-pH (a), Syt1-pH (b) and Syp-pH (c) during electrical stimulation (40 AP, 20 Hz) of surface-eclipsed hippocampal neurons. **(d)** Diffusion coefficients (D) that give the best fit between model traces and experimental data, displayed in (a-c). Mean ± s.e.m.; independent experiments: Syb2 (n = 5), Syt1 (n = 3), Syp (n = 3). Statistical analysis was done with a two-way ANOVA with repeated measures (a-c), time points 0.8-2 s) or a two-tailed unpaired t-test (d).

4.6.3 Endocytic adaptors restrict Syb2 diffusion

Endocytic adaptors are required for the efficient confinement of the NEP (chapters 4.5.2 and 4.5.4). However, it is not clear, whether they bind their diffusive cargo (chapter 4.6.2) at the moment of immobilization, during the phase of diffusion or even prior to the SV fusion with the plasma membrane. Thus, the question arises, whether endocytic adaptors influence Syb2 diffusion during the first seconds after insertion into the plasma membrane. Interestingly, Syb2-pH spreading seemed to be faster upon abolished AP180 / CALM binding (Figure 4-11a; Figure 4-14c). However, since the detected fluorescent signal was an overlay of signals originating from several SVs, it is unclear, whether this corresponds to faster diffusion or to altered exocytic kinetics. I next investigated how impaired AP180 or CALM binding affects the diffusion of newly exocytosed Syb2 (M46A). Therefore, the mathematical diffusion model was applied to the experimental determined spread of Syb2-pH (WT) and Syb2-pH (M46A), which was displayed in Figure 4-14.

The $FWHM^2$-traces from the diffusion model were again matched to the experimentally determined data by choosing appropriate diffusion coefficients. The good match indicated that Syb2 (WT) and the mutant of Syb2 (M46A) both spread by Brownian motion (Figure 4-17a,b). However, the diffusion of the mutant Syb2 (M46A) was significantly accelerated (Figure 4-17c) suggesting that indeed AP180 or CALM bind to Syb2, before or immediately after exocytosis, and thereby slow down Syb2 diffusion.

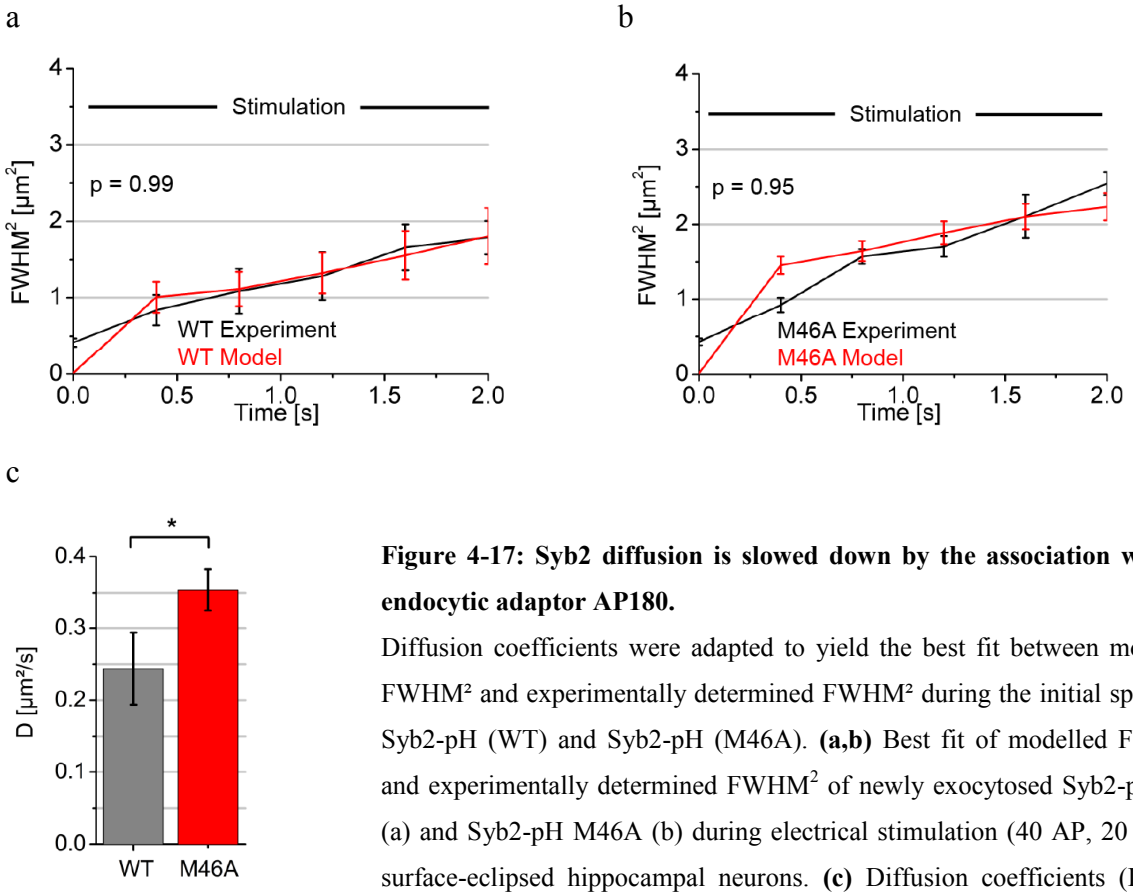

Figure 4-17: Syb2 diffusion is slowed down by the association with its endocytic adaptor AP180.

Diffusion coefficients were adapted to yield the best fit between modelled FWHM² and experimentally determined FWHM² during the initial spread of Syb2-pH (WT) and Syb2-pH (M46A). **(a,b)** Best fit of modelled FWHM² and experimentally determined FWHM^2 of newly exocytosed Syb2-pH WT (a) and Syb2-pH M46A (b) during electrical stimulation (40 AP, 20 Hz) of surface-eclipsed hippocampal neurons. **(c)** Diffusion coefficients (D) that give the best fit between model traces, displayed in (a,b), and experimental data. Mean ± s.e.m.; N = 3 independent experiments. Statistical analysis was done with a two-way ANOVA with repeated measures (a,b), time points 0.8-2 s) or a two-tailed paired t-test (c). * $p < 0.05$.

4.6.4 Inhibition of the clathrin terminal domain does not affect Syb2 diffusion

Pitstop 2 increases clathrin-coated pit lifetimes and sequesters endocytic proteins into arrested pits (von Kleist et al., 2011). This apparently interferes with Syb2 confinement (see chapter 4.5.1). Next, I wanted to investigate when those proteins that confine Syb2 bind to it. I therefore wanted to find out if they bind during the diffusion phase, like AP180 and CALM, or if they rather bind to Syb2 during immobilization. Therefore the diffusion model was applied to the experimentally determined spread of newly exocytosed Syb2-pH in Pitstop 2 and DMSO treated neurons, which is displayed in (Figure 4-9). Modelled FWHM²-traces matched the experimentally determined spread of newly exocytosed Syb2-pH after DMSO or Pitstop 2 treatment (Figure 4-18a,b). Again, the traces were consistent with diffusion, without

a contribution from active transport. Remarkably, in contrast to an abrogation of Syb2-binding to AP180 and CALM (see chapter 4.6.3), arresting clathrin-coated pits with Pitstop 2 had no effect on Syb2-pH diffusion rates (Figure 4-18c). These data suggest that the affected Syb2-confining proteins do not diffuse together with Syb2, but rather bind to newly exocytosed SV proteins during the confinement phase.

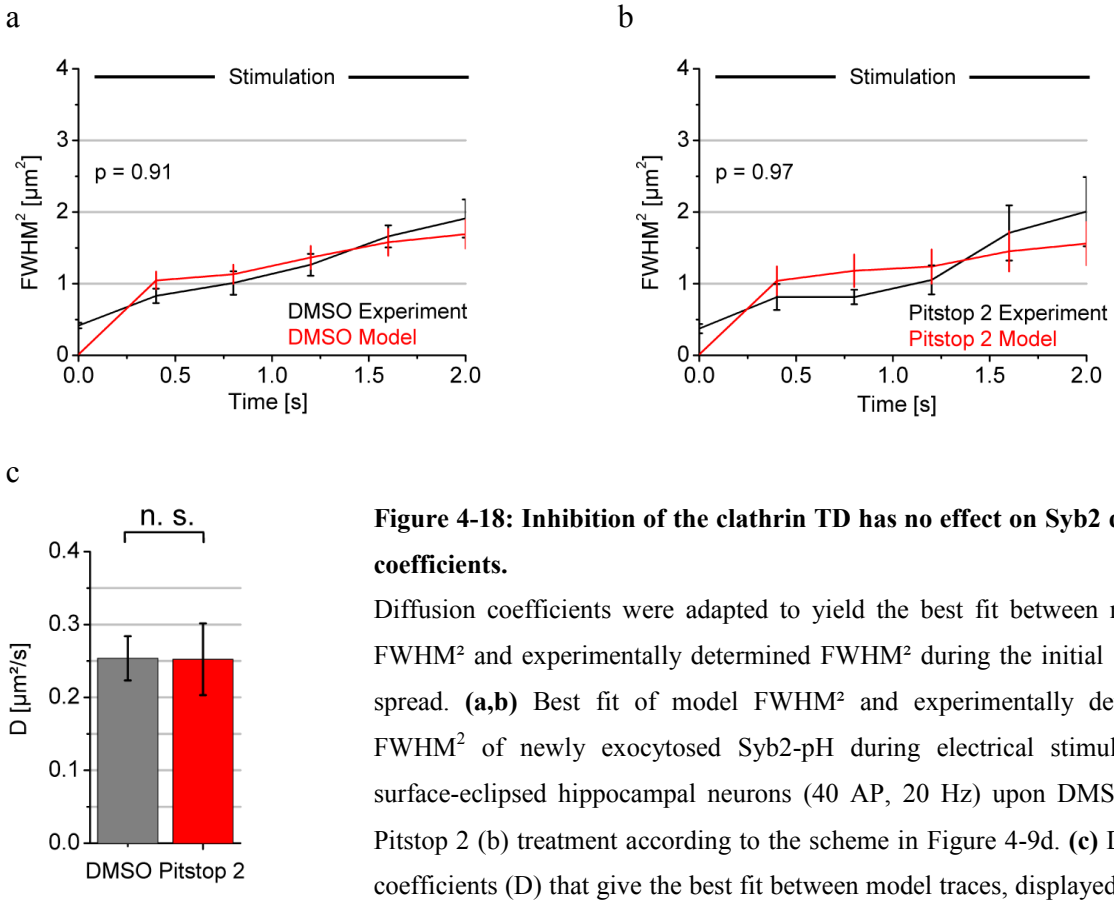

Figure 4-18: Inhibition of the clathrin TD has no effect on Syb2 diffusion coefficients.

Diffusion coefficients were adapted to yield the best fit between modelled FWHM² and experimentally determined FWHM² during the initial Syb2-pH spread. **(a,b)** Best fit of model FWHM² and experimentally determined FWHM² of newly exocytosed Syb2-pH during electrical stimulation of surface-eclipsed hippocampal neurons (40 AP, 20 Hz) upon DMSO (a) or Pitstop 2 (b) treatment according to the scheme in Figure 4-9d. **(c)** Diffusion coefficients (D) that give the best fit between model traces, displayed in (a,b), and experimental data. Mean ± s.e.m.; N = 3 independent experiments. Statistical analysis was done with a two-way ANOVA with repeated measures (a-d, time points 0.8-2 s) or a two-tailed paired t-test (e-f).

4.7 Spatial segregation of preexisting and newly exocytosed SV proteins

The RRetP is organized in nano-clusters in the plasma membrane of hippocampal neurons (Willig et al., 2006; Opazo et al., 2010; Hua et al., 2011). However it is not clear, if these clusters correspond to SVs that remained as patches after fusion with the plasma

membrane or if they reformed after dispersal. The latter possibility could lead to protein intermixing between SVs but also between newly exocytosed SV proteins and preexisting surface-stranded proteins. I therefore investigated, whether newly exocytosed SV proteins are distributed in nano-clusters, like the RRetP, and whether they intermix with unretrieved surface-stranded proteins.

4.7.1 A strategy to selectively label newly exocytosed SV proteins

In order to address the question, whether newly exocytosed proteins intermix with the preexisting pool of surface-stranded proteins, both pools were labeled with a sequential staining protocol, without membrane permeabilization. Transfected hippocampal neuron, expressing Syb2-c-myc were labeled with anti c-myc primary antibody, stimulated (40 APs, 20 Hz) and fixed. Unretrieved primary antibodies, binding preexisting surface-stranded proteins were saturated with an excess of Alexa 488-labeled Fab fragments. Newly exocytosed proteins were labeled in a second round with primary c-myc antibodies and Alexa 647-labeled Fab fragments (Figure 4-19a).

In the absence of electrical stimulation, widefield images and corresponding synaptic intensity profiles reveal a selective labeling of the Syb2 surface-stranded pool and, as expected, no labeling of the newly exocytosed pool (Figure 4-19b,c). This indicates that surface-stranded proteins were efficiently saturated. However, after electrical stimulation (40AP, 20 Hz) newly exocytosed Syb2 was efficiently labeled, in addition to the surface-stranded pool (Figure 4-19b,d). Interestingly both signals displayed only minor overlap, suggesting that both pools did not completely intermix. However, due to the limited resolution of conventional microscopy (Abbe, 1873) the precise nanoscale distribution of these synaptic protein pools could not be resolved.

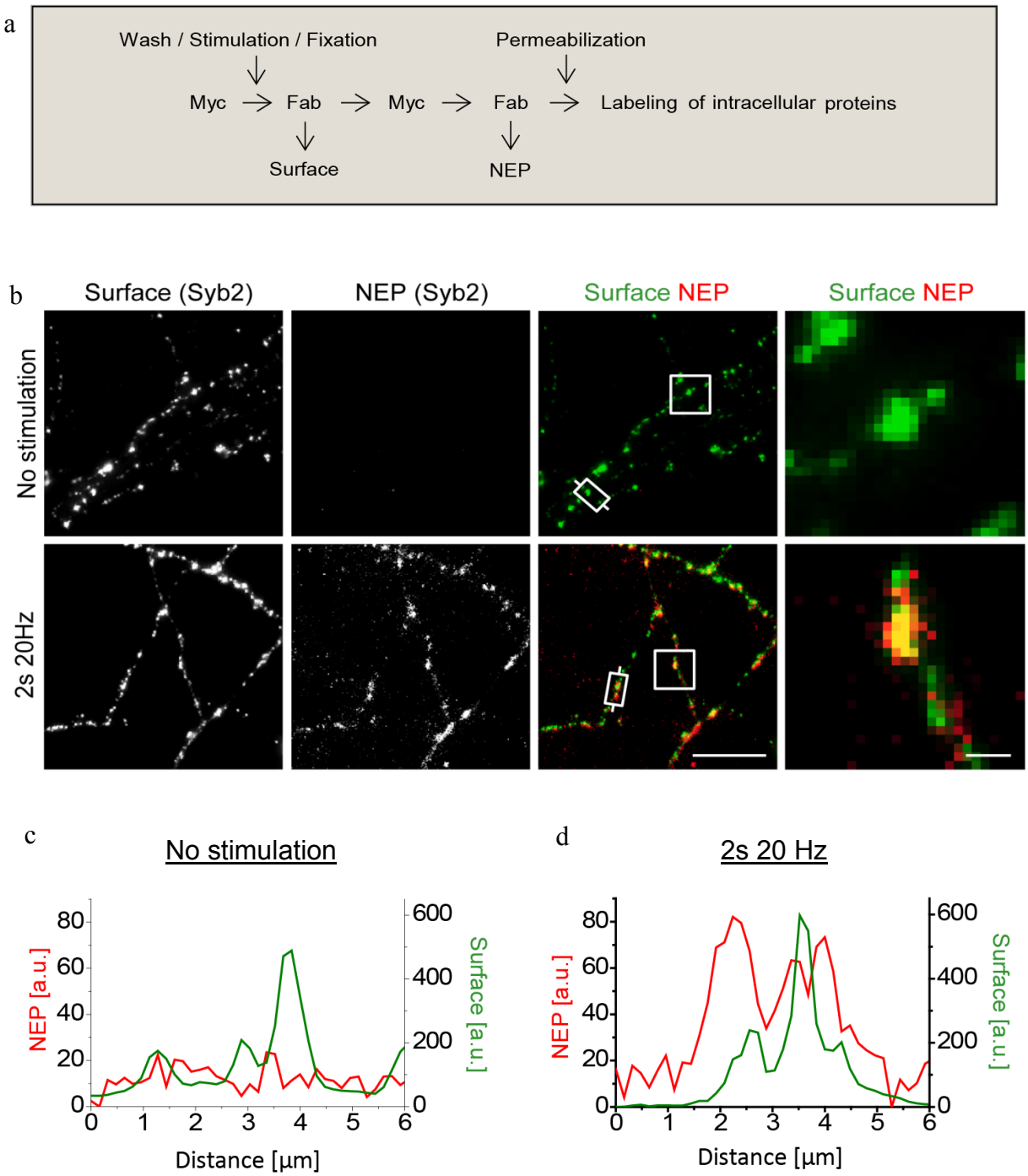

Figure 4-19: Distinct localization of newly exocytosed and surface-stranded Syb2.

Hippocampal neurons expressing Syb2-c-myc were stimulated (40 APs, 20 Hz) and stained for newly exocytosed Syb2 and for the surface-stranded pool of Syb2 (proteins that were localized on the neuronal surface before stimulation but were not recycled upon stimulation). **(a)** Schematic for the immunolabeling of the NEP of Syb2 and the surface-stranded pool (Surface). **(b)** Widefield images display only a partial overlap of NEP and Surface Syb2. Note the absence of NEP without stimulation. Scale bar, 10 µm, zoom 1 µm. **(c,d)** Intensity profiles of data shown in b, after electric field stimulation (c) and without stimulation (d).

4.7.2 Newly exocytosed SV proteins form nano-clusters

While widefield microscopy provides fast imaging rates that are required for the detection of spatiotemporal changes in NEP distribution, the resolution of this technique is restricted by the diffraction limit (Abbe, 1873). During the last two decades, techniques evolved that bypass the diffraction limit and thus increase the image resolution (Huang et al., 2009). In this section, SD-*d*STORM with a lateral resolution of 20 - 35 nm (Lampe et al., 2012; Lehmann et al., 2015) was used to gain further information about the sub-synaptic localization of newly exocytosed SV proteins and the unretrieved surface-stranded pool, which did not recycle upon stimulation.

Newly exocytosed and surface-stranded Syb-c-myc was labeled as described before (see chapter 4.7.1). SD-*d*STORM imaging of both pools showed nearly no overlap of both pools (Figure 4-20). This confirms the observation from the widefield images in Figure 4-19, that newly exocytosed and unretrieved surface-stranded proteins do not intermix. Interestingly, the SD-*d*STORM images show nano-cluster of newly exocytosed Syb2, which appear in the periphery of the less structured boutonic surface-stranded pool.

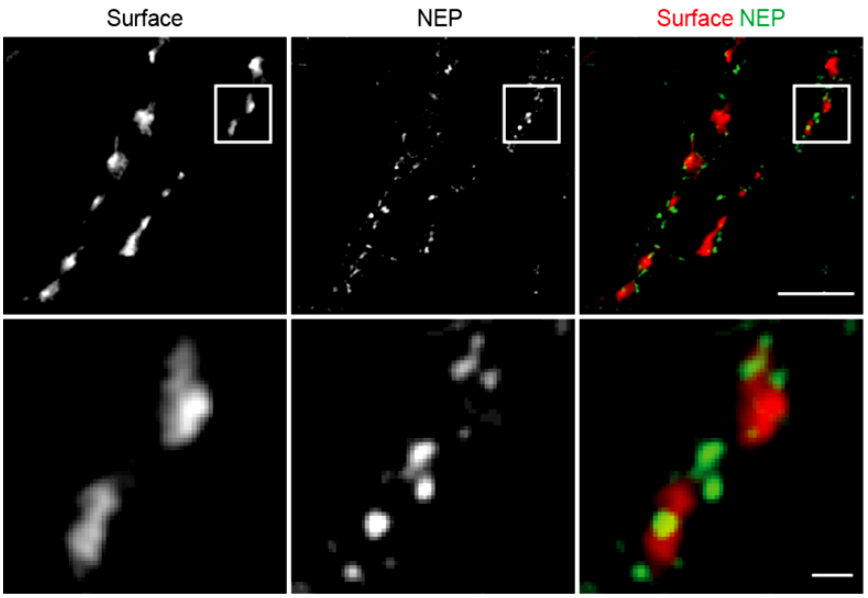

Figure 4-20: Sub-synaptic localization of newly exocytosed and surface-stranded Syb2.
SD-*d*STORM images of hippocampal neurons expressing Syb2-c-myc. The NEP and the surface-stranded pool (proteins that were localized on the neuronal surface before stimulation but were not retrieved upon stimulation) of Syb2-c-myc were immunolabeled according to the procedure described in Figure 4-19a. Note that newly

exocytosed Syb2 (Alexa 647-labeled) forms nano-clusters in the periphery of surface-stranded Syb2 (CF 680-labeled). Scale bar, 1 µm, zoom 100 nm.

4.8 Architecture of a presynaptic trap

Newly exocytosed SV proteins undergo diffusion (see chapter 4.6) and are presynaptically confined (see chapter 4.1.3). Thus, the question arises how this confinement is achieved. Since the clathrin-based endocytic machinery has a major function in the confinement of newly exocytosed SV proteins (see chapter 4.1.3), the localization of endocytic adaptors and clathrin within the synapse might provide further insights into the confinement process.

4.8.1 No major clathrin recruitment upon electrical stimulation

In contrast to AP180 and CALM, clathrin does not associate with Syb2 during the initial diffusion phase. This is indicated by the unaltered Syb2 diffusion rates upon clathrin TD inhibition by Pitstop 2 (Figure 4-18). I wanted to know, whether clathrin nevertheless relocates upon electrical stimulation, since previous publications reported contradictory results regarding clathrin re-localization. While one group reported a minor clathrin loss from synapses (~ 1 %) upon moderate electrical stimulation (40 AP, 20 Hz; Granseth et al., 2006), another group reported clathrin to accumulate at synapses, however only upon intense electrical stimulation (750 AP, 20 Hz; Mueller et al., 2004). In order to investigate this issue the localization and dynamics of clathrin light chain (LC) were analyzed. Widefield live-cell imaging of hippocampal neurons co-expressing either the fluorescently tagged active zone protein Munc13-1-mCherry (Stevens et al., 2005) or Syb2-pH together with fluorescently tagged clathrin LC revealed clathrin to accumulate at presynaptic boutons, close to the active zone (Figure 4-21a,b), where it shows an overlapping distribution with newly exocytosed Syb2-pH (Figure 4-21c,d). The distribution of eGFP- and mRFP (monomeric red fluorescent protein)-clathrin LC remained largely unchanged by electric field stimulation (40AP, 20 Hz; Figure 4-21a-d). However, nanoscale changes may still occur but may be hidden by the diffraction limit (Abbe, 1873). Note, the size of the active zone (~ 0.2 µm diameter, Schikorski and Stevens, 1997) is close to the diffraction limit of widefield microscopy.

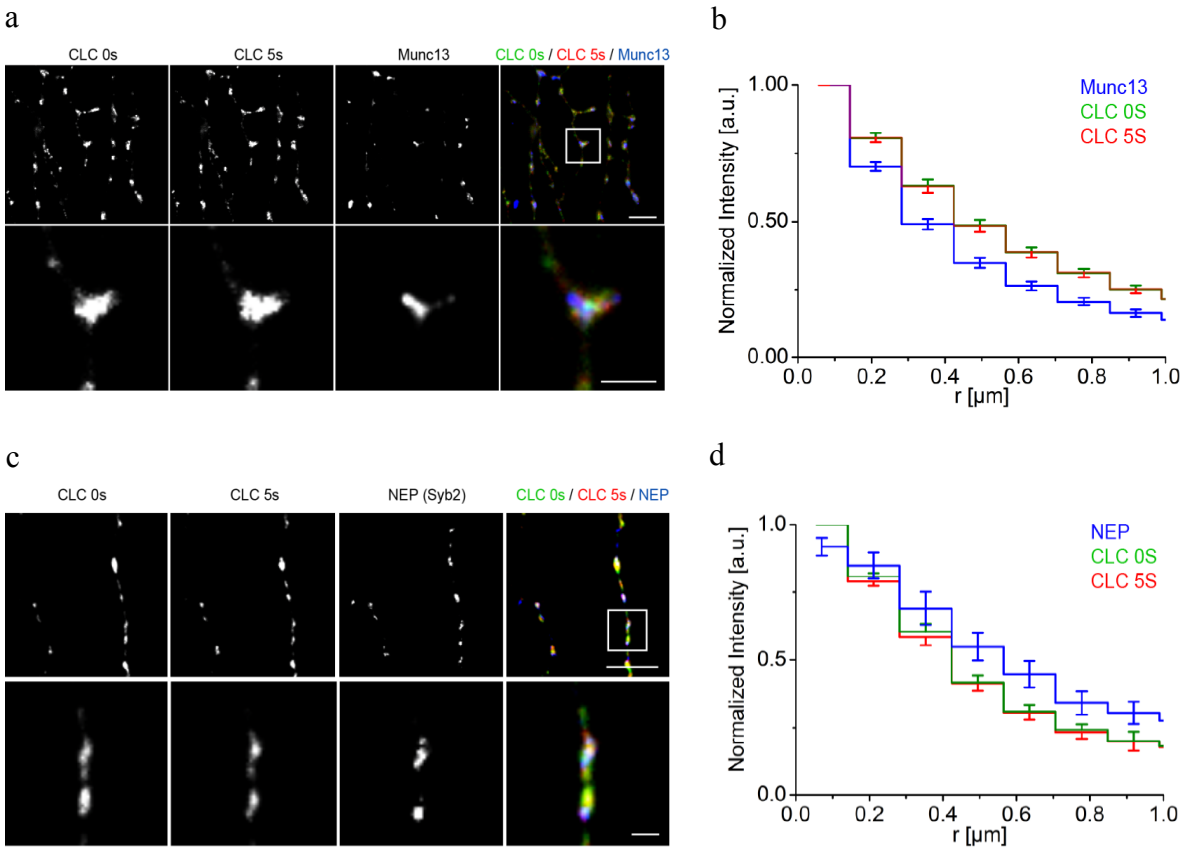

Figure 4-21: Subsynaptic distribution of clathrin and newly exocytosed SV proteins.

(a,b) Hippocampal neurons co-expressing Munc13-1-mCherry and eGFP-clathrin light chain (CLC) were stimulated in an electric field (40 AP, 20 Hz). (a) Munc13-1 (before stimulation) was overlaid with CLC before (0s) and after (5s) stimulation. Scale bar, 5 µm, zoom 2 µm. (b) Radial intensity profiles of Munc13-1 and CLC around maxima of Munc13-1 (mean ± s.e.m.; N = 8 neurons). **(c,d)** Surface-eclipsed hippocampal neurons expressing Syb2-pHluorin and mRFP-clathrin light chain (CLC) were stimulated in an electric field (40 AP, 20 Hz). (c) The NEP image was calculated as described in Figure **4-4** and overlaid with CLC before (0s) and after (5s) stimulation. Scale bar, 10 µm, zoom 1 µm. (d) Radial intensity profiles of NEP and CLC around maxima of the NEP (mean ± s.e.m.; N = 2 independent experiments).

4.8.2 AP180 and clathrin form nano-clusters in the periactive zone

As mentioned, in widefield microscopy, the diffraction limit might obscure nano-structures of the clathrin-based endocytic machinery, which may be relevant for NEP confinement. A higher resolution is therefore necessary to investigate if endocytic proteins form nano-scale synaptic traps outside the active zone. Therefore, the AP180 and clathrin localization was further investigated with multicolor 3-dimensional structured illumination microscopy (3D-SIM) in hippocampal neurons. 3D-SIM provides an approximately 2-fold gain in both lateral and axial resolution, compared to conventional diffraction-limited imaging (Gustafsson, 2000) and in contrast to SD-*d*STORM up to four different color channels. Hippocampal neurons were immunolabeled against the active zone protein bassoon (Dieck et al., 1998), clathrin heavy chain (HC) and the Syb2-specific endocytic adaptor AP180 (Koo et al., 2011a). Interestingly, both endocytic proteins clathrin and AP180 appeared as clusters in the periphery of active zones, which were labeled by bassoon (Figure 4-22a). Similar patterns were also observed if neurons were stimulated (40 AP, 20 Hz) prior to fixation and immunolabeling (Figure 4-22b). This indicates that, although some proteins may still redistribute upon stimulation (see also chapter 4.6.3), the majority of clathrin and AP180 molecules remains in the periactive zone.

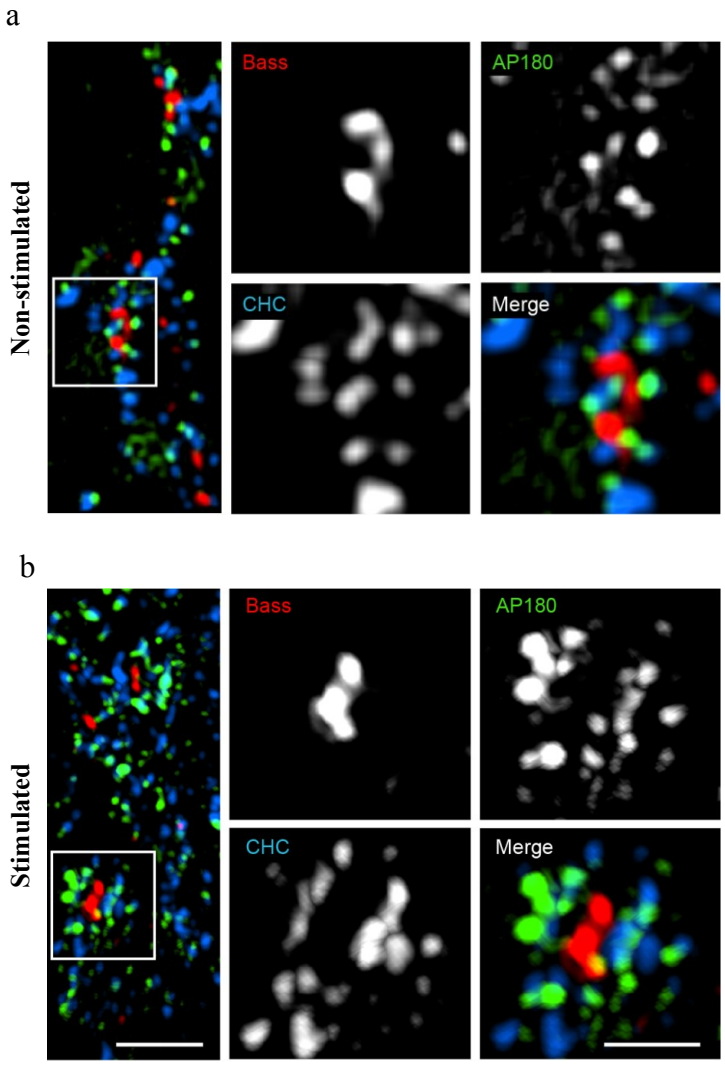

Figure 4-22: AP180 and clathrin preferentially localize in the periactive zone.
(a,b) 3D-Structured Illumination Microscopy (3D-SIM) analysis of non-stimulated (a) or stimulated with 40 AP, 20 Hz (b) hippocampal neurons, immunolabeled for bassoon (Bass), AP180 and clathrin heavy chain (CHC). Scale bar, 1 µm; zoom, 500 nm.

4.8.3 Newly exocytosed Syb2 co-clusters with AP180

AP180 is required for the efficient confinement of newly exocytosed Syb2 (see chapter 4.5) and AP180 and clathrin form clusters within the periactive zone (Figure 4-22). These findings are in agreement with a model where the clathrin-based endocytic machinery traps diffusive newly exocytosed SV proteins within the periactive zone. SD-*d*STORM was

used in order to investigate the exact spatial relationship between newly exocytosed SV proteins and the endocytic machinery. We chose SD-*d*STORM over SIM because of its superior lateral resolution of 20 – 35 nm (Lampe et al., 2012; Lehmann et al., 2015) compared to SIM (110 - 120 nm, Gustafsson, 2000). Note, in contrast to other *d*STORM techniques, SD-*d*STORM is free from registration errors (Lampe et al., 2012, 2015), a crucial requirement for precise co-localization experiments (Annibale et al., 2012).

Newly exocytosed Syb2-c-myc was labeled as described before (see chapter 4.7.1) on unpermeabilized hippocampal neurons. Additionally, AP180 and bassoon labeling was performed after membrane permeabilization. Strikingly, the SD-*d*STORM images reveal sub-synaptic clusters of newly exocytosed Syb2, together with AP180. Both proteins localize in a ring-like structure around the active zone, labeled by bassoon (Figure 4-23a). The cluster distribution resembles very much the sub-synaptic AP180 and clathrin distribution from the SIM experiment (see chapter 4.8.2). Diffraction-limited rendering of SD-*d*STORM images demonstrates that the AP180 and Syb2 nano-clusters are not resolvable by conventional widefield microscopy (Figure 4-23b).

Since SD-*d*STORM is based on the localization of single proteins, it offers the opportunity to directly perform spatial descriptive statistics of protein localizations. In order to determine the clustering properties of AP180 and newly exocytosed Syb2, the Ripley's L(r)-r function (Kiskowski et al., 2009) was applied to SD-*d*STORM localizations within synaptic regions, identified by a bassoon signal in corresponding widefield images. L(r)-r values equal 0 indicate complete spatial randomness, positive values indicate attraction and negative values represent repulsion (Kiskowski et al., 2009). Newly exocytosed Syb2 and AP180 indeed display positive L(r)-r values, above the upper 95 % confidence interval of complete spatial randomness (Figure 4-23c), indicating the attraction of both proteins. Peaks of the Ripley's L(r)-r function at ~ 100 nm (Syb2) and ~ 200 nm (AP180) prove the existence of nano-clusters of the corresponding size.

Two different proteins cannot completely overlap in SD-*d*STORM images, since the localization accuracy of SD-*d*STORM is high enough to resolve labeling heterogeneities (Lampe et al., 2012). The spatial relation between newly exocytosed Syb2 and AP180 clusters was therefore further analyzed in the SD-*d*STORM images by radial intensity profiles of both proteins that were centered at sub-synaptic clusters of newly exocytosed Syb2. Profiles of both proteins revealed similar intensity decay from the cluster center towards the periphery,

which shows that both proteins are in the same sub-synaptic cluster (Figure 4-23d). k-Nearest neighbor analysis (chapter 3.5.8) was applied to more precisely determine the distance between AP180 and newly exocytosed Syb2. Syb2 to AP180 distances were calculated from all corresponding SD-*d*STORM localizations in synaptic regions. The distribution of distances revealed a frequency peak at ~ 25 nm. This peak was not caused by noise as it was absent after the randomization by a toroidal shift of the AP180 channel (Figure 4-23e). The ~ 25 nm distance between AP180 and Syb2 molecules is well below the size of the corresponding nano-clusters (Figure 4-23c) and in the range of the experimental resolution (Lampe et al., 2012; Lehmann et al., 2015), which provides further evidence for the co-clustering of both proteins. This supports the idea of the clathrin-based endocytic machinery as a trap for diffusive newly exocytosed SV proteins within the periactive zone.

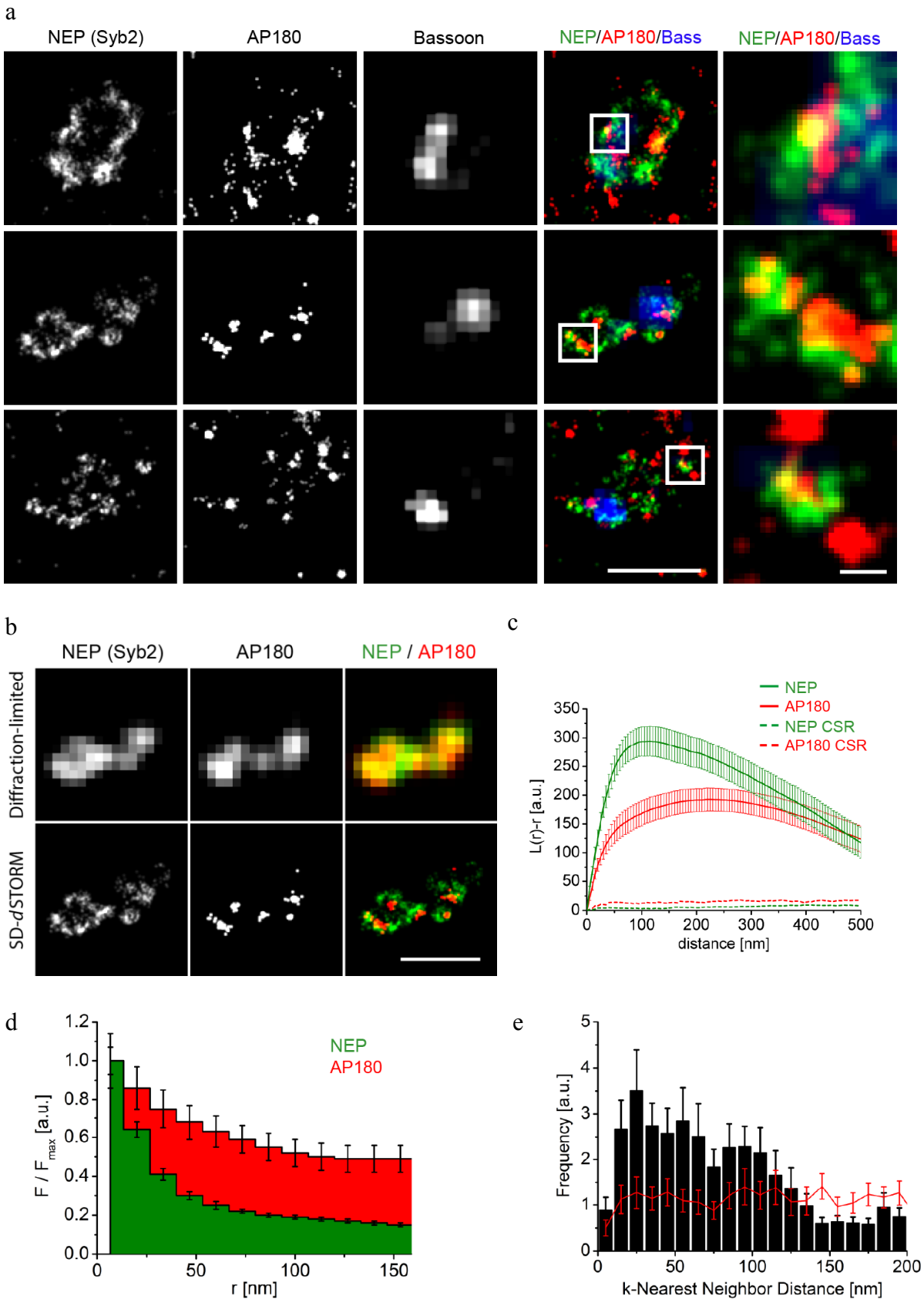

Figure 4-23: Newly exocytosed Syb2 co-clusters with it endocytic adaptor AP180.

SD-dSTORM imaging of newly exocytosed Syb2 (stimulation: 40 AP, 20 Hz) in hippocampal neurons expressing Syb2-c-myc **(a)** 2-color SD-*d*STORM analysis of the NEP (Alexa 647-labeled) and AP180 (CF 680-labeled), overlaid with widefield images of Bassoon. Scale bar, 1 µm; zoom, 100 nm. Note that Syb2-c-myc originates only from transfected neurons, whereas endogenous AP180 signal may also originate from untransfected cells. **(b)** "Diffraction-limited" rendering and SD-*d*STORM images of AP180 and newly exocytosed Syb2. Scale bar, 1 µm. **(c)** Ripley's L(r)-r function shows sub-synaptic clustering of the NEP and of AP180, indicated by positive L(r)-r values with a maximum at radii of about 100 nm (NEP) and 200 nm (AP180). Mean ± s.e.m.; n = 31 synapses. Dotted lines represent upper 95% confidence bands of complete spatial randomness (CSR; 10 simulations per synapse). **(d)** Radial intensity profiles of the NEP and AP180 signals centered on the maxima of sub-synaptic NEP clusters indicate that both proteins appear in common clusters (mean ± s.e.m.; n = 47 synapses). **(e)** *k*-Nearest neighbor analysis (k = 10) of the NEP and AP180 showing a maximum at 25 nm. The red line represents results after toroidal shift of one channel. Values above the red line indicate co-localization of the NEP and AP180. (mean ± s.e.m.; n = 31 synapses).

5 Discussion

In the present work, I present an assay to spatiotemporally study the fate of newly exocytosed SV proteins in hippocampal neurons, which had remained uncharacterized so far. I found that after moderate electrical stimulation, newly exocytosed SV proteins diffuse away from the AZ. This movement can be modelled by Brownian motion and requires no active transport. While only a minor fraction of SV proteins escapes into the axon (~ 10 %), the majority of proteins becomes rapidly confined within the presynaptic bouton, followed by their slow reclustering. I provide evidence that the clathrin-based endocytic machinery is required for efficient confinement. In line with that, the endocytic adaptor AP180 and newly exocytosed SV proteins were found together in nano-clusters in periactive zones. Here the endocytic proteins may act as a trap for newly exocytosed SV proteins.

5.1 Spatiotemporal dynamics of newly exocytosed SV proteins

Despite the increasing amount of knowledge on exo- and endocytosis at mammalian presynapses (Heuser and Reese, 1973; Südhof, 2004; Jung and Haucke, 2007; Haucke et al., 2011; Saheki and Camilli, 2012; Kononenko et al., 2014), relatively little is known about the fate of newly exocytosed SV proteins. Recent studies provide evidence that newly exocytosed SV proteins are not immediately retrieved. Instead, a preexisting readily retrievable pool on the neuronal surface is endocytosed preferentially (Fernández-Alfonso et al., 2006; Wienisch and Klingauf, 2006; Hua et al., 2011). It has remained controversial if newly exocytosed SV proteins are retained within synaptic boutons, or if they escape into the axon before being recollected. Previous studies either did not selectively address newly exocytosed SV proteins or used strong electrical stimulation protocols that exceeded the capacity of the RRetP (Fernández-Alfonso et al., 2006; Granseth et al., 2006; Li and Murthy, 2001; Opazo et al., 2010; Sankaranarayanan and Ryan, 2000; Wienisch and Klingauf, 2006)

A presynaptic restriction of newly exocytosed SV proteins would alleviate the need for re-sorting of SV proteins from a huge neuronal surface and transporting them back to synapses. Both, re-sorting and long-range transport, are probably too slow to ensure fast recycling with high reliability (Mutch et al., 2011) during sustained neurotransmission. I

therefore hypothesized, that the post-exocytic movement of newly exocytosed SV proteins is restricted to synaptic boutons.

5.1.1 Newly exocytosed SV proteins remain at the presynaptic surface

In this study, pHluorin imaging of surface-eclipsed neurons was used to selectively describe the fate of newly exocytosed SV proteins (chapter 4.1.3). In contrast to recent studies, a moderate electrical stimulation was used (40 APs, 20Hz), which releases the readily releasable pool (Schikorski and Stevens, 2001) but does not exceed the capacity of the RRetP (which is ~ 70 APs, Hua et al., 2011).

My data shows that upon exocytosis only a minor fraction of newly exocytosed Syb2 molecules escape into the axon (~ 10 %, Figure 4-2), while most proteins remain on the surface of synaptic boutons. In contrast to recent studies (Granseth et al., 2006; Opazo et al., 2010), the applied assay is not sensitive to vesicle movement, since vesicular pHluorin is efficiently quenched. The signal is also unbiased by dynamics of preexisting surface-stranded SV proteins, since surface fluorescence was efficiently removed prior to imaging (Figure 4-1). In line with recent studies that demonstrate a selective endocytosis of the preexisting RRetP (Fernández-Alfonso et al., 2006; Wienisch and Klingauf, 2006; Hua et al., 2011), no endocytosis of newly exocytosed SV proteins was detected (Figure 4-3).

Taken together, this confirms our hypothesis of a restriction of newly exocytosed SV proteins at the presynaptic plasma membrane by some kind of barrier. The minor axonal loss likely represents inefficiencies of this barrier. However, a protein loss from synapses could also be functionally relevant, as escaping SV proteins may contribute to an exchange of proteins between synapses, similar to the sharing of SVs between synaptic boutons (Darcy et al., 2006). Alternatively, escape may represent a degradation route for improperly folded or damaged proteins outside synapses.

5.1.2 Fast spreading, confinement and slow reclustering

Gaussian fitting is an established technique for the characterization of 2d diffusion from a point source (Crank, 1975; Schmoranzer et al., 2000; Sochacki et al., 2012). It is also a proper tool to describe post-exocytic dynamics of newly exocytosed SV proteins, since SVs

fuse at the active zone (~0.2 µm diameter, Schikorski and Stevens, 1997), which is a diffraction-limited spot in widefield microscopy. The noise-like residuals that were obtained from the fit confirm the suitability of the model (Figure 4-4). However, the synaptic orientation in our neuronal cultures is unknown compared to the plasma membrane of non-neuronal cells in previous studies (Schmoranzer et al., 2000) that was parallel to the projection plane in the microscope. A partial or complete side view would lead to the shortening of one axis in the projection plane. In order, to avoid a systematic underestimation of FWHMs, only the longer width of the 2d Gaussian fit was used for further analysis (see also chapter 3.5.5).

The Gaussian fit analysis on the presynaptically preserved ~ 90 % of the NEP (Figure 4-2) revealed three post-exocytic phases of mobility. Upon SV fusion with the plasma membrane, proteins spread for a few seconds, until they are confined within ~ 2 µm² (Figure 4-5). This corresponds to the approximate dimensions of a hippocampal synapse (Wilhelm et al., 2014). Confinement of newly exocytosed SV proteins is independent from the amount of cargo proteins (Figure 4-5c), indicating that the barrier is not saturated under these experimental conditions. I wondered, whether the initial spread might correspond to the addition of membrane from fused SVs. Earlier studies report the release of ~ 10 docked SVs upon application of the same stimulation procedure (Schikorski and Stevens, 1997, 2001). Assuming a SV diameter of 40 – 45 nm (Takamori, 2006), 10 SVs would, after fusion with the plasma membrane, transform into a patch of 0.05 – 0.06 µm², which is well below the dimensions of the post-exocytic spread. Thus, the initial spread corresponds to a true dispersion of SV proteins within the plasma membrane. However, proteins from newly exocytosed SVs do not necessarily spread independently and intermix. Spreading could as well represent the movement of several intact patches of fused SVs.

After spreading and confinement, SV proteins recluster into the much smaller area of ~ 1 µm². This shrinkage exceeds the membrane area of ~10 retrieved SVs (see the calculation above) and is, thus, not caused by membrane retrieval. Interestingly, reclustering takes ~ 40s. This is relatively long, considering that the RRetP is already exhausted after ~ 70 APs at 20 Hz (Hua et al., 2011). Reclustering might therefore limit the number of stimulus trains that a synapse can cope with and may be the rate-limiting step for reloading the RRetP and slow modes of endocytosis (e. g. CME). The major three SV proteins Syb2, Syt1 and Syp (Takamori, 2006) showed no statistically significant differences in the post-exocytic dynamics

(Figure 4-6), suggesting a common underlying mechanism of spreading, confinement and reclustering for all three proteins.

Spreading, confinement and reclustering are incompatible with kiss-and-run, since kiss-and-run is the transient fusion of SVs with the plasma membrane at active zones without full vesicle collapse or loss of membrane components (Ceccarelli et al., 1973; Richards et al., 2005; Harata et al., 2006). The observed initial spread is rather consistent with full SV collapse that is a prerequisite of clathrin-mediated endocytosis (Heuser and Reese, 1973, 1981).

5.2 Molecular players for post-exocytic confinement and reclustering

5.2.1 Filamentous actin is not involved in post-exocytic NEP dynamics

A promising candidate for a presynaptic diffusion barrier was actin. Actin filaments are implicated in the diffusion barrier for phospholipids and transmembrane proteins at the axonal initial segment of hippocampal neurons. This barrier that can be partially destroyed by the disruption of actin filaments by the incubation with Latrunculin A (Nakada et al., 2003). Nakada et al. propose that membrane proteins, at the axonal initial segment, are anchored to a dense actin meshwork and act like pickets that restrict diffusion. In line with that, super-resolution studies describe a cortical cyoskeleton of periodically alternating actin / spectrin rings in axons (Xu et al., 2013b; Zhong et al., 2014; Ganguly et al., 2015) that periodically ancor voltage-gated sodium channels in the axon.

Actin filaments are also enriched in periactive zones and they are required for efficient SV recycling (Shupliakov et al., 2002; Watanabe et al., 2013b; Ganguly et al., 2015). Furthermore, actin filaments are implicated in the maintenance of SV protein clusters in the plasma membrane of neuromuscular junctions of the *Drosophila* temperature-sensitive dynamin mutant shibire^{ts} (Dason et al., 2013). However, despite the role of actin in SV protein cluster preservation, my results show that actin filaments have no major function as a presynaptic diffusion barrier. Spread, confinement and reclustering remain unperturbed by Latrunculin A application (Figure 4-7). This also implies that spread and reclustering do not rely on the active transport on formin-dependent actin trails that were recently found in axons and synaptic boutons (Ganguly et al., 2015). However, even though synaptic actin filaments

were largely removed by the incubation with Latrunculin A, one cannot rule out that remaining short actin filaments remain intact and therefore prevent unlimited SV protein escape and aid reclustering.

5.2.2 Synaptophysin is not required for Syb2 confinement and reclustering

Dason and colleagues found out that, similar to the removal of actin filaments, an extraction of cholesterol results in a dispersal of SV protein clusters at the presynaptic plasma membrane of the *Drosophila* shibire^{ts} neuromuscular junctions (Dason et al., 2013). Cholesterol is highly enriched in SVs (Takamori, 2006). Syp, but not Syb2 can bind to cholesterol (Thiele et al., 2000). Furthermore, Syp facilitates Syb2 endocytosis (Pennuto et al., 2003; Wienisch and Klingauf, 2006; Gordon et al., 2011) in a stimulus- and frequency-dependent manner and recent data suggests that Syp is required to remove Syb2 from release sites upon high-frequency stimulation (Rajappa et al., 2016).

Since Syp and Syb2 form cholesterol-dependent (Mitter et al., 2003) heteromers (Calakos and Scheller, 1994; Edelmann et al., 1995; Becher et al., 1999), I speculated that Syp also mediates Syb2 confinement to cholesterol-rich presynaptic micro-domains. However, the post-exocytic Syb2 dynamics remained unchanged in Syp KO neurons (Figure 4-8). The function of Syp in Syb2 sorting may therefore rather be required at later timepoints, after confinement and reclustering, or upon stimulations exceeding the capacity of the RRetP (as indicated by recent data: Rajappa et al., 2016).

Althought the cholesterol-binding protein Syp is not required to limit Syb2 dispersal under these conditions, cholesterol still might be implicated in NEP confinement. This is due to the fact, that, beside SV proteins, also the endocytic proteins clathrin and AP-2 are enriched in detergent-resistant cholesterol-rich microdomains (Jia et al., 2006). Unfortunately, the removal of cholesterol from plasma membranes and SVs is incompatible with the detection of newly exocytosed SV proteins, since overall cholesterol extraction impairs SV recycling (Dason et al., 2010).

5.2.3 The clathrin-based endocytic machinery mediates post-exocytic confinement

Under low-to-moderate electrical stimulation, sorting and retrieval are mediated in part by the clathrin-based endocytic machinery (Figure 4-9f and Granseth et al., 2006; Kononenko et al., 2014). Even though confinement of newly exocytosed SV proteins and their sorting for endocytosis could be conducted by independent machineries, a participation of the clathrin-based endocytic machinery in NEP confinement would make a separate confinement-machinery unnecessary.

Indeed, my work indicates that the clathrin-based endocytic machinery is required for NEP confinement. An acute inhibition of the clathrin TD with Pitstop 2, depletion of the Syb2-specific endocytic adaptors AP180 and CALM, as well as the mutation of the AP180 and CALM binding site in Syb2, cause reduced confinement (Figure 4-9, Figure 4-11, Figure 4-14) of newly exocytosed Syb2. Impaired confinement is not a secondary effect of Syb2 protein accumulations on the neuronal surface upon interference with the specific endocytic adaptors (Figure 4-12), because NEP confinement turned out to be independent of Syb2 abundance (Figure 4-5c).

Although all three manipulations have similar effects on the confinement of newly exocytosed Syb2, one should differentiate between the perturbation of CME in general, by applying Pitstop 2, and the interference with the Syb2-specific endocytic adaptors AP180 and CALM. Pitstop 2 blocks CME per se by increasing clathrin-coated pit lifetimes. However, Pitstop 2 does not interfere with cargo recognition or sequestration into clathrin-coated pits (von Kleist et al., 2011). Therefore a direct effect of clathrin in confinement is unlikely. Instead, frozen clathrin-coated pits may sequester other proteins of the clathrin-based endocytic machinery away, which are therefore no longer available as confinement factors. In contrast to Pitstop 2 treatment, the depletion of AP180 and CALM or the mutation of Syb2 specifically affect Syb2 sorting (Grote and Kelly, 1996; Bushlin et al., 2008; Koo et al., 2011a).

Collectively this data indicates that endocytic sorting adaptors, among other proteins of the clathrin-based endocytic machinery, are a key element of NEP confinement. Nevertheless, none of the applied manipulations abolished confinement completely. Thus,

additional factors may aid the confinement process and thereby prevent the escape of newly exocytosed SV proteins into the axon.

5.2.4 Reclustering requires additional factors

Interfering with the clathrin-based endocytic machinery affects the extent but not the rate of reclustering (Figure 4-11, Figure 4-14). This suggests that a fraction of molecules still reclusters with unchanged rate into the pre-synaptic RRetP, while others do not recluster at all. Under these conditions, residual reclustering may be mediated by interactions with additional factors. Possible candidates are cholesterol- and PI(4,5)P_2-rich microdomains, since together they are able to concentrate SV proteins and endocytic proteins. Furthermore, both lipids are required for SV endocytosis (Thiele et al., 2000; Jia et al., 2006; Milosevic et al., 2005; Dason et al., 2010; McMahon and Boucrot, 2011; van den Bogaart et al., 2011). However, NEP reclustering might also be mediated by the interaction of different SV proteins among each other (Kwon and Chapman, 2011; Gordon et al., 2011; Kaempf et al., 2015). This would explain that various mouse mutants, which are deficient of single SV proteins, show general deficits in SV protein endocytosis (Syp KO: Gordon et al., 2011; Kwon and Chapman, 2011; Rajappa, 2016 / Syb2 KO: Deák et al., 2004; Xu et al., 2013a / Syt1 KO: Nicholson-Tomishima and Ryan, 2004 / VGlut1 KO: Pan et al., 2015).

5.3 Post-exocytic Syb2 missorting promotes Syb2 accumulation on the neuronal surface

As discussed in the last chapter, AP180 and CALM binding is required to recluster released Syb2 molecules. However, in the absence of both proteins only a fraction of them reclusters. Although newly exocytosed proteins are still confined close to the synapse by additional factors (chapter 5.2.3), those proteins that do not recluster may eventually get lost into the axon over longer periods of time. This loss can be observed in the super-resolved images, where the majority of the surface-stranded mutant Syb2 (M46A) has escaped into the axon, while surface-stranded Syb2 (WT) was situated exclusively at synaptic boutons (Figure 4-13), likely as part of a presynaptic RRetP. Proteins that escaped the synapse cannot

contribute to the presynaptic RRetP. They are likely inefficiently retrieved, since endocytosis mainly occurs at the periactive zone (Teng et al., 1999), where endocytic proteins are enriched (Roos and Kelly, 1999; Koh et al., 2007; Sundborger et al., 2011; Sakaba et al., 2013; Wahl et al., 2013). This is in agreement with recently published data from our group that shows delayed Syb2-pH endocytosis in AP180 KO or AP180 and CALM double-deficient neurons (Koo et al., 2015). The inefficient endocytosis leads to increased steady-state Syb2 surface-levels, as observed for AP180 single- or AP180 / CALM double-deficient neurons (Figure 4-12 and Koo et al., 2011). The fact that silencing neurons by the application of TTX completely rescues elevated Syb2-pH surface levels of AP180 and CALM deficient neurons (Figure 4-12a) proves that increased steady-state Syb2 surface-levels are indeed the long-term consequence of inefficient post-exocytic Syb2 mis-sorting. Since the depletion of AP180 and CALM leads to a stronger increase in Syb2 surface-levels than the depletion of AP180 alone (Figure 4-12), it is likely that both AP180 and CALM are required to mediate post-exocytic sorting processes like confinement and reclustering.

Interestingly, synaptic vesicles of AP180 KO neurons were found to be elongated and enlarged (Koo et al., 2015). Similar irregularly shaped SVs were also observed in Syb2 knockout neurons (Deák et al., 2004). At the first glance, the concordant defect of both mutants may appear contradictory, as the situation at the plasma membrane is entirely different for both mutants. AP180 KO neurons have increased Syb2 surface levels (Figure 4-12b), whereas Syb2 KO neurons contain no Syb2 at all. However, considering that the majority of surface-stranded Syb2 mis-localizes in the absence of endocytic adaptor binding (Figure 4-11, Figure 4-13, Figure 4-14), this would ultimately lead to a reduction of Syb2 molecules in the RRetP. In this regard, the situation in the RRetP of AP180 KO neurons resembles very much the situation in Syb2 KO neurons. Also non-neuronal cells require cargo for the maturation of clathrin-coated pits (Loerke et al., 2009). However, it remains unclear how the lack of cargo affects the formation of properly shaped SVs from the RRetP.

Taken together, fast and accurate sorting of the NEP by endocytic adaptors is an essential element of the SV cycle and required to form proper SVs.

5.4 Newly exocytosed SV proteins are diffusive until confinement

5.4.1 Release site clearance is a passive process

Sustained neurotransmission requires available release sites for the fast repetition of SV fusion with the plasma membrane. If release sites are blocked by SV proteins, this causes STD, a deceleration of synaptic responses. STD does not represent a consumption of SVs, since it happens much faster (Neher, 2010; Haucke et al., 2011). The mechanism, by which newly exocytosed SV proteins are removed from active zones has remained unknown so far.

I have shown that the initial post-exocytic spread of Syb2, Syt1 and Syp (Figure 4-16) matches the results from the mathematical diffusion model, without the requirement to introduce a parameter for active transport. This indicates that newly exocytosed Syb2, Syt1 and Syp are not actively transported from active zones, but undergo a few seconds of diffusion before being confined (Figure 4-5). This is in line with the finding that a disruption of actin filaments by the application of Latrunculin A does not alter post-exocytic Syb2 dynamics (Figure 4-7).

STD occurs particularly under high-frequency stimulation. However, several studies have observed that the disruption of the clathrin-based endocytic machinery induces stronger STD that occurs upon much milder electrical stimulation (Hosoi et al., 2009; Kawasaki et al., 2000; Sakaba et al., 2013; Hua et al., 2013). Considering that the endocytic adaptors AP180 or CALM rapidly trap newly exocytosed Syb2 (Figure 4-11, Figure 4-14), a NEP immobilization by the clathrin-based endocytic machinery outside active zones might support release site clearance by reducing the amount of diffusive cargo in the presynaptic plasma membrane.

5.4.2 Synaptic vesicles likely remain as patches after exocytosis

Although, my data demonstrates that release site clearance is a fast diffusion-driven process, SV proteins do not necessarily diffuse alone. Whether a SV remains as a patch upon fusion with the plasma membrane and thereby preserves its identity, or if SVs fully disperses and the proteins from different SVs intermix, followed by resorting of all proteins, has remained the topic of an ongoing debate (Haucke et al., 2011; Rizzoli, 2014). Patch diffusion

would alleviate the need for extensive protein sorting on the plasma membrane. Interestingly, super-resolution experiments show that SV proteins are organized as nano-clusters in plasma membranes of hippocampal neurons (Willig et al., 2006; Opazo et al., 2010; Hua et al., 2011). It has further been demonstrated that similar presynaptic SV protein clusters, found on the plasma membrane of the *Drosophila* neuromuscular junction, are cholesterol-dependent (Dason et al., 2013). This is in agreement with biochemical experiments that prove the existence of cholesterol-rich microdomains, which accumulate SV proteins (Thiele et al., 2000; Mitter et al., 2003; Jia et al., 2006). It is therefore tempting to speculate, that newly exocytosed proteins from one SV diffuse (Figure 4-16) as a patch, that is partially agglutinated by a locally high cholesterol level from the fused SV (Takamori, 2006).

My super-resolution experiments demonstrate that upon electrical stimulation unretrieved Syb2 molecules distribute diffusely over the bouton, while newly exocytosed Syb2 forms cluster, preferentially in the periphery of synaptic boutons (Figure 4-20). Even though these findings leave room for an exchange of proteins between newly exocytosed protein clusters from different vesicles, they clearly show that newly exocytosed SV proteins do not intermix with preexisting unretrieved SV proteins. The NEP rather preserves its identity. Like the NEP, also the RRetP appears as peripheral clusters (Willig et al., 2006; Opazo et al., 2010; Hua et al., 2011). This is in line with the idea that NEP clusters transform into the RRetP clusters. However, it remains unclear, why unretrieved surface-stranded SV proteins remain dispersed and do recluster.

A closer look on the diffusion coefficients that were obtained from the mathematical model provides further insights into the question, whether newly exocytosed SV proteins diffuse solitary or if they diffuse as a patch. Interestingly, the mathematic modeling reveals diffusion coefficients of ~ 0.2 – 0.3 µm² / s, with no statistically significant difference between Syb2, Syp and Syt1 (Figure 4-16). Since diffusion coefficients of transmembrane proteins correlate with the radius of their transmembrane segment (Saffman and Delbrück, 1975), this is incompatible with the solitary diffusion of single proteins. As the tetraspan membrane protein Syp (Arthur and Stowell, 2007) has a huge transmembrane segment, compared to the single pass transmembrane proteins Syb2 and Syt1 (Bowen and Brunger, 2006; Perin et al., 1991), Syp should diffuse slower than Syb2 and Syt1. However, in a patch all proteins would have the same speed. A further hint towards patch diffusion is the fact, that the obtained diffusion coefficient of newly exocytosed Syb2 (~ 0.2 µm² / s, Figure 4-16) is

strikingly slow in comparison to the diffusion coefficient of Syb2 alone, reconstituted in giant unilamellar vesicles (~ 5 μm² / s, Ramadurai et al., 2009). However, slower presynaptic diffusion rates may be partially due to molecular crowding (Wilhelm et al., 2014), which corresponds to reduced diffusion in situations where protein concentrations are so high that proteins cannot move freely because other molecules occupy too much space in the membrane (Ramadurai et al., 2009; Saka et al., 2014).

5.4.3 Endocytic adaptors bind their cargo prior to confinement

Since the diffusion of newly exocytosed Syb2 is rapidly confined by AP180 or CALM (Figure 4-11, Figure 4-14), the question arises: "When precisely do endocytic adaptors bind to newly exocytosed SV proteins?" It is conceivable that endocytic adaptors residing in endocytic structures, particularly in periactive zones, catch the diffusing NEP. Alternatively, endocytic adaptors could be also diffusive and bind the diffusing NEP. In a third scenario, endocytic adaptors bind to their cargo at SVs, before exocytosis.

My data shows that Syb2 spreading is accelerated by abolishing the binding to AP180 and CALM. The overlaid signals of post-exocytic dynamics from multiple fusion events (Figure 4-11a, Figure 4-14b) point towards accelerated Syb2 (M46A) diffusion, although changes in exocytic kinetics would equally affect the curve progression. However, the mathematic diffusion model clearly demonstrates that the binding mutant Syb2 M46A diffuses faster than Syb2 WT (Figure 4-17). Note that this happens before confinement, in the spreading phase, where Syb2 (M46A) is still diffusive. This suggests that AP180 or CALM, either before or briefly after SV fusion with the plasma membrane, bind to Syb2 and thereby slow down Syb2 diffusion as a complex. AP180 and CALM binding to Syb2 at SVs is in line with the recent observation, that the heterologous expression of Syb2, in non-neuronal cells suffices to recruit heterologously expressed AP180 to vesicular membranes (Koo et al., 2015). A diffusive Syb2 -AP180 or -CALM complex is further supported by the finding that a strong neuronal depolarization with KCl induces an AP180 delocalization out of synapses (Wu et al., 2010), similar to the dispersal of SV proteins observed upon intense stimulation (Fernández-Alfonso et al., 2006; Li and Murthy, 2001; Wienisch and Klingauf, 2006). Therefore, Syb2 might drag AP180 into the axon upon strong electrical stimulation. Such a delocalization of AP180 is incompatible with all AP180 being preassembled in endocytic structures at the

plasma membrane before binding to Syb2. In contrast to the severe AP180 delocalization upon intense KCl induced depolarization (Wu et al., 2010), a moderate electrical stimulation has no major effects on the AP180 localization, as indicated by the SIM experiments in Figure 4-22. The fraction of AP180 that may redistribute with the newly exocytosed Syb2 is likely too small to be seen in a fixed-cell experiment. The accumulation of AP180 in periactive zones of un-stimulated neurons suggests that although some AP180 molecules likely relocate together with the NEP (Figure 4-11a, Figure 4-14b, Figure 4-17) most AP180 molecules are assembled in endocytic structures, likely together with the RRetP.

Considering the rather large effect of AP180 or CALM on the Syb2 diffusion coefficient (~ 50 % deceleration, Figure 4-17), not only AP180 and CALM, but also further binding partners of both adaptors may rapidly associate with diffusive Syb2. If indeed newly exocytosed SV proteins diffuse as patches, such interactions may be critical to keep Syb2 in SV-derived patches.

Freezing clathrin-coated pits by the application of Pitstop 2 affects Syb2 confinement (Figure 4-9). However, since Pitstop 2 treatment, in contrast to the interference with AP180 and CALM binding, only affects confinement and leaves the Syb2 diffusion coefficient unchanged (Figure 4-18) the affected confinement factors must immobilize the Syb2 - AP180 or - CALM complex after the diffusion phase. Pitstop 2 effects on Syb2 confinement most likely rely on the sequestration of endocytic proteins into frozen pits (as discussed in chapter 5.2.3). As a large number of endocytic players is sequestered into clathrin-coated pits by Pitstop 2 (von Kleist et al., 2011), the identity of these confinement factors remains unknown. Possible candidates are proteins and lipids that are implicated in the nucleation of CME, like the scaffold protein Eps15 or $PI(4,5)P_2$, which both interact with AP180 and CALM (Ford et al., 2001; Morgan et al., 2003). It is not clear whether the diffusive Syb2-AP180 or -CALM complex is immobilized prior to the recruitment of clathrin, which can be aided by AP180 and CALM (Ahle and Ungewickell, 1986; Ford et al., 2001), or if the complex is concentrated within preassembled clathrin structures at the plasma membrane. However, the fact that no major clathrin redistribution was observed upon electrical stimulation in live-cell widefield microscopy (Figure 4-21) or fixed-cell SIM imaging (Figure 4-22) argues for the latter scenario. This is in agreement with findings from experiments with neuroendocrine PC12 cells, where clathrin participates in structures that capture newly exocytosed proteins (Sochacki et al., 2012).

5.5 The clathrin-based endocytic machinery clusters newly exocytosed SV proteins in the periactive zone

A fast immobilization of newly exocytosed SV proteins by the clathrin-based endocytic machinery is required to confine proteins within the presynapse (chapter 5.2.3) and might further support release site clearance by trapping diffusive (chapter 5.4.1) SV proteins outside active zones and thus reducing the amount of diffusive SV proteins within the synapse. Particularly, periactive zones are characterized by the accumulation of various endocytic proteins in close proximity to the active zone (Roos and Kelly, 1999; Koh et al., 2007; Sundborger et al., 2011; Sakaba et al., 2013; Wahl et al., 2013) and are therefore suitable to fulfill the function of a fast trap for newly exocytosed SV proteins.

Indeed, my data shows that clathrin and AP180 accumulate around active zones (Figure 4-22), where clathrin and AP180 partially co-localize. The partial colocalization of clathrin and AP180 is in agreement with a model where endocytic structures are preassembled at plasma membranes, while some AP180 diffuses together with newly exocytosed cargo (see also chapter 5.4.3). The overlapping signal of clathrin and AP180 in the SIM images (Figure 4-22) might represent the fraction of both proteins that is assembled together with the RRetP clusters, while the non-overlapping signal might correspond to vacant clathrin-positive binding sites for newly exocytosed SV proteins on the plasma membrane or AP180 bound to Syb2 at SVs, respectively. Remarkably, SIM resolves a patch-like distribution of clathrin and AP180 around bassoon-positive active zones, which remains undetectable in widefield microscopy (Figure 4-23b). Comparable nano-scale pattern have not been described for other endocytic proteins yet.

Interestingly, newly exocytosed Syb2 reveals a similar patch-like distribution around active zones in SD-*d*STORM (Figure 4-23). With the Ripley's analysis it was possible to show co-clustering between newly exocytosed Syb2 and AP180. Interestingly, clusters of newly exocytosed Syb2 have a diameter of ~100 nm, which is very close to what has been observed for RRetP clusters of Syt1 and Syp (Syt1: 80 – 100 nm, Syp: ~ 100 nm; Willig et al., 2006; Opazo et al., 2010). Like newly exocytosed SV proteins, also RRetP patches are distributed in the periphery of active zones, as reported for the RRetP of Syt1 (Hua et al., 2011). Collectively, this data suggests that the NEP transforms into the RRetP upon its immobilization in endocytic structures at periactive zones. Strikingly, the surface area of a

100 nm flat cluster equals the surface area of a spherical SV with a diameter of 50 nm. This is very close to the size of a native spherical SV with a diameter of 40 - 45 nm (Takamori, 2006). Thus, newly exocytosed SV proteins could preassemble into sub-diffraction units that may be ready for endocytosis and for the conversion into single SVs. Alternatively, they could remain as assemblies (see also chapter 5.4.2) with a preserved size over the whole SV cycle.

6 Conclusion and Outlook

In this work I spatiotemporally describe the fate of newly exocytosed SV proteins and indentify molecular factors that mediate their dynamics. I show that SV proteins, after exocytosis, rapidly spread via Brownian motion, before most molecules are confined in the area of a synapse. Nevertheless, ~ 10 % of the molecules rapidly escape into the axon. After confinement, SV proteins recluster in periactive zones, without intermixing with unretrieved surface-stranded proteins. There they contribute to nano-clusters, together with the endocytic adaptor AP180. Likewise, I found clathrin in nano-clusters near active zones, partially overlapping with AP180. I furthermore demonstrate that interfering with the Syb2-specific endocytic adaptors AP180 and CALM accelerates Syb2 diffusion and reduces Syb2 confinement and the amount (but not the speed) of Syb2 reclustering. Blocking the clathrin TD with Pitstop 2 phenocopies the effects on confinement and reclustering. Even though both treatments increase the covered area of newly released Syb2, they do not induce a rapid loss into the axon. However, steady-state experiments demonstrate that Syb-specific endocytic adaptors are finally required to prevent a major loss into the axon over a long time periods.

I therefore propose a model (Figure 6-1) where newly exocytosed SV proteins diffuse away from active zones after SVs collapsed into the plasma membrane. Most proteins are rapidly captured by endocytic adaptors and recluster in periactive zones, likely by the contribution of additional components of the clathrin-based endocytic machinery. There they form nano-clusters, which likely give rise to the RRetP that will be retrieved when the next action potentials arrives the synapse. Abrogated endocytic adaptor binding accelerates NEP diffusion by reducing the size of the complex. In addition confinement and the extent of reclustering are reduced, since the clathrin-based endocytic machinery cannot bind the NEP. However, a fraction of proteins still reclusters by additional, yet unknown, factors that may also prevent a further escape of SV proteins in the absence of endocytic adaptor binding. Since not all proteins recluster efficiently, finally more and more non-clustered proteins get lost into the axon over time. Over long time periods synapses with deficient endocytic machinery run out of SV proteins, leading to the lack of functional SVs and defective neurotransmission that was previously observed in AP180 KO neurons (Koo et al., 2015).

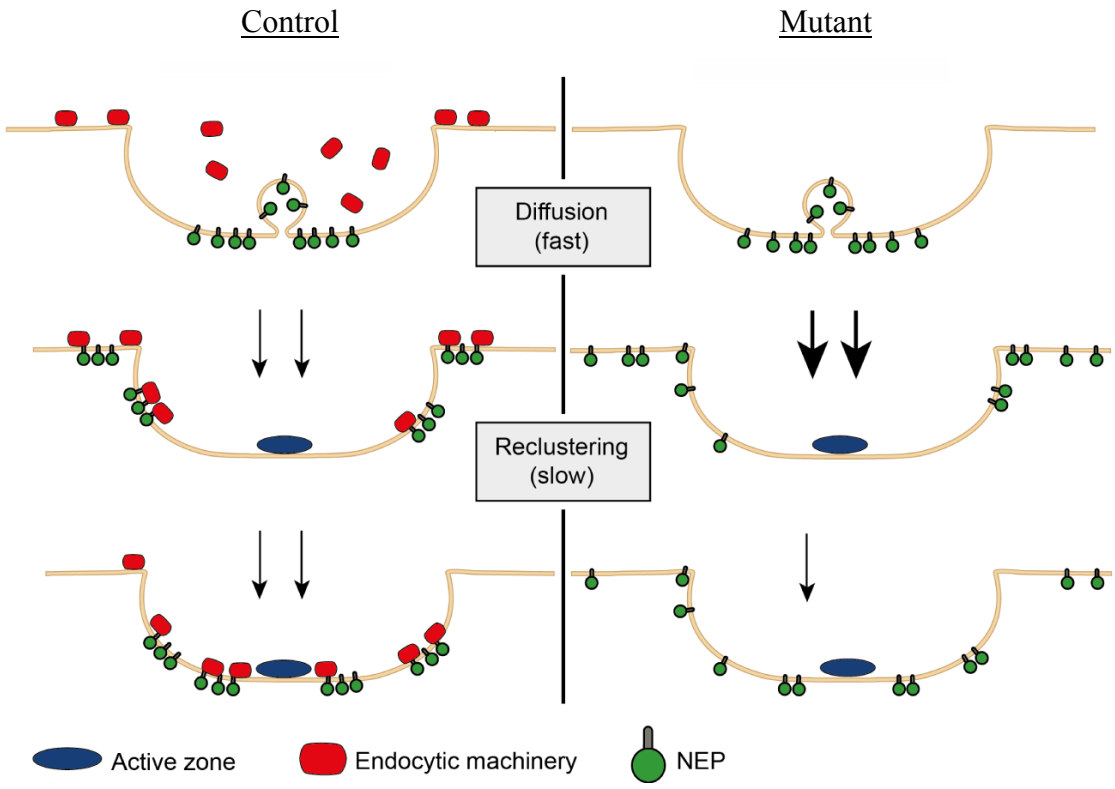

Figure 6-1: Summarizing model of protein diffusion, confinement, and reclustering.
Schematic model of SV protein confinement and reclustering and the role of the endocytic machinery: Following rapid diffusion (Control, top; Figure 4-16) newly exocytosed SV proteins remain confined within the presynaptic bouton (Control, middle; Figure 4-6), aided by their association with the endocytic machinery (Figure 4-23). Confinement is followed by SV protein reclustering within the periactive zone (Control, bottom; Figure 4-6). In cases where the association with endocytic adaptor is abrogated (Mutant), diffusion of newly exocytosed SV proteins is accelerated (bold arrows; Figure 4-17) and confinement is compromised (Figure 4-11, Figure 4-14). Some proteins still recluster efficiently, while others are being lost over time (Figure 4-12, Figure 4-13).

It was established, that a moderate electrical stimulation leads to clathrin-mediated endocytosis (Augustine et al., 2006; Granseth et al., 2006; Kononenko et al., 2014) of a preassembled RRetP (Fernández-Alfonso et al., 2006; Wienisch and Klingauf, 2006; Hua et al., 2011). However, the fate of newly exocytosed SV proteins remained unknown under such conditions. My work hopefully contributes to a better understanding of how the RRetP is created from newly exocytosed SV proteins. The findings raise new questions and further research will be required to particularize and complement the image of diffusional spread, confinement and reclustering of newly exocytosed SV proteins.

In this work, I demonstrate that the clathrin-based endocytic machinery is required for NEP confinement. The literature reports many more proteins that are involved in CME (McMahon and Boucrot, 2011). It would thus be interesting to investigate, which endocytic proteins beside AP180 and CALM, are further involved in NEP confinement. Studying confinement in neurons, systematically depleted for different components of the clathrin-based endocytic machinery, might provide insights on the maturation stage of the endocytic structures that immobilize the NEP in periactive zones. Another issue is patch diffusion. Whether released SV proteins remain as clusters or not was debated in the literature (Haucke et al., 2011; Rizzoli, 2014). My findings of slow Syb2, Syt1 and Syp diffusion at equal speed, together with the spatial segregation of NEP clusters from unretrieved surface-stranded SV proteins point towards patch diffusion. However, more direct evidence is required to validate such a scenario. Another unsolved question is, whether SV-derived cholesterol contributes to the remaining NEP confinement and reclustering in AP180- and CALM-deficient neurons. However, considering that cholesterol extraction from SVs impairs SV recycling (Dason et al., 2010), this remains a difficult issue. Whether a network of interactions between SV proteins promotes confinement and reclustering may be addressed by systematically combining KOs and KDs of diverse SV components.

7 Bibliography

Abbe, E. (1873). Beiträge zur Theorie des Mikroskops und der mikroskopischen Wahrnehmung. Arch. Für Mikrosk. Anat. *9*, 413–418.

Ahle, S., and Ungewickell, E. (1986). Purification and properties of a new clathrin assembly protein. EMBO J. *5*, 3143–3149.

Annibale, P., Scarselli, M., Greco, M., and Radenovic, A. (2012). Identification of the factors affecting co-localization precision for quantitative multicolor localization microscopy. Opt. Nanoscopy *1*, 9.

Arthur, C.P., and Stowell, M.H.B. (2007). Structure of synaptophysin: A hexameric MARVEL domain channel protein. Struct. Lond. Engl. 1993 *15*, 707–714.

Augustine, G.J., Morgan, J.R., Villalba-Galea, C.A., Jin, S., Prasad, K., and Lafer, E.M. (2006). Clathrin and synaptic vesicle endocytosis: studies at the squid giant synapse. Biochem. Soc. Trans. *34*, 68–72.

Becher, A., Drenckhahn, A., Pahner, I., Margittai, M., Jahn, R., and Ahnert-Hilger, G. (1999). The Synaptophysin–Synaptobrevin Complex: a Hallmark of Synaptic Vesicle Maturation. J. Neurosci. *19*, 1922–1931.

Bennett, M.K., Calakos, N., Kreiner, T., and Scheller, R.H. (1992). Synaptic vesicle membrane proteins interact to form a multimeric complex. J. Cell Biol. *116*, 761–775.

Bloom, O., Evergren, E., Tomilin, N., Kjaerulff, O., Löw, P., Brodin, L., Pieribone, V.A., Greengard, P., and Shupliakov, O. (2003). Colocalization of synapsin and actin during synaptic vesicle recycling. J. Cell Biol. *161*, 737–747.

van den Bogaart, G., Holt, M.G., Bunt, G., Riedel, D., Wouters, F.S., and Jahn, R. (2010). One SNARE complex is sufficient for membrane fusion. Nat. Struct. Mol. Biol. *17*, 358–364.

van den Bogaart, G., Meyenberg, K., Risselada, H.J., Amin, H., Willig, K.I., Hubrich, B.E., Dier, M., Hell, S.W., Grubmüller, H., Diederichsen, U., et al. (2011). Membrane protein sequestering by ionic protein-lipid interactions. Nature *479*, 552–555.

Boucrot, E., Ferreira, A.P.A., Almeida-Souza, L., Debard, S., Vallis, Y., Howard, G., Bertot, L., Sauvonnet, N., and McMahon, H.T. (2015). Endophilin marks and controls a clathrin-independent endocytic pathway. Nature *517*, 460–465.

Bowen, M., and Brunger, A.T. (2006). Conformation of the synaptobrevin transmembrane domain. Proc. Natl. Acad. Sci. U. S. A. *103*, 8378–8383.

Bradford, M.M. (1976). A rapid and sensitive method for the quantitation of microgram quantities of protein utilizing the principle of protein-dye binding. Anal. Biochem. *72*, 248–254.

Brodin, L., Löw, P., and Shupliakov, O. (2000). Sequential steps in clathrin-mediated synaptic vesicle endocytosis. Curr. Opin. Neurobiol. *10*, 312–320.

Bushlin, I., Petralia, R.S., Wu, F., Harel, A., Mughal, M.R., Mattson, M.P., and Yao, P.J. (2008). Clathrin Assembly Protein AP180 and CALM Differentially Control Axogenesis and Dendrite Outgrowth in Embryonic Hippocampal Neurons. J. Neurosci. Off. J. Soc. Neurosci. *28*, 10257–10271.

Calakos, N., and Scheller, R.H. (1994). Vesicle-associated membrane protein and synaptophysin are associated on the synaptic vesicle. J. Biol. Chem. *269*, 24534–24537.

Ceccarelli, B., Hurlbut, W.P., and Mauro, A. (1973). Turnover of Transmitter and Synaptic Vesicles at the Frog Neuromuscular Junction. J. Cell Biol. *57*, 499–524.

Chapman, E.R., Hanson, P.I., An, S., and Jahn, R. (1995). Ca2+ regulates the interaction between synaptotagmin and syntaxin 1. J. Biol. Chem. *270*, 23667–23671.

Chen, X., Barg, S., and Almers, W. (2008). Release of the Styryl Dyes from Single Synaptic Vesicles in Hippocampal Neurons. J. Neurosci. *28*, 1894–1903.

Coué, M., Brenner, S.L., Spector, I., and Korn, E.D. (1987). Inhibition of actin polymerization by latrunculin A. FEBS Lett. *213*, 316–318.

Crank, J. (1975). The mathematics of diffusion (Oxford, [Eng]: Clarendon Press).

Cremona, O., Di Paolo, G., Wenk, M.R., Lüthi, A., Kim, W.T., Takei, K., Daniell, L., Nemoto, Y., Shears, S.B., Flavell, R.A., et al. (1999). Essential role of phosphoinositide metabolism in synaptic vesicle recycling. Cell *99*, 179–188.

Darcy, K.J., Staras, K., Collinson, L.M., and Goda, Y. (2006). Constitutive sharing of recycling synaptic vesicles between presynaptic boutons. Nat. Neurosci. *9*, 315–321.

Dason, J.S., Smith, A.J., Marin, L., and Charlton, M.P. (2010). Vesicular Sterols Are Essential for Synaptic Vesicle Cycling. J. Neurosci. *30*, 15856–15865.

Dason, J.S., Smith, A.J., Marin, L., and Charlton, M.P. (2013). Cholesterol and F-actin are Required for Clustering of Recycling Synaptic Vesicle Proteins in the Presynaptic Plasma Membrane. J. Physiol. jphysiol.2013.265447.

Daumke, O., Roux, A., and Haucke, V. (2014). BAR Domain Scaffolds in Dynamin-Mediated Membrane Fission. Cell *156*, 882–892.

Deák, F., Schoch, S., Liu, X., Südhof, T.C., and Kavalali, E.T. (2004). Synaptobrevin is essential for fast synaptic-vesicle endocytosis. Nat. Cell Biol. *6*, 1102–1108.

Dieck, S., Sanmartí-Vila, L., Langnaese, K., Richter, K., Kindler, S., Soyke, A., Wex, H., Smalla, K.H., Kämpf, U., Fränzer, J.T., et al. (1998). Bassoon, a novel zinc-finger CAG/glutamine-repeat protein selectively localized at the active zone of presynaptic nerve terminals. J. Cell Biol. *142*, 499–509.

Di Paolo, G., Moskowitz, H.S., Gipson, K., Wenk, M.R., Voronov, S., Obayashi, M., Flavell, R., Fitzsimonds, R.M., Ryan, T.A., and De Camilli, P. (2004). Impaired PtdIns(4,5)P2 synthesis in nerve terminals produces defects in synaptic vesicle trafficking. Nature *431*, 415–422.

Diril, M.K., Wienisch, M., Jung, N., Klingauf, J., and Haucke, V. (2006). Stonin 2 is an AP-2-dependent endocytic sorting adaptor for synaptotagmin internalization and recycling. Dev. Cell *10*, 233–244.

Dittman, J.S., and Kaplan, J.M. (2006). Factors regulating the abundance and localization of synaptobrevin in the plasma membrane. Proc. Natl. Acad. Sci. U. S. A. *103*, 11399–11404.

Dreyling, M.H., Martinez-Climent, J.A., Zheng, M., Mao, J., Rowley, J.D., and Bohlander, S.K. (1996). The t(10;11)(p13;q14) in the U937 cell line results in the fusion of the AF10 gene and CALM, encoding a new member of the AP-3 clathrin assembly protein family. Proc. Natl. Acad. Sci. U. S. A. *93*, 4804–4809.

Droese, S., Bindseil, K.U., Bowman, E.J., Siebers, A., Zeeck, A., and Altendorf, K. (1993). Inhibitory effect of modified bafilomycins and concanamycins on P- and V-type adenosinetriphosphatases. Biochemistry (Mosc.) *32*, 3902–3906.

Edelmann, L., Hanson, P.I., Chapman, E.R., and Jahn, R. (1995). Synaptobrevin binding to synaptophysin: a potential mechanism for controlling the exocytotic fusion machine. EMBO J. *14*, 224–231.

El-Shaarawi, A.H., and Piegorsch, W.W. (2002). Encyclopedia of Environmetrics (Wiley).

Fdez, E., Martínez-Salvador, M., Beard, M., Woodman, P., and Hilfiker, S. (2010). Transmembrane-domain determinants for SNARE-mediated membrane fusion. J. Cell Sci. *123*, 2473–2480.

Ferguson, S.M., and De Camilli, P. (2012). Dynamin, a membrane-remodelling GTPase. Nat. Rev. Mol. Cell Biol. *13*, 75–88.

Fernández-Alfonso, T., Kwan, R., and Ryan, T.A. (2006). Synaptic Vesicles Interchange Their Membrane Proteins with a Large Surface Reservoir during Recycling. Neuron *51*, 179–186.

Fernández-Chacón, R., Königstorfer, A., Gerber, S.H., García, J., Matos, M.F., Stevens, C.F., Brose, N., Rizo, J., Rosenmund, C., and Südhof, T.C. (2001). Synaptotagmin I functions as a calcium regulator of release probability. Nature *410*, 41–49.

Ford, M.G.J., Pearse, B.M.F., Higgins, M.K., Vallis, Y., Owen, D.J., Gibson, A., Hopkins, C.R., Evans, P.R., and McMahon, H.T. (2001). Simultaneous Binding of PtdIns(4,5)P2 and Clathrin by AP180 in the Nucleation of Clathrin Lattices on Membranes. Science *291*, 1051–1055.

Gandhi, S.P., and Stevens, C.F. (2003). Three modes of synaptic vesicular recycling revealed by single-vesicle imaging. Nature *423*, 607–613.

Ganguly, A., Tang, Y., Wang, L., Ladt, K., Loi, J., Dargent, B., Leterrier, C., and Roy, S. (2015). A dynamic formin-dependent deep F-actin network in axons. J. Cell Biol. *210*, 401–417.

Gasnier, B. (2000). The loading of neurotransmitters into synaptic vesicles. Biochimie *82*, 327–337.

Geppert, M., Goda, Y., Hammer, R.E., Li, C., Rosahl, T.W., Stevens, C.F., and Südhof, T.C. (1994). Synaptotagmin I: a major Ca2+ sensor for transmitter release at a central synapse. Cell *79*, 717–727.

Gerona, R.R., Larsen, E.C., Kowalchyk, J.A., and Martin, T.F. (2000). The C terminus of SNAP25 is essential for Ca(2+)-dependent binding of synaptotagmin to SNARE complexes. J. Biol. Chem. *275*, 6328–6336.

Gordon, S.L., and Cousin, M.A. (2014). The Sybtraps: Control of Synaptobrevin Traffic by Synaptophysin, α-Synuclein and AP-180. Traffic *15*, 245–254.

Gordon, S.L., Leube, R.E., and Cousin, M.A. (2011). Synaptophysin is required for synaptobrevin retrieval during synaptic vesicle endocytosis. J. Neurosci. *31*, 14032–14036.

Granseth, B., Odermatt, B., Royle, S.J., and Lagnado, L. (2006). Clathrin-Mediated Endocytosis Is the Dominant Mechanism of Vesicle Retrieval at Hippocampal Synapses. Neuron *51*, 773–786.

Grote, E., and Kelly, R.B. (1996). Endocytosis of VAMP is facilitated by a synaptic vesicle targeting signal. J. Cell Biol. *132*, 537–547.

Gustafsson, M.G. (2000). Surpassing the lateral resolution limit by a factor of two using structured illumination microscopy. J. Microsc. *198*, 82–87.

Harata, N.C., Choi, S., Pyle, J.L., Aravanis, A.M., and Tsien, R.W. (2006). Frequency-Dependent Kinetics and Prevalence of Kiss-and-Run and Reuse at Hippocampal Synapses Studied with Novel Quenching Methods. Neuron *49*, 243–256.

Harel, A., Wu, F., Mattson, M.P., Morris, C.M., and Yao, P.J. (2008). Evidence for CALM in Directing VAMP2 Trafficking. Traffic *9*, 417–429.

Haucke, V., and De Camilli, P. (1999). AP-2 recruitment to synaptotagmin stimulated by tyrosine-based endocytic motifs. Science *285*, 1268–1271.

Haucke, V., Neher, E., and Sigrist, S.J. (2011). Protein scaffolds in the coupling of synaptic exocytosis and endocytosis. Nat Rev Neurosci *12*, 127–138.

Heilemann, M., van de Linde, S., Schüttpelz, M., Kasper, R., Seefeldt, B., Mukherjee, A., Tinnefeld, P., and Sauer, M. (2008). Subdiffraction-Resolution Fluorescence Imaging with Conventional Fluorescent Probes. Angew. Chem. Int. Ed. *47*, 6172–6176.

Henne, W.M., Boucrot, E., Meinecke, M., Evergren, E., Vallis, Y., Mittal, R., and McMahon, H.T. (2010). FCHo proteins are nucleators of clathrin-mediated endocytosis. Science *328*, 1281–1284.

Heuser, J.E., and Reese, T.S. (1973). Evidence for Recycling of Synaptic Vesicle Membrane During Transmitter Release at the Frog Neuromuscular Junction. J. Cell Biol. *57*, 315–344.

Heuser, J.E., and Reese, T.S. (1981). Structural changes after transmitter release at the frog neuromuscular junction. J. Cell Biol. *88*, 564–580.

Hosoi, N., Holt, M., and Sakaba, T. (2009). Calcium Dependence of Exo- and Endocytotic Coupling at a Glutamatergic Synapse. Neuron *63*, 216–229.

Hua, Y., Sinha, R., Thiel, C.S., Schmidt, R., Huve, J., Martens, H., Hell, S.W., Egner, A., and Klingauf, J. (2011). A readily retrievable pool of synaptic vesicles. Nat Neurosci *14*, 833–839.

Hua, Y., Woehler, A., Kahms, M., Haucke, V., Neher, E., and Klingauf, J. (2013). Blocking Endocytosis Enhances Short-Term Synaptic Depression under Conditions of Normal Availability of Vesicles. Neuron *80*, 343–349.

Huang, B., Bates, M., and Zhuang, X. (2009). Super-resolution fluorescence microscopy. Annu. Rev. Biochem. *78*, 993–1016.

Hui, E., Johnson, C.P., Yao, J., Dunning, F.M., and Chapman, E.R. (2009). Synaptotagmin-Mediated Bending of the Target Membrane Is a Critical Step in Ca2+-Regulated Fusion. Cell *138*, 709–721.

Imig, C., Min, S.-W., Krinner, S., Arancillo, M., Rosenmund, C., Südhof, T.C., Rhee, J., Brose, N., and Cooper, B.H. (2014). The Morphological and Molecular Nature of Synaptic Vesicle Priming at Presynaptic Active Zones. Neuron *84*, 416–431.

Jahn, R., and Scheller, R.H. (2006). SNAREs — engines for membrane fusion. Nat. Rev. Mol. Cell Biol. *7*, 631–643.

Jia, J.-Y., Lamer, S., Schümann, M., Schmidt, M.R., Krause, E., and Haucke, V. (2006). Quantitative proteomics analysis of detergent-resistant membranes from chemical synapses: evidence for cholesterol as spatial organizer of synaptic vesicle cycling. Mol. Cell. Proteomics MCP *5*, 2060–2071.

Jung, N., and Haucke, V. (2007). Clathrin-mediated endocytosis at synapses. Traffic Cph. Den. *8*, 1129–1136.

Kaempf, N., Kochlamazashvili, G., Puchkov, D., Maritzen, T., Bajjalieh, S.M., Kononenko, N.L., and Haucke, V. (2015). Overlapping functions of stonin 2 and SV2 in sorting of the calcium sensor synaptotagmin 1 to synaptic vesicles. Proc. Natl. Acad. Sci. *112*, 7297–7302.

Katz, B., and Miledi, R. (1967). The timing of calcium action during neuromuscular transmission. J. Physiol. *189*, 535–544.

Kawasaki, F., Hazen, M., and Ordway, R.W. (2000). Fast synaptic fatigue in shibire mutants reveals a rapid requirement for dynamin in synaptic vesicle membrane trafficking. Nat. Neurosci. *3*, 859–860.

Khvotchev, M.V., and Südhof, T.C. (2004). Stimulus-dependent dynamic homo- and heteromultimerization of synaptobrevin/VAMP and synaptophysin. Biochemistry (Mosc.) *43*, 15037–15043.

Kiskowski, M.A., Hancock, J.F., and Kenworthy, A.K. (2009). On the Use of Ripley's K-Function and Its Derivatives to Analyze Domain Size. Biophys. J. *97*, 1095–1103.

von Kleist, L., Stahlschmidt, W., Bulut, H., Gromova, K., Puchkov, D., Robertson, M.J., Macgregor, K.A., Tomlin, N., Pechstein, A., Chau, N., et al. (2011). Role of the clathrin terminal domain in regulating coated pit dynamics revealed by small molecule inhibition. Cell *146*, 471–484.

Koh, T.-W., Verstreken, P., and Bellen, H.J. (2004). Dap160/Intersectin Acts as a Stabilizing Scaffold Required for Synaptic Development and Vesicle Endocytosis. Neuron *43*, 193–205.

Koh, T.-W., Korolchuk, V.I., Wairkar, Y.P., Jiao, W., Evergren, E., Pan, H., Zhou, Y., Venken, K.J.T., Shupliakov, O., Robinson, I.M., et al. (2007). Eps15 and Dap160 control synaptic vesicle membrane retrieval and synapse development. J. Cell Biol. *178*, 309–322.

Kononenko, N.L., and Haucke, V. (2015). Molecular Mechanisms of Presynaptic Membrane Retrieval and Synaptic Vesicle Reformation. Neuron *85*, 484–496.

Kononenko, N.L., Pechstein, A., and Haucke, V. (2013a). The tortoise and the hare revisited. eLife *2*.

Kononenko, N.L., Diril, M.K., Puchkov, D., Kintscher, M., Koo, S.J., Pfuhl, G., Winter, Y., Wienisch, M., Klingauf, J., Breustedt, J., et al. (2013b). Compromised fidelity of endocytic synaptic vesicle protein sorting in the absence of stonin 2. Proc. Natl. Acad. Sci. *110*, E526–E535.

Kononenko, N.L., Puchkov, D., Classen, G.A., Walter, A.M., Pechstein, A., Sawade, L., Kaempf, N., Trimbuch, T., Lorenz, D., Rosenmund, C., et al. (2014). Clathrin/AP-2 Mediate Synaptic Vesicle Reformation from Endosome-like Vacuoles but Are Not Essential for Membrane Retrieval at Central Synapses. Neuron *82*, 981–988.

Koo, S.J., Markovic, S., Puchkov, D., Mahrenholz, C.C., Beceren-Braun, F., Maritzen, T., Dernedde, J., Volkmer, R., Oschkinat, H., and Haucke, V. (2011a). SNARE motif-mediated sorting of synaptobrevin by the endocytic adaptors clathrin assembly lymphoid myeloid leukemia (CALM) and AP180 at synapses. Proc. Natl. Acad. Sci. *108*, 13540–13545.

Koo, S.J., Puchkov, D., and Haucke, V. (2011b). AP180 and CALM: Dedicated endocytic adaptors for the retrieval of synaptobrevin 2 at synapses. Cell. Logist. *1*, 168–172.

Koo, S.J., Kochlamazashvili, G., Rost, B., Puchkov, D., Gimber, N., Lehmann, M., Tadeus, G., Schmoranzer, J., Rosenmund, C., Haucke, V., et al. (2015). Vesicular

Synaptobrevin/VAMP2 Levels Guarded by AP180 Control Efficient Neurotransmission. Neuron.

Kwon, S.E., and Chapman, E.R. (2011). Synaptophysin regulates the kinetics of synaptic vesicle endocytosis in central neurons. Neuron *70*, 847–854.

Lampe, A., Haucke, V., Sigrist, S.J., Heilemann, M., and Schmoranzer, J. (2012). Multi-colour direct STORM with red emitting carbocyanines. Biol. Cell *104*, 229–237.

Lampe, A., Tadeus, G., and Schmoranzer, J. (2015). Spectral demixing avoids registration errors and reduces noise in multicolor localization-based super-resolution microscopy. Methods Appl. Fluoresc. *3*, 034006.

de Lange, R.P.J., de Roos, A.D.G., and Borst, J.G.G. (2003). Two modes of vesicle recycling in the rat calyx of Held. J. Neurosci. Off. J. Soc. Neurosci. *23*, 10164–10173.

Lehmann, M., Lichtner, G., Klenz, H., and Schmoranzer, J. (2015). Novel organic dyes for multicolor localization-based super-resolution microscopy. J. Biophotonics n/a – n/a.

Li, Z., and Murthy, V.N. (2001). Visualizing postendocytic traffic of synaptic vesicles at hippocampal synapses. Neuron *31*, 593–605.

Loerke, D., Mettlen, M., Yarar, D., Jaqaman, K., Jaqaman, H., Danuser, G., and Schmid, S.L. (2009). Cargo and Dynamin Regulate Clathrin-Coated Pit Maturation. PLoS Biol. *7*.

Lois, C., Hong, E.J., Pease, S., Brown, E.J., and Baltimore, D. (2002). Germline transmission and tissue-specific expression of transgenes delivered by lentiviral vectors. Science *295*, 868–872.

Marie, B., Sweeney, S.T., Poskanzer, K.E., Roos, J., Kelly, R.B., and Davis, G.W. (2004). Dap160/Intersectin Scaffolds the Periactive Zone to Achieve High-Fidelity Endocytosis and Normal Synaptic Growth. Neuron *43*, 207–219.

Maritzen, T., Koo, S.J., and Haucke, V. (2012). Turning CALM into excitement: AP180 and CALM in endocytosis and disease. Biol. Cell Auspices Eur. Cell Biol. Organ. *104*, 588–602.

Martens, S., and McMahon, H.T. (2008). Mechanisms of membrane fusion: disparate players and common principles. Nat. Rev. Mol. Cell Biol. *9*, 543–556.

McMahon, H.T., and Boucrot, E. (2011). Molecular mechanism and physiological functions of clathrin-mediated endocytosis. Nat. Rev. Mol. Cell Biol. *12*, 517–533.

McMahon, H.T., and Gallop, J.L. (2005). Membrane curvature and mechanisms of dynamic cell membrane remodelling. Nature *438*, 590–596.

McMahon, H.T., Bolshakov, V.Y., Janz, R., Hammer, R.E., Siegelbaum, S.A., and Südhof, T.C. (1996). Synaptophysin, a major synaptic vesicle protein, is not essential for neurotransmitter release. Proc. Natl. Acad. Sci. U. S. A. *93*, 4760–4764.

Miesenböck, G., De Angelis, D.A., and Rothman, J.E. (1998). Visualizing secretion and synaptic transmission with pH-sensitive green fluorescent proteins. Nature *394*, 192–195.

Miller, T.M., and Heuser, J.E. (1984). Endocytosis of synaptic vesicle membrane at the frog neuromuscular junction. J. Cell Biol. *98*, 685–698.

Milosevic, I., Sørensen, J.B., Lang, T., Krauss, M., Nagy, G., Haucke, V., Jahn, R., and Neher, E. (2005). Plasmalemmal phosphatidylinositol-4,5-bisphosphate level regulates the releasable vesicle pool size in chromaffin cells. J. Neurosci. Off. J. Soc. Neurosci. *25*, 2557–2565.

Milosevic, I., Giovedi, S., Lou, X., Raimondi, A., Collesi, C., Shen, H., Paradise, S., O'Toole, E., Ferguson, S., Cremona, O., et al. (2011). Recruitment of endophilin to clathrin-coated pit necks is required for efficient vesicle uncoating after fission. Neuron *72*, 587–601.

Mitter, D., Reisinger, C., Hinz, B., Hollmann, S., Yelamanchili, S.V., Treiber-Held, S., Ohm, T.G., Herrmann, A., and Ahnert-Hilger, G. (2003). The synaptophysin/synaptobrevin interaction critically depends on the cholesterol content. J. Neurochem. *84*, 35–42.

Mohrmann, R., Wit, H. de, Verhage, M., Neher, E., and Sørensen, J.B. (2010). Fast Vesicle Fusion in Living Cells Requires at Least Three SNARE Complexes. Science *330*, 502–505.

Morgan, J.R., Prasad, K., Jin, S., Augustine, G.J., and Lafer, E.M. (2003). Eps15 Homology Domain-NPF Motif Interactions Regulate Clathrin Coat Assembly during Synaptic Vesicle Recycling. J. Biol. Chem. *278*, 33583–33592.

Mueller, V.J., Wienisch, M., Nehring, R.B., and Klingauf, J. (2004). Monitoring Clathrin-Mediated Endocytosis during Synaptic Activity. J. Neurosci. *24*, 2004–2012.

Mutch, S.A., Kensel-Hammes, P., Gadd, J.C., Fujimoto, B.S., Allen, R.W., Schiro, P.G., Lorenz, R.M., Kuyper, C.L., Kuo, J.S., Bajjalieh, S.M., et al. (2011). Protein quantification at the single vesicle level reveals that a subset of synaptic vesicle proteins are trafficked with high precision. J. Neurosci. Off. J. Soc. Neurosci. *31*, 1461–1470.

Nakada, C., Ritchie, K., Oba, Y., Nakamura, M., Hotta, Y., Iino, R., Kasai, R.S., Yamaguchi, K., Fujiwara, T., and Kusumi, A. (2003). Accumulation of anchored proteins forms membrane diffusion barriers during neuronal polarization. Nat. Cell Biol. *5*, 626–632.

Neher, E. (2010). What is Rate-Limiting during Sustained Synaptic Activity: Vesicle Supply or the Availability of Release Sites. Front. Synaptic Neurosci. *2*.

Nicholson-Fish, J.C., Kokotos, A.C., Gillingwater, T.H., Smillie, K.J., and Cousin, M.A. (2015). VAMP4 Is an Essential Cargo Molecule for Activity-Dependent Bulk Endocytosis. Neuron *88*, 973–984.

Nicholson-Tomishima, K., and Ryan, T.A. (2004). Kinetic efficiency of endocytosis at mammalian CNS synapses requires synaptotagmin I. Proc. Natl. Acad. Sci. U. S. A. *101*, 16648–16652.

Opazo, F., Punge, A., Bückers, J., Hoopmann, P., Kastrup, L., Hell, S.W., and Rizzoli, S.O. (2010). Limited Intermixing of Synaptic Vesicle Components upon Vesicle Recycling. Traffic *11*, 800–812.

Pan, P.-Y., Marrs, J., and Ryan, T.A. (2015). Vesicular Glutamate Transporter 1 Orchestrates Recruitment of Other Synaptic Vesicle Cargo Proteins during Synaptic Vesicle Recycling. J. Biol. Chem. *290*, 22593–22601.

Pennuto, M., Bonanomi, D., Benfenati, F., and Valtorta, F. (2003). Synaptophysin I Controls the Targeting of VAMP2/Synaptobrevin II to Synaptic Vesicles. Mol. Biol. Cell *14*, 4909–4919.

Perin, M.S., Brose, N., Jahn, R., and Südhof, T.C. (1991). Domain structure of synaptotagmin (p65). J. Biol. Chem. *266*, 623–629.

Posor, Y., Eichhorn-Grünig, M., and Haucke, V. (2015). Phosphoinositides in endocytosis. Biochim. Biophys. Acta *1851*, 794–804.

Puszkin, S., Perry, D., Li, S., and Hanson, V. (1992). Neuronal protein NP185 is developmentally regulated, initially expressed during synaptogenesis, and localized in synaptic terminals. Mol. Neurobiol. *6*, 253–283.

Rajappa, R., Gauthier-Kemper, A., Böning, D., Hüve, J., and Klingauf, J. (2016). Anatomy and dynamics of a supramolecular membrane protein cluster. Cell Rep. *14*, 1369–1381.

Ramadurai, S., Holt, A., Krasnikov, V., van den Bogaart, G., Killian, J.A., and Poolman, B. (2009). Lateral diffusion of membrane proteins. J. Am. Chem. Soc. *131*, 12650–12656.

Rayleigh, J.W.S. (1879). Investigations in optics, with special reference to the spectroscope. (London: s.n.]).

Richards, D.A., Guatimosim, C., and Betz, W.J. (2000). Two Endocytic Recycling Routes Selectively Fill Two Vesicle Pools in Frog Motor Nerve Terminals. Neuron *27*, 551–559.

Richards, D.A., Bai, J., and Chapman, E.R. (2005). Two modes of exocytosis at hippocampal synapses revealed by rate of FM1-43 efflux from individual vesicles. J. Cell Biol. *168*, 929–939.

Riedl, J., Crevenna, A.H., Kessenbrock, K., Yu, J.H., Neukirchen, D., Bista, M., Bradke, F., Jenne, D., Holak, T.A., Werb, Z., et al. (2008). Lifeact: a versatile marker to visualize F-actin. Nat. Methods *5*, 605.

Rizzoli, S.O. (2014). Synaptic vesicle recycling: steps and principles. EMBO J. *33*, 788–822.

Rizzoli, S.O., and Betz, W.J. (2005). Synaptic vesicle pools. Nat. Rev. Neurosci. *6*, 57–69.

Roos, J., and Kelly, R.B. (1999). The endocytic machinery in nerve terminals surrounds sites of exocytosis. Curr. Biol. *9*, 1411–1414.

Rowlingson, B.S., and Diggle, P.J. (1993). Splancs: Spatial point pattern analysis code in S-plus. Comput. Geosci. *19*, 627–655.

Saffman, P.G., and Delbrück, M. (1975). Brownian motion in biological membranes. Proc. Natl. Acad. Sci. U. S. A. *72*, 3111–3113.

Saheki, Y., and Camilli, P.D. (2012). Synaptic Vesicle Endocytosis. Cold Spring Harb. Perspect. Biol. *4*, a005645.

Saka, S.K., Honigmann, A., Eggeling, C., Hell, S.W., Lang, T., and Rizzoli, S.O. (2014). Multi-protein assemblies underlie the mesoscale organization of the plasma membrane. Nat. Commun. *5*.

Sakaba, T., Kononenko, N.L., Bacetic, J., Pechstein, A., Schmoranzer, J., Yao, L., Barth, H., Shupliakov, O., Kobler, O., Aktories, K., et al. (2013). Fast neurotransmitter release regulated by the endocytic scaffold intersectin. Proc. Natl. Acad. Sci. *110*, 8266–8271.

Sanger, F., and Coulson, A.R. (1975). A rapid method for determining sequences in DNA by primed synthesis with DNA polymerase. J. Mol. Biol. *94*, 441–448.

Sankaranarayanan, S., and Ryan, T.A. (2000). Real-time measurements of vesicle-SNARE recycling in synapses of the central nervous system. Nat. Cell Biol. *2*, 197–204.

Sankaranarayanan, S., De Angelis, D., Rothman, J.E., and Ryan, T.A. (2000). The use of pHluorins for optical measurements of presynaptic activity. Biophys. J. *79*, 2199–2208.

Schikorski, T., and Stevens, C.F. (1997). Quantitative Ultrastructural Analysis of Hippocampal Excitatory Synapses. J. Neurosci. *17*, 5858–5867.

Schikorski, T., and Stevens, C.F. (2001). Morphological correlates of functionally defined synaptic vesicle populations. Nat. Neurosci. *4*, 391–395.

Schindelin, J., Arganda-Carreras, I., Frise, E., Kaynig, V., Longair, M., Pietzsch, T., Preibisch, S., Rueden, C., Saalfeld, S., Schmid, B., et al. (2012). Fiji: an open-source platform for biological-image analysis. Nat. Methods *9*, 676–682.

Schlossman, D.M., Schmid, S.L., Braell, W.A., and Rothman, J.E. (1984). An enzyme that removes clathrin coats: purification of an uncoating ATPase. J. Cell Biol. *99*, 723–733.

Schmid, E.M., and McMahon, H.T. (2007). Integrating molecular and network biology to decode endocytosis. Nature *448*, 883–888.

Schmoranzer, J., Goulian, M., Axelrod, D., and Simon, S.M. (2000). Imaging Constitutive Exocytosis with Total Internal Reflection Fluorescence Microscopy. J. Cell Biol. *149*, 23–32.

Schneggenburger, R., Meyer, A.C., and Neher, E. (1999). Released Fraction and Total Size of a Pool of Immediately Available Transmitter Quanta at a Calyx Synapse. Neuron *23*, 399–409.

Schneider, C.A., Rasband, W.S., and Eliceiri, K.W. (2012). NIH Image to ImageJ: 25 years of image analysis. Nat. Methods *9*, 671–675.

Schoch, S., Deák, F., Königstorfer, A., Mozhayeva, M., Sara, Y., Südhof, T.C., and Kavalali, E.T. (2001). SNARE function analyzed in synaptobrevin/VAMP knockout mice. Science *294*, 1117–1122.

Shapiro, A.L., Viñuela, E., and Maizel, J.V. (1967). Molecular weight estimation of polypeptide chains by electrophoresis in SDS-polyacrylamide gels. Biochem. Biophys. Res. Commun. *28*, 815–820.

Shi, L., Shen, Q.-T., Kiel, A., Wang, J., Wang, H.-W., Melia, T.J., Rothman, J.E., and Pincet, F. (2012). SNARE Proteins: One to Fuse and Three to Keep the Nascent Fusion Pore Open. Science *335*, 1355–1359.

Shupliakov, O., Löw, P., Grabs, D., Gad, H., Chen, H., David, C., Takei, K., de Camilli, P., and Brodin, L. (1997). Synaptic Vesicle Endocytosis Impaired by Disruption of Dynamin-SH3 Domain Interactions. Science *276*, 259–263.

Shupliakov, O., Bloom, O., Gustafsson, J.S., Kjaerulff, O., Löw, P., Tomilin, N., Pieribone, V.A., Greengard, P., and Brodin, L. (2002). Impaired recycling of synaptic vesicles after acute perturbation of the presynaptic actin cytoskeleton. Proc. Natl. Acad. Sci. *99*, 14476–14481.

Sinha, R., Ahmed, S., Jahn, R., and Klingauf, J. (2011). Two synaptobrevin molecules are sufficient for vesicle fusion in central nervous system synapses. Proc. Natl. Acad. Sci. U. S. A.

Sochacki, K.A., Larson, B.T., Sengupta, D.C., Daniels, M.P., Shtengel, G., Hess, H.F., and Taraska, J.W. (2012). Imaging the post-fusion release and capture of a vesicle membrane protein. Nat. Commun. *3*, 1154.

Stahlschmidt, W., Robertson, M.J., Robinson, P.J., McCluskey, A., and Haucke, V. (2014). Clathrin Terminal Domain-Ligand Interactions Regulate Sorting of Mannose 6-Phosphate Receptors Mediated by AP-1 and GGA Adaptors. J. Biol. Chem. *289*, 4906–4918.

Stevens, D.R., Wu, Z.-X., Matti, U., Junge, H.J., Schirra, C., Becherer, U., Wojcik, S.M., Brose, N., and Rettig, J. (2005). Identification of the minimal protein domain required for priming activity of Munc13-1. Curr. Biol. CB *15*, 2243–2248.

Stobrawa, S.M., Breiderhoff, T., Takamori, S., and Jentsch, T.J. (2001). Disruption of ClC-3, a chloride channel expressed on synaptic vesicles, leads to a loss of the hippocampus. Neuron *29*, 185–196.

Stuurman, N., Edelstein, A.D., Amodaj, N., Hoover, K.H., and Vale, R.D. (2010). Computer Control of Microscopes using μManager. Curr. Protoc. Mol. Biol. Ed. Frederick M Ausubel Al *CHAPTER*, Unit14.20.

Südhof, T.C. (2004). The Synaptic Vesicle Cycle. Annu. Rev. Neurosci. *27*, 509–547.

Südhof, T.C. (2013). Neurotransmitter Release: The Last Millisecond in the Life of a Synaptic Vesicle. Neuron *80*, 675–690.

Sun, J.-Y., Wu, X.-S., and Wu, L.-G. (2002). Single and multiple vesicle fusion induce different rates of endocytosis at a central synapse. Nature *417*, 555–559.

Sundborger, A., Soderblom, C., Vorontsova, O., Evergren, E., Hinshaw, J.E., and Shupliakov, O. (2011). An endophilin–dynamin complex promotes budding of clathrin-coated vesicles during synaptic vesicle recycling. J Cell Sci *124*, 133–143.

Tadeus, G., Lampe, A., and Schmoranzer, J. (2015). SDmixer —a versatile software tool for spectral demixing of multicolor single molecule localization data. Methods Appl. Fluoresc. *3*, 037001.

Takamori, S. (2006). Molecular anatomy of a trafficking organelle. Cell *127*, 831–846.

Teng, H., and Wilkinson, R.S. (2000). Clathrin-Mediated Endocytosis near Active Zones in Snake Motor Boutons. J. Neurosci. *20*, 7986–7993.

Teng, H., Cole, J.C., Roberts, R.L., and Wilkinson, R.S. (1999). Endocytic Active Zones: Hot Spots for Endocytosis in Vertebrate Neuromuscular Terminals. J. Neurosci. *19*, 4855–4866.

Thiele, C., Hannah, M.J., Fahrenholz, F., and Huttner, W.B. (2000). Cholesterol binds to synaptophysin and is required for biogenesis of synaptic vesicles. Nat. Cell Biol. *2*, 42–49.

Thomas, L., Hartung, K., Langosch, D., Rehm, H., Bamberg, E., Franke, W.W., and Betz, H. (1988). Identification of synaptophysin as a hexameric channel protein of the synaptic vesicle membrane. Science *242*, 1050–1053.

Towbin, H., Staehelin, T., and Gordon, J. (1992). Electrophoretic transfer of proteins from polyacrylamide gels to nitrocellulose sheets: procedure and some applications. 1979. Biotechnol. Read. Mass *24*, 145–149.

Traub, L.M. (2005). Common principles in clathrin-mediated sorting at the Golgi and the plasma membrane. Biochim. Biophys. Acta *1744*, 415–437.

Ungewickell, E., Ungewickell, H., Holstein, S.E., Lindner, R., Prasad, K., Barouch, W., Martin, B., Greene, L.E., and Eisenberg, E. (1995). Role of auxilin in uncoating clathrin-coated vesicles. Nature *378*, 632–635.

Voglmaier, S.M., Kam, K., Yang, H., Fortin, D.L., Hua, Z., Nicoll, R.A., and Edwards, R.H. (2006). Distinct Endocytic Pathways Control the Rate and Extent of Synaptic Vesicle Protein Recycling. Neuron *51*, 71–84.

Wahl, S., Katiyar, R., and Schmitz, F. (2013). A Local, Periactive Zone Endocytic Machinery at Photoreceptor Synapses in Close Vicinity to Synaptic Ribbons. J. Neurosci. *33*, 10278–10300.

Watanabe, S., Liu, Q., Davis, M.W., Hollopeter, G., Thomas, N., Jorgensen, N.B., and Jorgensen, E.M. (2013a). Ultrafast endocytosis at Caenorhabditis elegans neuromuscular junctions. eLife *2*.

Watanabe, S., Rost, B.R., Camacho-Pérez, M., Davis, M.W., Söhl-Kielczynski, B., Rosenmund, C., and Jorgensen, E.M. (2013b). Ultrafast endocytosis at mouse hippocampal synapses. Nature *504*, 242–247.

Watanabe, S., Trimbuch, T., Camacho-Pérez, M., Rost, B.R., Brokowski, B., Söhl-Kielczynski, B., Felies, A., Davis, M.W., Rosenmund, C., and Jorgensen, E.M. (2014). Clathrin regenerates synaptic vesicles from endosomes. Nature *advance online publication*.

Wenk, M.R., Pellegrini, L., Klenchin, V.A., Di Paolo, G., Chang, S., Daniell, L., Arioka, M., Martin, T.F., and De Camilli, P. (2001). PIP kinase Igamma is the major PI(4,5)P(2) synthesizing enzyme at the synapse. Neuron *32*, 79–88.

Wienisch, M., and Klingauf, J. (2006). Vesicular proteins exocytosed and subsequently retrieved by compensatory endocytosis are nonidentical. Nat. Neurosci. *9*, 1019–1027.

Wilhelm, B.G., Mandad, S., Truckenbrodt, S., Kröhnert, K., Schäfer, C., Rammner, B., Koo, S.J., Claßen, G.A., Krauss, M., Haucke, V., et al. (2014). Composition of isolated synaptic boutons reveals the amounts of vesicle trafficking proteins. Science *344*, 1023–1028.

Willig, K.I., Rizzoli, S.O., Westphal, V., Jahn, R., and Hell, S.W. (2006). STED microscopy reveals that synaptotagmin remains clustered after synaptic vesicle exocytosis. Nature *440*, 935–939.

Wolter, S., Löschberger, A., Holm, T., Aufmkolk, S., Dabauvalle, M.-C., van de Linde, S., and Sauer, M. (2012). rapidSTORM: accurate, fast open-source software for localization microscopy. Nat. Methods *9*, 1040–1041.

Wu, F., Mattson, M.P., and Yao, P.J. (2010). Neuronal activity and the expression of clathrin-assembly protein AP180. Biochem. Biophys. Res. Commun. *402*, 297–300.

Xu, J., Luo, F., Zhang, Z., Xue, L., Wu, X.-S., Chiang, H.-C., Shin, W., and Wu, L.-G. (2013a). SNARE Proteins Synaptobrevin, SNAP-25, and Syntaxin Are Involved in Rapid and Slow Endocytosis at Synapses. Cell Rep. *3*, 1414–1421.

Xu, K., Zhong, G., and Zhuang, X. (2013b). Actin, Spectrin, and Associated Proteins Form a Periodic Cytoskeletal Structure in Axons. Science *339*, 452–456.

Yao, J., Kwon, S.E., Gaffaney, J.D., Dunning, F.M., and Chapman, E.R. (2011). Uncoupling the roles of synaptotagmin I as a dual Ca2+ sensor during endo- and exocytosis of synaptic vesicles. Nat. Neurosci. *15*, 243–249.

Zhang, B., Koh, Y.H., Beckstead, R.B., Budnik, V., Ganetzky, B., and Bellen, H.J. (1998). Synaptic Vesicle Size and Number Are Regulated by a Clathrin Adaptor Protein Required for Endocytosis. Neuron *21*, 1465–1475.

Zhong, G., He, J., Zhou, R., Lorenzo, D., Babcock, H.P., Bennett, V., and Zhuang, X. (2014). Developmental mechanism of the periodic membrane skeleton in axons. eLife *3*.

Zhou, S., Sousa, R., Tannery, N.H., and Lafer, E.M. (1992). Characterization of a novel synapse-specific protein. II. cDNA cloning and sequence analysis of the F1-20 protein. J. Neurosci. *12*, 2144–2155.

8 Appendix

8.1 Abbreviations

Table 8-1: List of abbreviations.

Abbreviation	Meaning
aa	amino acid
amp	ampicillin
AP	action potential
AP-2	adaptor protein complex 2
APV	DL-2-Amino-5-phosphonopentanoic acid
AraC	Cytosine β-D-arabinofuranoside
AZ	active zone
CALM	clathrin-assembly lymphoid myeloid leukaemia protein
CLASP	clathrin-associated sorting protein
CME	clathrin-mediated endocytosis
CMV	cytomegalovirus
CNQX	6-Cyano-7-nitroquinoxaline-2,3-dione
d STORM	direct stochastic optical reconstruction microscopy
DIV	days in *vitro*
DMSO	Dimethylsulfoxid
DOL	degree of labeling
DTT	Dithiothreitol
E. coli	*Escherichia coli*
EGFP	enhanced green fluorescent protein
FCS	fetal calf serum
FWHM	full with at half maximum
GFP	green fluorescent protein
GSDB	goat serum dilution buffer
HBSS	Hank's Balanced Salt Solution
HEPES	4-(2-hydroxyethyl)-1-piperazineethanesulfonic acid
HRP	horseradish peroxidase
hygro	hygromycin
KD	knockdown
KO	knockout
LatA	Latrunculin A
MEA	β-mercaptoethylamine
MEM	Minimum Essential Media
MES	2-(N-morpholino)ethansulfonic acid
mRFP	monomeric red fluorescent protein
NA	numerical aperture

NBA	Neurobasal A
neo	neomycin
NEP	newly exocytosed pool of SV proteins
n. s.	not significant
NSF	N-ethylmaleimide-sensitive-factor
P #	postnatal day #
PAZ	periactive zone
PCR	polymerase chain reaction
PFA	Paraformaldehyde
PLL	poly-L-lysine
P / S	Penicillin / Streptomycin
pub	published
ROI	region of interest
RRetP	readily releasable pool of SV proteins
RRP	readily releasable pool
scr	scrambled
SD-*d*STORM	spectral-demixing direct stochastic optical reconstruction microscopy
shRNA	small hairpin RNA
SIM	structured illumination microscopy
SNAP	soluble NSF factor attachment protein
SNAP-25	Synaptosomal-associated protein 25
SNARE	soluble NSF attachment receptor
STED	stimulated emission depletion
SV	synaptic vesicle
SV2	synaptic vesicle glycoprotein 2
Syb2	synaptobrevin 2
Syb2-pH	pHluorin tagged synaptobrevin 2
Syp	synaptophysin
Syp-pH	pHluorin tagged synaptophysin
Syt1	synaptotagmin1
Syt1-pH	pHluorin tagged synaptotagmin1
TD	terminal domain
TES	2-[(2-Hydroxy-1,1-bis(hydroxymethyl)ethyl)amino]ethanesulfonic acid
TEV	Tobacco Etch Virus
TM	melting temperature
Tris	Tris(hydroxymethyl)aminomethane
TTX	tetrodotoxin
v / v	volume / volume
VGLUT1	vesicular glutamate transporter
w / v	weight / volume
WT	wild type

8.2 List of figures

8.3 Publications

Publications containing parts of this thesis

Gimber, N., Tadeus, G., Maritzen, T., Schmoranzer, J., and Haucke, V. (2015). Diffusional spread and confinement of newly exocytosed synaptic vesicle proteins. *Nature Communications*. 6, 8392. DOI: http://dx.doi.org/10.1038/ncomms9392.

Koo, S.J., Kochlamazashvili, G., Rost, B., Puchkov, D., **Gimber, N.**, Lehmann, M., Tadeus, G., Schmoranzer, J., Rosenmund, C., Haucke, V., et al. (2015). Vesicular Synaptobrevin/VAMP2 Levels Guarded by AP180 Control Efficient Neurotransmission. *Neuron*, 88, 330-44. DOI: http://dx.doi.org/10.1016/j.neuron.2015.08.034.

Additional publications

Weinert, S., Jabs, S., Supanchart, C., Schweizer, M., **Gimber, N.**, Richter, M., Rademann, J., Stauber, T., Kornak, U., and Jentsch, T.J. (2010). Lysosomal pathology and osteopetrosis upon loss of H+-driven lysosomal Cl- accumulation. *Science* 328, 1401–1403. DOI: http://dx.doi.org/10.1126/science.1188072.

Eberle, A.B., Hessle, V., Helbig, R., Dantoft, W., **Gimber, N.**, and Visa, N. (2010). Splice-site mutations cause Rrp6-mediated nuclear retention of the unspliced RNAs and transcriptional down-regulation of the splicing-defective genes. *PloS One* 5, e11540. DOI: http://dx.doi.org/10.1371/journal.pone.0011540.